Thesis

Wake Vortices and Tropical Cyclogenesis Downstream of Sumatra over the Indian Ocean

Submitted by

Caitlin Marie Fine

Department of Atmospheric Science

In partial fulfillment of the requirements

For the Degree of Master of Science

Colorado State University

Fort Collins, Colorado

Summer 2015

Master's Committee:

Advisor: Richard H. Johnson

Wayne H. Schubert
Michael J. Kirby

Abstract

Wake Vortices and Tropical Cyclogenesis Downstream of Sumatra over the Indian Ocean

A myriad of processes acting singly or in concert may contribute to tropical cyclogenesis, including convectively coupled waves, breakdown of the inter-tropical convergence zone (ITCZ), or upper-level troughs. This thesis investigates the role that topographic effects from the island of Sumatra may play in initiating tropical cyclogenesis (TC genesis) in the eastern Indian Ocean. If easterly flow is split by the mountains of Sumatra, counter-rotating lee vortices may form downstream. Because Sumatra straddles the equator, though the wake vortices rotate in opposite directions, they will both be cyclonic when winds are easterly upon Sumatra, and may intensify further into tropical cyclones. The phenomenon of cross-equatorial cyclone pairs, or "twin" tropical cyclones, in the Indian Ocean originating from Sumatra was first noted by Kuettner (1989). TC genesis appears to be particularly favored during the pre-onset phase of the Madden Julian Oscillation (MJO), when easterly flow encroaches upon Sumatra and the resulting cyclonic wake vortices encounter convectively coupled waves and enhanced moisture associated with the MJO in the Indian Ocean.

Operational analysis data from the Year of Tropical Convection (YOTC) and Dynamics of the Madden Julian Oscillation (DYNAMO) campaigns were used to evaluate the impacts of Sumatra's topography upon the flow. The YOTC data encompass two years, from May 2008 to April 2010, while the special observing period of DYNAMO was conducted from October to December 2011. This research also presents three case studies of twin tropical cyclones west of Sumatra in the Indian Ocean, which were all determined to originate from

Sumatran wake vortices and occurred between October and December of 2008, 2009, and 2011.

Multiple cyclonic wake vortices and vorticity streamers were observed downstream of Sumatra during periods of easterly flow, most frequently between October and December. Froude numbers calculated for the region upstream of Sumatra with regard to easterly flow between October and December favored flow blocking and splitting, more so for Sumatra's northern tip due to the higher terrain there. Correlations between zonal wind and relative vorticity are more significant near Sumatra's northern tip than near and downstream of the island's southern tip. Cyclonic vorticity was maximized at the level of Sumatra's topography for most easterly wind days west of both the north and south ends of the island, suggesting that topography was contributing to vorticity generation.

Thirteen tropical cyclones in the Indian Ocean during the YOTC and DYNAMO campaigns were determined to develop from cyclonic wake vortices downstream of Sumatra, including three tropical cyclone pairs. Over 75% of these tropical cyclones formed between October and December. In four cases, wake vortices were generated by anomalously easterly low-level flow that preceded the active phase of the Madden Julian Oscillation. These vortices proceeded to encounter the MJO convective envelope, which is frequently accompanied by convectively coupled waves and may have altered the environment to be more moist and favorable for tropical cyclogenesis. In many cases, equatorial westerly winds, which may have been related to westerly wind bursts from the MJO or to convectively coupled equatorial Rossby waves, intensified low-level cyclonic circulations. It is suggested that diabatic heating in the vicinity of twin tropical cyclones may disturb the atmosphere enough to invigorate extant convectively coupled Kelvin waves, or contribute to the formation of a Kelvin wave.

The research presented herein describes the interaction of the flow with steep topography on Sumatra and its role in tropical cyclogenesis over the Indian Ocean, a mechanism for TC genesis that has heretofore received little attention.

Acknowledgements

This research was supported by NSF grant AGS-1360237 and a one-year Americal Meteorological Society Graduate Fellowship.

I would like to thank my adviser, Dr. Richard Johnson, for his support, understanding of my unique situation in the U.S. Navy, and keen insight into all things meteorological, and the members of my committee, Drs. Wayne Schubert and Michael Kirby, for their helpful comments. I would also like to thank the members of the Johnson group- in particular Paul Ciesielski and Rick Taft- for helping me obtain relevant data and address complicated technical difficulties, and the CSU Atmospheric Science Department staff for helping me navigate many bureaucratic and paperwork-related challenges. Finally, thanks to Dr. Kathy Straub for her code to filter outgoing longwave radiation for the different convectively coupled equatorial wave modes, which otherwise would have been a daunting task, and Brian McNoldy, for his help with tropical cyclone track maps.

I would like to thank the United States Naval Academy's Oceanography Department, in particular Dr. David Smith, Dr. Brad Barrett, and Commander Elizabeth Sanabia, PhD, USN. Without their encouragement and the facilitation of many unique professional and academic opportunities, I would not have been prepared for the rigors of research and graduate school. I learned many life lessons from them that were applicable in academia, and will be applicable in the fleet.

I would like to thank my family, who has been with me since the beginning- my mother, Dr. Anne Marie Fine, and my brother, Colin Fine, for their love, advice, and unwavering support, and my father, Captain Gregory Fine, USNR (ret.), who would be proud.

I would like to thank my friends, both new and old, for their support, fun diversions, and many great conversations, whether related to meteorology or not.

This thesis is typset in LaTeX using a document class designed by Leif Anderson.

Table of Contents

List of Tables

List of Figures

CHAPTER 1

Introduction

Many tropical phenomena and modes of variability interact in the Indian Ocean, including thermally driven, seasonal monsoonal flows, tropical cyclones, convectively coupled equatorial waves, the Madden Julian Oscillation, the interannual Indian Ocean dipole, and on a more local scale, sea breezes and mountain flows along the edges of continents. A number of field campaigns have been conducted, and more are planned, to investigate these myriad processes that influence weather, agriculture, economics, and quality of life for the billions of people who live in the region, as well as for billions more in other parts of the world due to meteorological teleconnections and global economic ties. On the eastern edge of the Indian Ocean lies the Maritime Continent, composed of many large, mountainous tropical islands, including the cross-equatorial island of Sumatra. Sumatra and the Maritime Continent have been implicated in influencing the propagation of the Madden Julian Oscillation (Inness and Slingo 2006; Wu and Hsu 2009), and contributing to local rainfall maxima via a pronounced diurnal cycle of convection and mutual reinforcement between sea and mountain breezes (Yang and Slingo 2001; Mori et al. 2004; Qian 2008; Wu et al. 2009; Peatman et al. 2014). In addition, and of more specific relevance to this thesis, Sumatra has been shown to interfere with lower-tropospheric flow and generate wake vortices that may then develop into tropical cyclones in the Indian Ocean (Kuettner 1989).

When wind flows around or over an obstacle, relative vorticity may be generated downstream (e. g., Smith 1979). In the case of winds impinging upon an equatorial obstacle such as the island of Sumatra, wake vortices form downstream (e. g., Smolarkiewicz and Rotunno

1989; Schär and Smith 1993a). These wake vortices rotate in opposite directions. When easterly wind encounters Sumatra, wake vortices from each end of Sumatra emerge downstream in the Indian Ocean, and both are cyclonic because Sumatra straddles the equator. Such counter-rotating, cyclonic wake vortices have been observed to intensify into twin tropical cyclones on either side of the equator (Kuettner 1989). Tropical cyclones that formed from Sumatran wake vortices have curved poleward, to make landfall in the low-lying countries bordering the Bay of Bengal or Australia, and have also propagated far to the west to strike Madagascar or the Arabian Peninsula and the Horn of Africa. In addition to the very visible impacts of tropical cyclone damage, some wake vortices (as will be shown) have been observed to pass through the convective envelope that marks the Madden Julian Oscillation's active phase, or through other types of convectively coupled equatorial waves.

This study will use data from the virtual Year of Tropical Convection campaign from 2008 to 2010 and the Dynamics of the Madden Julian Oscillation field campaign in late 2011 to investigate modification of flow by Sumatra's topography, the formation of wake vortices near Sumatra, the intensification of those wake vortices into tropical cyclones, and any interaction between wake vortices and tropical waves. This study hopes to inform the contribution of orographic flow disturbance to cyclonic, counter-rotating vortices downstream of Sumatra over the Indian Ocean, the difference between developing and non-developing wake vortices, and the behavior of convectively coupled equatorial waves and wake vortices in close proximity to one another and the Maritime Continent.

1.1. DYNAMO and YOTC Overview

The Year of Tropical Convection (YOTC) was a virtual field campaign conducted from May 2008 to April 2010 (Moncrieff et al. 2012). YOTC was coordinated through the World

Climate Research Program and World Weather Research Programs research entity, The Observing System Research and Predictability Experiment (THORPEX) (Moncrieff et al. 2012). As a "virtual" field campaign, YOTC served to focus the community's efforts on assimilating, modeling, and hindcasting using the myriad of data available on a regular basis in the tropics, such as geostationary and low-earth orbit satellite imagery, soundings, buoys, oceanic floats, and data from other observational platforms. YOTC was intended to gather data in one database to facilitate inquiry into and improve the understanding and prediction skill of tropical phenomena such as the Madden-Julian Oscillation (MJO), convectively coupled equatorial waves, interaction between the tropics and extratropics, monsoons in different tropical regions, the diurnal cycle, and tropical cyclone activity.

For a more complete description of all the climatic and weather events that occurred during YOTC, refer to Waliser et al. (2012); only the salient points will be discussed here. The first half of the YOTC virtual campaign period exhibited moderate La Niña, the cold phase of of the El Niño Southern Oscillation (ENSO), conditions, while a moderate warm phase El Niño event emerged in the second half of the timeframe (Waliser et al. 2012). Sea surface temperatures (SSTs) in the Indian Ocean were below average at the beginning of YOTC, and warmed to as much as 0.5 °C above average in the eastern Indian Ocean basin by the summer of 2009, while the western Indian Ocean basin was consistently approximately 0.5 °C warmer than the eastern side throughout.

Six active MJO events were identified, passing by the approximate longitude of Sumatra in early June 2008, early September 2008, early February 2009, early April 2009, early November 2009, and late December 2009/early January 2010; the strongest events, in terms of outgoing longwave radiation (OLR) anomalies, occurred from April 2009 and later (Waliser et al. 2012). From April to May 2009, notable interaction between convectively coupled waves

and the MJO was observed. The November 2009 MJO event featured the most negative OLR anomalies observed during the YOTC period. The December 2009 and January 2010 MJO convective envelope extended farther west than any of the other MJO events during YOTC.

Between May 2008 and April 2010, tropical cyclones made landfall in Madagascar, Bangladesh, Myanmar, Australia, and elsewhere; the most notable of these was Cyclone Nargis, which inflicted a storm surge upon low-lying Myanmar and the Irrawaddy River delta, potentially claiming over 130,000 lives (Red Cross 2011). Field projects involving aircraft reconnaissance into typhoons were conducted in the western North Pacific at this time, but do not concern this research (Waliser et al. 2012). Eleven tropical cyclones were subjectively identified to be related to wake vortices stemming from flow blocking or splitting near Sumatra, including two cross-equatorial tropical cyclone pairs. The wake vortex precursors to two cyclones appeared to pass through the MJO convective envelope in late January 2009 and early January 2010. This study will focus on the two twin tropical cyclone events that occurred during YOTC, and another tropical cyclone pair that grew out of Sumatran wake vortices during another field campaign in late 2011.

The Dynamics of the MJO (DYNAMO) field project was conducted between October 2011 and March 2012 primarily in the Indian Ocean basin, where MJO convection initiates (Johnson and Ciesielski 2013). Its goals were to observe and better understand the roles of tropospheric moistening, cloud population, and air-sea interaction during MJO initiation. There were three contributing entities to the project overarchingly known as DYNAMO: Dynamics of the MJO (DYNAMO), Cooperative Indian Ocean Experiment on Intraseasonal Variability in the Year 2011 (CINDY2011), and the Atmospheric Radiation Measurement Program (ARM) MJO Investigation Experiment (AMIE). A special observing period of enhanced temporal and spatial observations occurred between October and November 2011.

Quadrilateral sounding arrays, where soundings were launched between 4 to 8 times daily, were established in the 70-80°E region in both hemispheres, and are depicted in Fig. 1.1; the shape of the arrays changed occasionally as ships or other stations briefly became non-operational or left the site (Johnson and Ciesielski 2013).

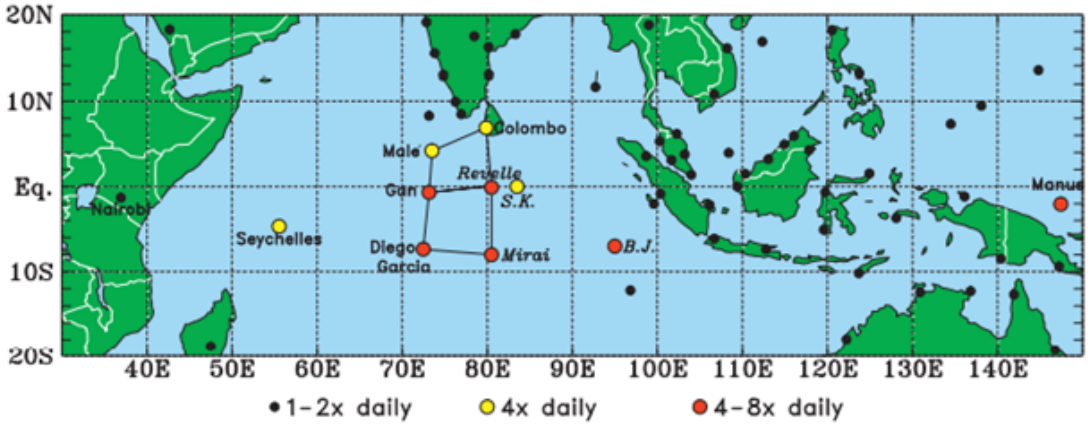

FIGURE 1.1. The northern and southern sounding arrays used in DYNAMO's special observing period, and other sounding launch sites in the Indian Ocean basin. From Johnson and Ciesielski (2013).

The sounding arrays included two ships, the RV *Mirai* and the RV *Revelle*, which measured oceanic quantities such as SST and latent heat fluxes in addition to atmospheric variables. Soundings were launched from other locations as well around the Indian Ocean basin, but less frequently, from one to two times daily. Thirteen research flights were conducted to sample various phases of the MJO as well. C-band, S-band, and Ka-band radars, which are able to detect different cloud populations and microphysical properties, were also situated within the sounding arrays (Yoneyama et al. 2013; Feng et al. 2014).

For a more complete description of the climatic conditions and weather events that occurred during DYNAMO, please refer to Johnson and Ciesielski (2013) or Gottschalck et al. (2013). The beginning of the DYNAMO special observing period in October coincided with a burgeoning cold phase ENSO, or La Niña, event. Near Sumatra, SSTs were below

average, but within 1 °C of the mean; in the western Indian Ocean, SSTs were elevated by nearly 1 °C (Gottschalck et al. 2013). In November and December, the cool anomalies near Sumatra vanished, while positive SST anomalies lingered, especially along the equator and in parts of the southern Indian Ocean. Two MJO events were observed during the early part of DYNAMO, crossing the longitude of Sumatra in late October 2011 and late November 2011, the November 2011 event characterized by stronger OLR anomalies, distinct westerly wind bursts, and two prominent Kelvin waves (Johnson and Ciesielski 2013). A third subseasonal event with some MJO characteristics that did not meet the real-time multivariate MJO (RMM) index metric to be classified as an MJO occurred in late December (Gottschalck et al. 2013). OLR and precipitation anomalies related to the active MJO were less obvious in the southern sounding array, which was marked, rather, by persistent rain and convection from the inter-tropical convergence zone (ITCZ) (Johnson and Ciesielski 2013). At times, persistent rain and troughs in surface flow both north and south of the equator demarcated a double-ITCZ pattern (Johnson and Ciesielski 2013).

Tropical Storm 05A, which reached tropical storm strength on 26 November 2011, will be addressed in this research, as will Moderate Tropical Cyclone Alenga (01S), which was classified as a tropical storm on 5 December 2011 (JTWC 2011a, 2012). Tropical Storm 05A appeared to stem from a wake vortex that formed when easterly flow was split by Sumatra, then propagated westward and encountered the active MJO envelope with Kelvin waves embedded within it. The wake vortex precursor to Moderate Tropical Cyclone Alenga spun up near Sumatra, possibly due to blocking and cyclonic deflection of westerly flow, within the MJOs convective envelope, then propagated westward and out of the convective envelope. Another pair of cross-equatorial tropical cyclones, Very Severe Cyclonic Storm Thane (06B) and Tropical Cyclone Benilde (04S), was attributed to interaction between the subseasonal,

MJO-like event in late December 2011 and an equatorial Rossby wave (Gottschalck et al. 2013). However, these storms sprang from monsoon troughs, and will not be analyzed further (JTWC 2011b).

CHAPTER 2

Background

2.1. The Madden-Julian Oscillation

The Madden-Julian Oscillation is the dominant mode of intraseasonal variability in the tropics (Zhang 2005). It was first formally noted in the 1970's by Madden and Julian (1971, 1972) as a pattern in atmospheric circulation and pressure anomalies between meteorological observing stations in eastern Africa, the Indian Ocean, and the western Pacific Ocean. From the Indian Ocean to the International Date Line, a convective and rainy, or "active", phase, and a dry, or "suppressed", phase, comprise the MJO (Madden and Julian 1971). The rainfall and OLR signatures of the MJO dissipate east of the date line, but zonal wind anomalies and velocity potential related to the MJO propagate around the world in the upper troposphere (Madden and Julian 1994). Many different scales of organized systems move both westward and eastward within the broadly-defined convective envelope of the MJO, including convectively-coupled equatorial waves, though the MJO as an entity propagates eastwards (Nakazawa 1988). The MJO is often defined using the Real-Time Multivariate MJO index (RMM) index, which considers 850 and 200 hPa circulation anomalies as well as outgoing longwave radiation (OLR), which is a proxy for cloud cover (Wheeler and Hendon 2004); other methods of diagnosing a MJO event also exist (e. g., Kiladis et al. 2014).

Energy from the MJO, even east of the International Date Line when its convective envelope has vanished, impacts phenomena both locally and globally (Zhang 2013). This study is primarily concerned with the local impacts of the Madden-Julian Oscillation and its interaction with wake vortices downstream of Sumatra, as observed during the Year of Tropical Convection and Dynamics of the MJO field campaigns, which were conducted from

2008 to 2010, and 2011 to 2012, respectively. Anomalous easterlies in the lower troposphere precede the arrival of the active phase of the MJO (Madden and Julian 1972). Depending on conditions, this easterly flow may be split by the mountains of Sumatra, resulting in cyclonic lee vortices in both hemispheres. In certain observed cases during YOTC and DYNAMO, these wake vortices propagated westward and encountered an environment modified by the MJO, the MJO itself, and other convectively coupled equatorial waves. Both environmental modification, including that of midlevel (300-700 hPa) moisture and sea surface temperatures (SSTs), as well as the complex dynamics of convectively coupled equatorial waves and the MJO, may have made the environment more favorable for tropical cyclogenesis or assisted the wake vortices in intensifying in these instances.

2.1.1. Impacts of the MJO. Multiple theories have been suggested to explain the initiation and propagation of the MJO, but the initiation and propagation mechanisms of the MJO are still relatively unknown; Zhang (2005) and Lau and Waliser (2011) provide a thorough overview of the challenges and uncertainties in the MJO field. Models currently struggle to reproduce an MJO-like signal with the appropriate characteristics (Lau and Waliser 2011). Models that could accurately portray the MJO would likely see an increase in their predictive skill (Zhang 2013). For example, statistical models that predict phenomena such as tropical cyclones in the southern Indian Ocean based on relationships to MJO phase show predictive skill out to between 10-20 days (Vitart et al. 2010). Understanding the convective and dynamical features that occur in the vicinity of the MJO, and how the MJO and its components and nearby phenomena interact, is critical to extending predictive skill with regard to the MJO, which can then enhance preparedness for the different severe weather events and climatic elements discussed below.

The MJO may exert influence over many local and remote phenomena, though only relevant impacts are discussed below. The MJO may influence local rainfall or flow patterns by modifying the onset date of the South Asian (Goswami 2011; Hsu 2011), or Australian seasonally reversing monsoons (Wheeler et al. 2009), possibly by affecting the local meridional circulation (Zhang et al. 2009). Though the MJO is an intraseasonal mode of variability, it may affect lower frequency variability as well, such as the El Nio Southern Oscillation (ENSO). ENSO is the predominant interannual mode of variability in the tropical Pacific Ocean, involves the warm pool and associated convective maximum sliding eastward or westward, and projects temperature (sea and air) and precipitation impacts around the world. Recent strong ENSO warm phase events have been preceded by unusually intense MJO episodes (McPhaden 1999, 2004, 2008). In particular, strong westerly wind bursts racing outwards from MJO-related convection are hypothesized to play a role by interacting with the warm pool near the Philippines and enhancing air-sea exchange and coupling, which is crucial to ENSO (Seiki and Takayabu 2007). The MJO is also suggested to influence the Indian Ocean Dipole, a zonal sea surface temperature gradient that exists across the Indian Ocean basin and occasionally reverses, as surface wind anomalies associated with the MJO can influence upper-ocean structure and mixing processes (Rao et al. 2009). ENSO and the IOD may then themselves modify environmental conditions in the Indian Ocean basin, potentially creating favorable conditions for MJO or tropical cyclone initiation, constituting a complicated feedback process.

Significant links have been demonstrated between certain phases of the MJO and tropical cyclogenesis in the Atlantic Ocean, Gulf of Mexico, Caribbean Sea, tropical eastern Pacific Ocean, southern Indian Ocean, and northern Indian Ocean (Frank and Roundy 2006). In the Indian Ocean basin, simulations have suggested that large cyclonic Rossby gyres in the

wake of the active MJO may also contribute to twin tropical cyclogenesis on either side of the equator (Ferreira et al. 1996). Additionally, elongated potential vorticity (PV) anomalies left in the wake of the MJO could become unstable and trigger cyclogenesis (Ferreira et al. 1996). Strong upper-level divergence anomalies associated with the active MJO may also prime the atmosphere to be more favorable for tropical cyclogenesis (Liebmann et al. 1994). This study is interested in the potential local influence of the Madden-Julian Oscillation on nascent tropical cyclones in the Indian Ocean basin.

2.1.2. Characteristics of the MJO. The MJO, as a whole, propagates eastwards at approximately 5 m s^{-1} (Zhang 2005). After uncoupling from convection around the International Date Line, the MJO's energy propagates more quickly (Milliff and Madden 1996; Matthews 2000); as a result, the MJO has a 30-60 day global period (Zhang 2005).

In Fig. 2.1, the initiation of the MJO's convection and circulation anomalies in the Indian Ocean, the movement of the MJO's convective envelope and the trailing suppressed phase eastward into the Pacific, and the dissipation of convection near the International Date Line, are evident. It is also demonstrated in Fig. 2.1 that the circulation anomalies proceed around the globe even in the absence of the convective signal. The convective maximum often diverts southwards upon reaching the mountainous Maritime Continent before returning to the equator (Wu and Hsu 2009). It has been theorized that wake vortices generated by flow interaction with the topography of the Maritime Continent, in particular Sumatra, interact with convectively coupled Kelvin waves and slow or block their propagation entirely (Flatau 2015).

As illustrated in Fig. 2.1, the active phase of the MJO is characterized by large-scale convergence of surface winds, divergence aloft, and anomalously low OLR (Madden and Julian 1994). Convergence at the surface contributes to the anomalously westerly winds

behind the convective envelope at low levels, and anomalously easterly winds ahead of the MJOs convective envelope (Madden and Julian 1972).

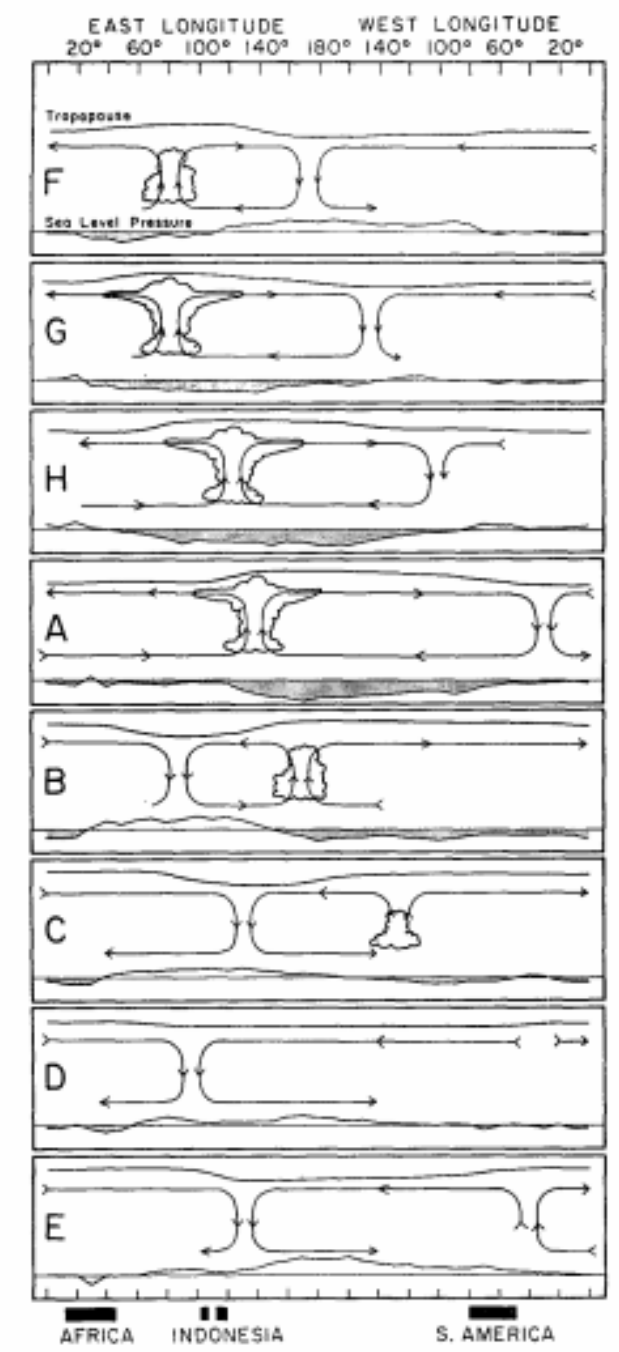

FIGURE 2.1. Circulation and convection anomalies associated with the Madden-Julian Oscillation. Longitude is on the x-axis. Phases correspond to the geographic regions in which the convective signal is found on the y-axis. From Madden and Julian (1972)

.

Depending on velocity and environmental conditions, these easterly winds may be split by Sumatra, leading to cyclonic wake vortices. In areas of convection, divergence aloft is enhanced, leading to upper level easterlies behind the convective envelope, and upper level westerlies ahead of it (Madden and Julian 1972). The troposphere moistens significantly as an active MJO event develops, though the mechanism by which it moistens is still debated (Zhang 2005). Low-level cyclonic potential vorticity appears in the wake of the MJO as two off-equatorial band where equatorial westerlies that accompany the MJO's convective envelope meet with poleward trade easterlies (Schubert and Masarik 2006). The majority of this PV appears to be generated by diabatic heating within the convective envelope (MacRitchie and Roundy 2012). These PV strips may become unstable and lead to tropical cyclogenesis in regions where convection is enhanced (Ferreira et al. 1996).

Westerly wind bursts (WWBs), which race ahead of the MJO, have been observed in conjunction with the MJO's active phase, and in conjunction with Kelvin waves (Luther et al. 1983; Moum et al. 2014). Westerly wind bursts and general gustiness from convection and cold pools enhance air-sea latent and sensible heat fluxes, which play a major role in many theories that seek to explain MJO initiation (de Szoeke et al. 2015). Wind stress also accelerates oceanic currents and mixing in the upper ocean, changes which may persist and moderate sea surface temperatures for weeks after the MJO has passed (McPhaden et al. 1992; Moum et al. 2014).

Components of MJO convection may include convectively coupled equatorial waves, which may propagate to the east (in the case of Kelvin waves) or westward (in the case of equatorial Rossby or mixed Rossby-gravity waves) (Hendon and Salby 1996). Convectively coupled waves will be introduced in more detail in the following subsection. Other

features, such as mesoscale convective systems or squall lines, may exist within the broader context of the MJO as well (Nakazawa 1988; Khouider et al. 2012).

The suppressed phase of the MJO is characterized by widespread subsidence, low atmospheric moisture content, and light winds (Madden and Julian 1972). Dry air entrainment due to Rossby gyres left in the wake of the MJO may reduce convection, or result in a shift in convection locations (Kerns and Chen 2014). Shallow diurnal warm layers, sometimes several degrees C above average, form in the oceanic mixed layer, as there is little wind to induce mixing upper-ocean mixing (Lindstrom et al. 1987; McPhaden et al. 1992). Before an active MJO event arrives, convection transitions from shallow convection, which may be related to suppression from a previous MJO, to deep convection (Ruppert and Johnson 2015). The diurnal cycle is prominent in SSTs, which again are starkly elevated due to diurnal warm layers, and in cumulus congestus formation, which aids in moistening the low-to-mid troposphere (Ruppert and Johnson 2015).

2.1.3. Convectively Coupled Equatorial Wave Modes. Gill (1980) demonstrated that, for an equatorial heat source, equatorially trapped Kelvin waves arise and propagate eastward, and equatorial Rossby waves are generated and move westward. This heat source is to a first order analogous to the Madden-Julian Oscillation, which is a large, roughly equatorial source of diabatic heating that may generate or interact with multiple scales of convection, including convectively coupled equatorial waves. Indeed, over 10 years of observation, the active phase of the MJO was associated with more frequent generation of convectively coupled waves (Schreck et al. 2012). Convectively coupled waves have been linked to tropical cyclogenesis, which will be discussed in further detail in a later section.

As shown in Fig. 2.2, equatorially trapped Kelvin waves involve circulation and pressure anomalies centered on the equator itself, while equatorial Rossby waves feature circulation and pressure anomalies symmetric about the equator (Matsuno 1966).

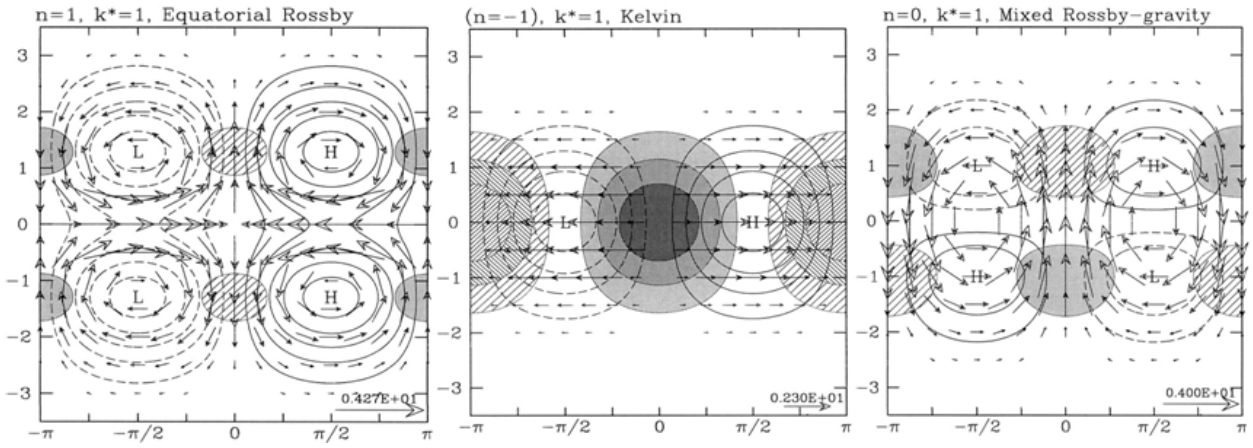

FIGURE 2.2. The pressure and circulation anomalies associated with equatorial Rossby waves (left), equatorially-trapped Kelvin waves (middle), and mixed Rossby gravity waves (right). From Wheeler et al. (2000), after Matsuno (1966).

Mixed Rossby-gravity waves, or Yanai waves, were first discovered in the stratosphere; in the tropics, they appear as anomalies antisymmetric about the equator (Yanai and Maruyama 1966). Accordingly, mixed Rossby-gravity waves are identified when filtering OLR for antisymmetric components, as seen in Fig. 2.2, while equatorial Rossby and Kelvin waves appear in the symmetrically filtered OLR anomaly fields (Wheeler and Kiladis 1999). Higher-frequency inertial gravity waves may also exist in the tropics, excited by convection or orography (Wheeler and Kiladis 1999).

The phase speed and group velocity of Kelvin waves are the same sign when solved in a shallow water framework, and so Kelvin waves transport energy eastwards (Matsuno 1966). Equatorial Rossby waves and mixed Rossby gravity waves flux energy eastwards as well,

though they propagate westwards, because their phase speeds and group velocities are of opposite sign (Matsuno 1966). These waves demonstrate circulation and convective anomalies throughout the troposphere and have been shown to flux energy upwards or downwards as well and interact with the stratosphere (Wallace and Kousky 1968; Lindzen and Matsuno 1968; Zangvil and Yanai 1980). These convectively coupled equatorial waves propagate more quickly than the MJO itself, and have a faster period (Wheeler and Kiladis 1999; Straub and Kiladis 2002). The easterly propagation of Kelvin waves and the MJO, and their relative frequencies, are illustrated in Fig. 2.3b, where the lower-frequency MJO lies on the right side of the plot, near the abcissa, and Kelvin waves occupy a space higher on the ordinate (and thus are characterized by a higher frequency), also on the right side of Fig. 2.3b. Equatorial Rossby waves propagate westward, and thus are found on the left side of Fig. 2.3b. Mixed Rossby-gravity waves are found in Fig. 2.3a, and inhabit a range of frequencies somewhat between those of equatorial Rossby waves and Kelvin waves.

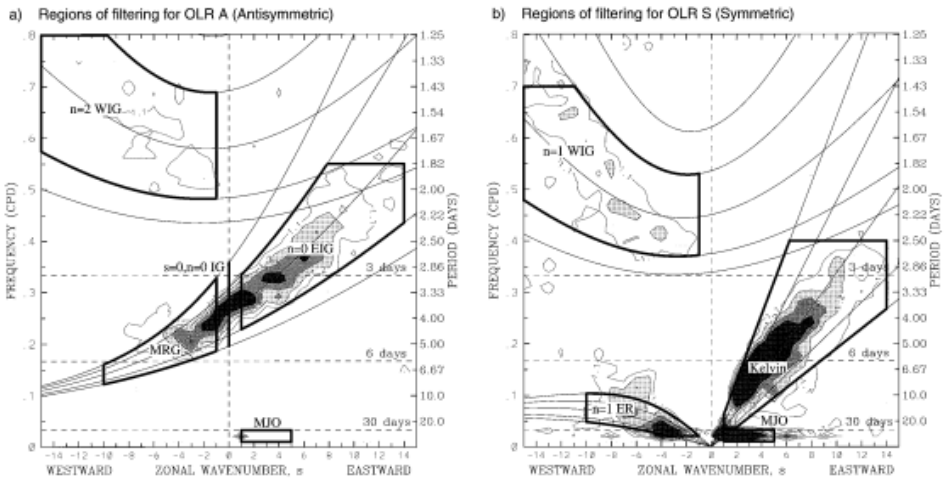

FIGURE 2.3. A wavenumber (x-axis) and frequency (y-axis) diagram of a) longitude-time OLR filtered for antisymmetric OLR components and b) longitude-time OLR filtered for symmetric components of OLR, normalized by a background spectrum. From Wheeler and Kiladis (1999).

The variance of equatorial waves follows a geographic and seasonal distribution, whose characteristics are presented in a series of figures in Wheeler and Kiladis (1999). Enhanced equatorial Rossby wave activity and significant Kelvin wave activity are present near Sumatra in boreal winter, when, it shall be demonstrated, the majority of cyclonic wake vortices form around Sumatras tips and propagate westward. MJO-band OLR variance is concentrated in the summer hemisphere. In the northern hemisphere, MJO band variance is maximized from the Bay of Bengal to the Philippines, while in the southern hemisphere, MJO band variance is distinctive to the south of the Maritime Continent (Wheeler and Kiladis 1999).

Convectively coupled Kelvin waves occur particularly frequently in conjunction with the MJOs active phase; the outflow and intensity from the Kelvin wave-associated deep convection is modulated by the MJO (Roundy 2008). Convectively coupled Kelvin waves have also been shown to generate potential vorticity, some of which is incorporated into the MJOs structure after the Kelvin wave propagates away, some of which remains in the environment (MacRitchie and Roundy 2012). The relative contributions of convectively coupled Kelvin waves, which have been shown to produce potential vorticity poleward of their convective centers, or equatorial Rossby waves, to potential vorticity production in the active MJO are debated (MacRitchie and Roundy 2012; Zhang and Ling 2012).

The MJO influences multiple temporal and spatial scales of weather and climatic events around the globe (Moncrieff et al. 2012). Multiple field campaigns, both in the past few years and planned, have sought or seek to untangle the many processes involved with the MJO, and the MJO's significant impact on many different phenomena both locally and globally. This research focuses on wake vortices that form due to topographic effects on flow downstream of Sumatra, and how, in some observed cases, wake vortices may interact with the MJO in the Indian Ocean basin.

2.2. Tropical Cyclogenesis

Tropical cyclones (TCs) are mesoscale-α to synoptic-scale, warm-core, low pressure systems with closed circulations that can feature heavy precipitation and strong winds (Riehl 1948). Tropical cyclones are composed of a primary and secondary circulation (Frank 1977). The primary circulation refers to tangential winds roughly in either gradient or cyclostrophic wind balance, while the secondary circulation consists of air flowing inwards in the boundary layer, gaining buoyancy from the warm, moist ocean, rising and condensing into rainbands or the eyewall, and diverging aloft (Frank 1977). In most observing regions, tropical cyclones from 34-64 knots (kt) are known as tropical storms, and those above 64 knots are variously known as typhoons (western North Pacific Ocean basin), hurricanes (Atlantic and East Pacific Ocean basins), tropical cyclones (South Indian Ocean basin), or very severe cyclonic storms (North Indian Ocean basin). It has been recognized for some time that conservation of angular momentum, thermodynamics of latent and sensible heat release, and air-sea exchange are all crucial factors in a tropical cyclones lifecycle, though debate continues over the relative importance of various mechanisms for tropical cyclogenesis and intensification (Ooyama 1969). This research will examine the environmental and dynamical conditions surrounding the intensification of wake vortices, generated by flow incident upon Sumatra's mountains, into tropical cyclones.

Six necessary but not sufficient conditions for tropical cyclogenesis are: 1) the sea surface temperature must exceed 26.5 °C, as is the case in most tropical seas for over half of the year; 2) the incipient tropical cyclone's latitude must usually be at least 5° poleward of the equator so the requisite amount of Coriolis force is present; 3) vertical wind shear must be low, or the disturbance will have its cloud tops shorn off and dissipate; 4) low-level vorticity must be large and cyclonic, usually due to a pre-existing disturbance, to provide the necessary

spin; 5) instability, which enables vertical motion, must be present; and 6) mid-tropospheric air must be humid (Gray 1968). Not all disturbances that meet these criteria develop into tropical cyclones.

2.2.1. Environmental Factors Supporting Tropical Cyclogenesis. Putting aside the debate over the correct mechanism for tropical cyclogenesis, there are a myriad of processes, oscillations, and features which may impact tropical cyclogenesis by modifying the environment or influencing dynamical or energetic aspects of a given tropical disturbance. The different basins have pronounced seasonal distributions of tropical cyclones, based on climatological factors that may affect the six necessary but not sufficient conditions for tropical cyclogenesis above (Gray 1968).

In the northwestern Pacific and entire Indian Ocean basins, the summer and winter monsoons are important sources of geographic and temporal variability of tropical cyclogenesis. Monsoon troughs are lower-tropospheric features wherein westerlies converge with trade easterlies to the east of the monsoon low feature, leading to preferential rising motion in a moist region (Holland 1995). A significant amount of tropical cyclones develop within monsoon troughs, which can then affect the track of an existing tropical cyclone, in the western north Pacific and both hemispheric Indian Ocean basins (Lander 1996). Tropical upper tropospheric troughs often occur in the same region as low-level monsoon troughs; TUTTs often make TC development more favorable by reducing vertical wind shear and increasing outflow aloft (Sadler 1976; Hanley et al. 2001). During DYNAMO and YOTC, several TCs were observed to form within evident monsoon troughs in both hemispheres. Wind shear associated with the southeastern Asian monsoon discourages tropical cyclone formation when monsoonal flow is well established (Gray 1968). Most tropical cyclones associated with Sumatran wake vortices have been observed in the monsoon transition months

of May to June and October to December, when shear is reduced and easterly winds impinge upon Sumatra (Kuettner 1989).

The tropical cyclones considered in this study form very close to the equator and the intertropical convergence zone, or ITCZ, a zonally elongated band of persistent convection, which may be located at 5-10° latitude poleward of the equator depending on which hemisphere is experiencing summer. Usually, potential vorticity increases towards the poles due to planetary vorticity f, which is a function of the sin of the latitude, and increasing static stability, due to decreasing temperatures and surface heights. If this meridional potential vorticity gradient is reversed, however, the ITCZ may become unstable through a combination of baroclinic and barotropic processes (Ferreira and Schubert 1997). Tropical cyclones have been observed to form out of the undulating ITCZ, which is also known as an ITCZ "breakdown" (Ferreira and Schubert 1997). Advection of vorticity out of the ITCZ by southerly wind into the region of a nascent tropical cyclone has been observed in the eastern Pacific Ocean (Farfán and Zehnder 1997). The orientation of a monsoon or midlatitude trough relative to the ITCZ has also been shown to influence the likelihood of tropical cyclogenesis (Briegel and Frank 1997).

Tropical cyclone frequency may fluctuate according to phases of intraseasonal and interannual modes of variability. During warm phases of ENSO, tropical cyclone frequency in the northern and southern Indian Ocean basins is reduced (Jury 1993; Singh et al. 2000). Suggested explanations include increased vertical wind shear during warm phase ENSO years and changes in the Hadley cell north-south circulation or in the Walker cell east-west tropical circulation (Jury 1993). Sea surface temperatures in the Indian Ocean and those in the Pacific Ocean show a close association, so the shift in SST patterns that occurs with

ENSO may affect SSTs, and thus tropical cyclone development ,in the Indian Ocean as well (Camargo et al. 2007).

The Indian Ocean Dipole (IOD) involves tight coupling between the ocean and atmosphere, and its anomalous SST distribution influences precipitation and large-scale circulation patterns over the Indian Ocean (Saji et al. 1999). The IOD has been shown to impact the southeastern Asian monsoon more significantly than does ENSO, so the two interannual modes of variability may either combine or counteract one another in influencing circulation and tropical cyclone likelihood in the Indian Ocean basin (Ashok et al. 2004). The phase of the North Atlantic Oscillation, an anomalous sea surface pressure pattern that may modify midlatitude westerlies and the jet stream, has been demonstrated to impact tropical cyclogenesis in the Indian Ocean basin as well (Frank and Young 2007).

As discussed further in the MJO section, the MJO is also a significant source of intraseasonal variability in tropical cyclone formation in many different tropical cyclogenesis regions. Many of these sources of variability may feed back upon one another, and thus it may be difficult to isolate the influence of each process in an individual case. The phases of these oscillations and their impact upon large-scale environmental conditions in the Indian Ocean basin during the YOTC and DYNAMO periods is noted in the overview of those campaigns.

2.2.2. Convectively Coupled Equatorial Waves and Tropical Cyclogenesis. Convectively coupled Kelvin, mixed Rossby-gravity, and equatorial Rossby waves have all been linked to tropical cyclogenesis (Frank and Roundy 2006). Studies of tropical cyclogenesis and mixed Rossby-gravity waves tend to focus on the Pacific Ocean, where the climatological variance of mixed Rossby-gravity waves is greatest (Dickinson and Molinari 2002). Equatorial Rossby waves were found to increase incidences of tropical cyclogenesis in the southern Indian Ocean, based on their modulation of vertical wind shear and 850mb

low-level vorticity to be more favorable for TC spin up (Bessafi and Wheeler 2006). Equatorial Rossby waves themselves occur more frequently in the southern Indian Ocean during the austral summer, corresponding to the climatological peak of tropical cyclogenesis in the southern Indian Ocean (Frank and Roundy 2006). Kelvin waves were found to contribute to southern Indian Ocean tropical cyclogenesis to a lesser, but still significant, degree than did equatorial Rossby waves (Bessafi and Wheeler 2006).

In the Indian Ocean, over a composited number of Kelvin wave events, cyclonic gyres associated with diabatic potential vorticity generation via latent heat release were connected to tropical cyclogenesis (Roundy 2008). Kelvin waves are often found within the multiscale structure of the active MJO; in two case studies in the western North Pacific, Kelvin waves and the MJO interacted to produce a strip of unstable potential vorticity near the equator, where MJO-related westerlies undercut trade easterlies, which led to tropical cyclogenesis (Schreck and Molinari 2011). This mechanism by which a zonally oriented potential vorticity anomaly forms and becomes unstable is similar to Ferreira and Schubert (1997), but was precipitated by a combination of the MJO and Kelvin waves. A similar meridional arrangement of zonal winds contributed to the formation of three pairs of cross-equatorial twin tropical cyclones in the Pacific Ocean (Schreck and Molinari 2009). In those cases, equatorial Rossby waves were implicated as the source of the anomalous equatorial westerlies (Schreck and Molinari 2009).

Strong Kelvin and equatorial Rossby wave activity was noted during the YOTC and DYNAMO periods, often in conjunction with an active MJO event (Waliser et al. 2012; Gottschalck et al. 2013). The superposition of a convectively coupled Kelvin wave, equatorial Rossby wave, and the MJO convective envelope was noted prior to the development of Tropical Storm 05A out of a wake vortex that propagated westward from Sumatra (Gottschalck

et al. 2013). Anomalous equatorial westerlies were observed during YOTC and DYNAMO to impinge upon Sumatra when cyclonic wake vortices were evident off of Sumatras tips, which preceded the detachment and westward propagation of the wake vortices, and eventual development into tropical cyclones. The MJO, other convectively coupled waves, and environmental variations may have conspired to make wake vortex production and tropical cyclone development off Sumatra more probable.

2.3. Topographic Effects on Flow

Topography may affect or force flow by many different mechanisms, generating impacts that range in scale from local orographic flows to planetary scale Rossby waves (Baines 1997). Mountainous obstacles may block flow or force it upwards. Flow blocking may produce along-mountain jets, or wake vortices if the obstacle is isolated (Baines 1997). Shunting flow upwards assists condensation and enhances precipitation on the windward side, and may provide an impetus for atmospheric waves, such as gravity waves (Clark and Peltier 1977). For mountainous islands or coastal landmasses, afternoon sea breezes flow inwards and upslope, and contribute to precipitation maxima on the slopes of the mountains (Mahrer and Pielke 1977). Flow over topography may result in an air mass sinking adiabatically or super-adiabatically on the lee side and lead to windstorms with differing characteristics (Klemp and Lilly 1975). There are potential vorticity (PV) implications for flow that is forced upwards as well, and thus multiple paths for flow to gain vorticity as it encounters topography (Thorpe et al. 1993). This research will address flow blocking and splitting around the mountainous island of Sumatra, which under easterly flow regimes may lead to counter-rotating, cyclonic wake vortices that in both hemispheres. Near Sumatra, sea breezes, mountain circulations, outflow from a pronounced daily cycle of convection, and

wake vortices may all interact and increase the complexity of flow characteristics (e. g. Mori et al. 2004; Qian 2008; Wu et al. 2009). Several cases were observed in the YOTC and DYNAMO campaigns where wake vortices from Sumatra developed into tropical cyclones.

2.3.1. Flow Blocking and Splitting Due to Topography. Flow is more likely to be blocked or split by a mountainous obstacle when the Froude number, a measure of wind speed u to stratification in the flow (N, the Brunt-Väisälä frequency) and the height of the obstacle h, is less than one (Smolarkiewicz and Rotunno 1989).

$$Fr = \frac{U}{Nh} \tag{1}$$

That the flow be stratified, or statically stable, is crucial to flow past an obstacle resulting in wake effects and vorticity downstream of the obstacle, as a homogenous air mass impinging upon an obstruction does not produce lasting vorticity (Schär and Smith 1993a).

The Froude number in (1) is not the only metric that decides whether flow splitting or blocking occurs. A horizontal aspect ratio (β) between the obstacles height and length determines a critical height, below which flow is blocked or split, above which flow overtops the obstacle (Epifanio 2003). A non-dimensional mountain height (ϵ), which is the inverse of the Froude number, describes the amplitude and nature of the disturbance that the mountain exerts on the flow Fig. 2.4 (Epifanio 2003). For a low-amplitude non-dimensional height, meaning low flow speed, a short obstacle, or weak static stability, gravity waves will be preferentially generated, as seen in the phase space in Fig. 2.4 (Epifanio 2003). Wave breaking may occur for slightly higher obstacles, or faster flow speeds (Fig. 2.4). For larger non-dimensional heights-tall obstacles, extremely stratified flow, or fast flow speeds-flow splitting and lee vortex formation are preferred (Fig. 2.4) (Epifanio 2003).

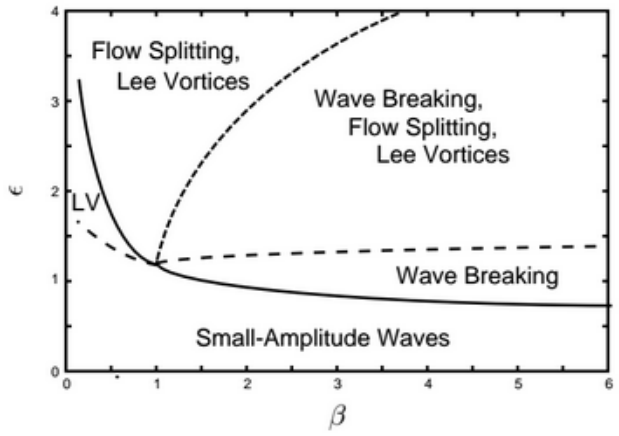

FIGURE 2.4. The phenomena that occur to hydrostatic flow encountering an isolated obstacle for values of non-dimensional mountain heights (ϵ) and horizontal aspect ratios between the length and width of the barrier (β). From Epifanio (2003).

There are several mechanisms by which flow may acquire vorticity while flowing around or over a mountainous obstruction. Linear theory suggests that friction impacts a viscous boundary layer in the homogenous air mass that is incident upon an obstacle, and that a pressure gradient forms at the impact point on the cylinder, inducing the fluid boundary layer to separate from the obstacle and advect that vorticity into the free fluid layer (Smith 1979). Simulations involving a stratified air mass incident upon an obstacle with a free-slip boundary condition, and hence no friction, run by Smolarkiewicz and Rotunno (1989), still demonstrated lee vortex formation, shown in Fig. 2.5.

Smolarkiewicz and Rotunno (1989) note that no wake vortices formed when Fr<0.1 or Fr>0.5, and thus boundary layer separation may still be responsible for forming lee vortices under those conditions. Isentropes, lines of constant potential temperature, deflect upwards on the upstream side of the obstacle, and deform downwards on the downstream side of the obstacle, baroclinically generating horizontal vorticity which is then tilted into the vertical

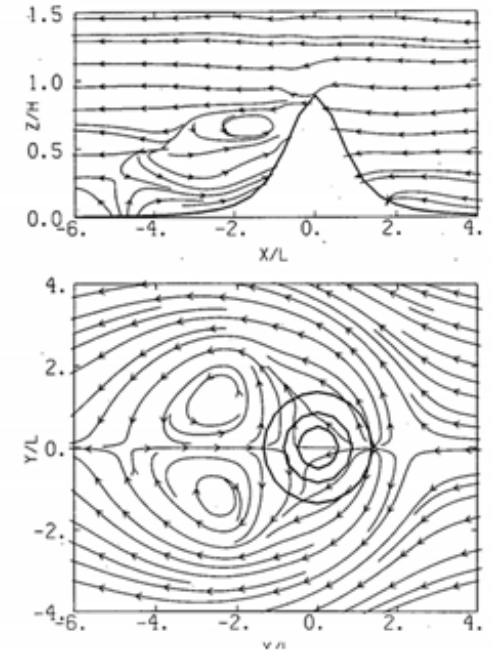

FIGURE 2.5. Vertical cross-section (top) and plan view (bottom) of streamlines around an isolated obstacle. Counter-rotating wake vortices are evident. From Smolarkiewicz and Rotunno (1989).

(Smolarkiewicz and Rotunno 1989). This requires potential vorticity q to be conserved as in (2), which may not always be the case in regions of wave breaking. (Smith 1989).

Potential vorticity conservation is also invoked in a popular theory for lee cyclone generation, wherein isentropes forced upwards on the windward side of an obstacle decrease the height H of the layer, which requires compensation from the relative vorticity term ζ, as seen in the shallow-water potential vorticity equation (2) and Fig. 2.6 (Holton 2004).

$$\frac{Dq}{Dt} = 0, \text{where } q = \frac{\zeta + f}{H} \tag{2}$$

In the case of easterly flow over a mountain range, such as that seen in the tropics where trade easterlies encounter a mountainous island, and illustrated in Fig. 2.6, the air parcel diverts equatorward. In returning to its original trajectory and the column expanding, it

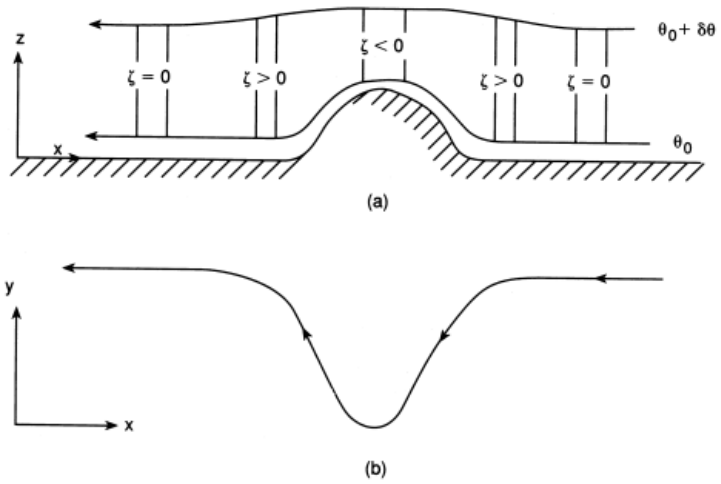

FIGURE 2.6. An idealized cross-section (top) and plan view (bottom) of layer height and changes in absolute vorticity and parcel path as easterly flow moves over an obstacle. From Holton (2004).

acquires cyclonic vorticity, which leads to reduced pressure and a lee cyclone in the area (Smith 1982).

Hydraulic jumps are posited to be another source of vorticity in flows impinging upon an obstacle (Schär and Smith 1993a). Hydraulic jumps are nonlinear events that occur when flow descending a mountainous obstacle encounters a lower-velocity environmental flow, converting kinetic energy into potential energy (Houghton and Kasahara 1968). The boundary layer and the air mass above it decouple, and the free air layer abruptly rises as it gains potential energy, creating a shock or discontinuity, seen in Fig. 2.7 (Houghton and Kasahara 1968).

Dissipation in the region of the hydraulic jump reduces the local Bernoulli function B in equation (5), creating a gradient in Bernoulli function values between the hydraulic jump and its surroundings (Schär and Smith 1993a). In equation (4), a gradient in Bernoulli function is related to vorticity flux J, oriented perpendicular to the flow (Schär and Smith 1993a). In equation (3), it is evident that if J is non-zero, then the relative vorticity time-tendency term

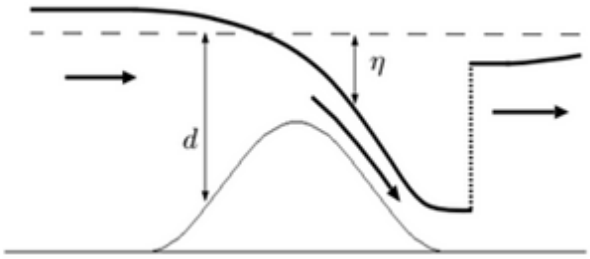

FIGURE 2.7. Idealized shallow-water flow over an obstacle, through a hydraulic jump. A discontinuity is indicated with the dotted line. From Epifanio (2003).

must also be non-zero, as vertical vorticity (ζ) is being produced along the streamlines that separate the hydraulically altered flow from flow that was split by the obstacle. Through the generation of relative vorticity and the jump in layer height, PV is also produced, not conserved, in hydraulic jumps.

$$\frac{\partial \zeta}{\partial t} + \nabla J = 0 \tag{3}$$

$$J = \zeta u = \hat{\mathbf{k}} \times (\nabla B + \frac{\partial \mathbf{u}}{\partial t}) \tag{4}$$

$$B = \frac{u^2}{2} + g\eta \tag{5}$$

Generation of vertical vorticity in flow undergoing a hydraulic jump via gradients in the Bernoulli function is illustrated in Fig. 2.8.

Counter-rotating wake vortices may sometimes detach from their parent mountain and propagate downstream in a periodic pattern. These wake vortex streets are often observed by satellites downstream of islands in regions of endemic oceanic stratus decks (Etling 1989). If flow overtops the obstacle and hydraulic jumps occur, potential vorticity is formed via the

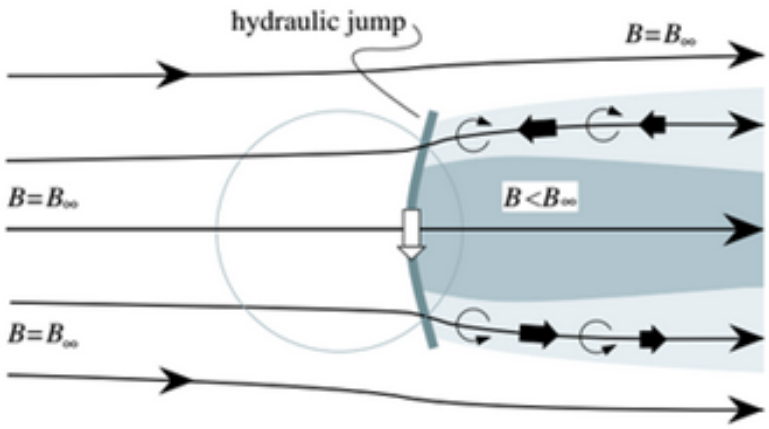

FIGURE 2.8. Cyclonic and anticyclonic vorticity production as flow undergoes a hydraulic jump downstream of an obstacle. Shading indicates a reduced Bernoulli function value. From Schär and Smith (1993a).

Bernoulli function gradient, as demonstrated in equations (3), (4), and (5), and Fig. 2.8 (Schär and Smith 1993a). If the wake is strong enough such that reverse flow separates the two vortices, shear increases, fluids with different Bernoulli function values are joined at the topography itself (Fig. 2.8), and the lee vortices will become susceptible to barotropic instability (Pierrehumbert 1984). The wake may then elongate and undulate, becoming asymmetric, and transitioning to a vortex-shedding state within the order of hours (Schär and Durran 1997). It has been shown that vorticity may be produced baroclinically, in the absence of friction, and it follows that vortex shedding may then occur regardless of the viscosity of the fluid (Etling 1989). That being said, vorticity generation in the boundary layer via friction and the advection of that vorticity into the mean flow, may still contribute to vortex formation when Fr<0.1 and Fr>0.5, and thus viscosity should be considered (Smolarkiewicz and Rotunno 1989). Also, elongated wakes are more prevalent in regimes with low viscosity, and are more prone to barotropic instability, which may instigate wake vortex shedding (Schär and Smith 1993b). The mechanics of vortex shedding discussed here may

be applicable to determining why lee vortices formed off Sumatra's northern and southern tips either persist attached to the landmass, or propagate westward.

2.3.2. Topographic Impacts on Tropical Cyclones. One necessary but not sufficient condition for tropical cyclogenesis is enhanced low-level vorticity (Gray 1968). This research examines counter-rotating, cyclonic wake vortices formed in both hemispheres by flow blocking or splitting near Sumatra, which in some cases underwent tropical cyclogenesis. This phenomenon of flow splitting and cross-equatorial twin tropical cyclones near Sumatra was most frequently observed during the October to December months in two separate periods of data, from 1966 to 1967 and 1976 to 1977 (Kuettner 1989). Cyclone tracks from those years show several pairs of tropical cyclones forming concurrently in the eastern Indian Ocean, west of Sumatra, on opposite sides of the equator, and propagating westward (Kuettner 1989). Observations taken during the October to December period in the region near Sumatra support the existence of counter-rotating wake vortices that are cyclonic in both hemispheres, as seen in Fig. 2.9 (Kuettner 1989).

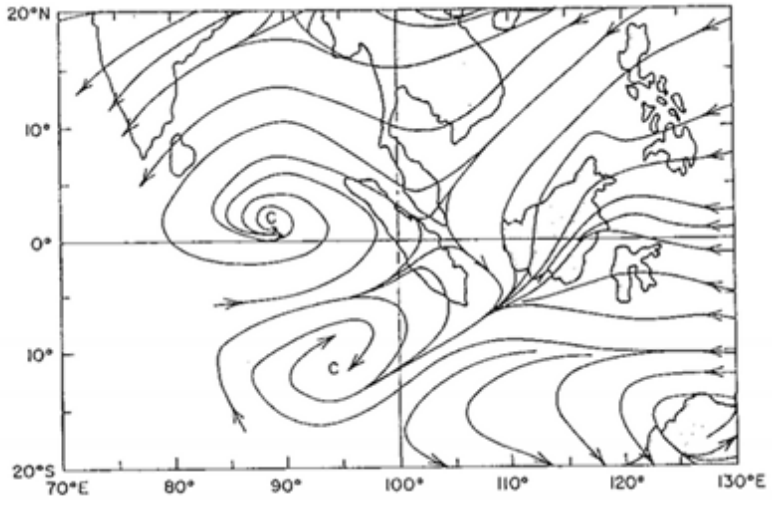

Figure 2.9. 850 hPa streamline analysis on 20 December 1978 from observations made during the MONEX (Monsoon Experiment) field campaign. From Kuettner (1989).

October to December, the most prolific months for cyclonic wake vortex production from Sumatra, lie within the monsoon transition period. Deep easterly flow regimes dominate near Sumatra in the shoulder seasons, from October to December, and May to June, between the summer monsoon, when low-level westerlies and upper-level easterlies prevail, and the winter monsoon, when the opposite circulation is seen; monsoonal flow creates vertical shear, which may inhibit tropical cyclogenesis (Kuettner 1989).

Other studies have been conducted to analyze the contribution of topography to tropical cyclogenesis in cyclone regions with upstream topography, such as the eastern Pacific Ocean. African Easterly Waves (AEWs), which propagate eastward from Africa and feature enhanced precipitation and cyclonic circulation on one side of the wave axis, and suppressed and anticyclonic conditions on the other, have been identified as one of the main contributors to eastern Pacific tropical cyclogenesis (Avila and Pasch 1992). These AEWs cross over Mexico and Central America, and the southwest-northeast oriented Sierra Madre, and mostly east-west oriented Central American mountain ranges, to reach the eastern Pacific Ocean (Farfán and Zehnder 1997). In simulations and several observed cases, prior to the AEW in question reaching the isthmus formed by Mexico and Central America, a northeasterly jet formed along the south side of the Sierra Madre due at least partially to flow blocking (Farfán and Zehnder 1997). A cyclonic vorticity maximum formed downstream of the mountains; this, along with the northward advection of vorticity from Intertropical Convergence Zone (ITCZ) instabilities into the lee cyclone region, contributed to higher cyclonic vorticity in the eastern Pacific (Zehnder et al. 1999). The AEW then passed through the region, increasing moisture and upward motion over the cyclonic vorticity maximum, leading to tropical cyclogenesis (Zehnder et al. 1999). While African Easterly Waves do not occur in the vicinity of Sumatra, orography does contribute to a cyclonic vorticity maximum during

easterly wind periods downstream of Sumatra, in close proximity to the ITCZ, which may contribute to tropical cyclogenesis, as in the studies discussed here.

The role of topography in modifying the track and intensity of extant tropical cyclones has also been examined. Tropical cyclones approaching mountainous islands, such as Taiwan, Hispaniola, and the Phillipines, have been observed to move cyclonically around the northern sides of the islands (Brand and Blelloch 1973; Wang 1980). Under the appropriate conditions, wake vortices form downstream of the island in question. The low-level TC circulation is blocked on the windward side of the island, but the upper-level TC circulation diverts to the north of the island, as expected from PV conservation arguments, then rejoins with the topographically-induced low level cyclonic vorticity on the lee side of the island (Wei-Jen Chang 1982). Propagation speed increases as the tropical cyclone approaches the obstruction, and tangential wind speed is shown to weaken during and after the cyclones passage over the mountains (Wei-Jen Chang 1982; Bender et al. 1987). While this study is primarily concerned with the impacts of Sumatra's topography upon tropical cyclogenesis, many of the processes that affect TC propagation near mountainous obstacles are pertinent to tropical cyclogenesis downstream of topography as well.

2.4. Summary of Background Information

The relevant literature pertaining to the Madden Julian Oscillation, topographic effects on the flow, and their applications to tropical cyclogenesis, has been discussed. In summary:

(1) Anomalous surface easterlies precede the active phase of the MJO (e. g., Madden and Julian 1971, 1972). Enhanced surface convergence, divergence aloft, and high atmospheric moisture levels accompany the MJO convective envelope.

(2) Easterly flow impinging upon Sumatra could acquire cyclonic relative vorticity and produce a wake vortex by several different mechanisms, including flow splitting for blocked flow (e. g., Epifanio 2003), or potential vorticity conservation for flow that overtops the obstacle (e. g., Thorpe et al. 1993).

(3) Wake vortices have been shown to contribute to tropical cyclogenesis downstream of Sumatra (Kuettner 1989) and in other basins as well (Farfán and Zehnder 1997). In the case of Sumatra, orographic effects on easterly flow may produce cyclonic counter-rotating wake vortices, which can develop into twin tropical cyclones on either side of the equator (Kuettner 1989).

(4) Tropical cyclogenesis occurs most frequently in the southern and northern Indian Oceans in transition periods between the summer and winter monsoons, as strong vertical shear regimes discourage tropical cyclogenesis in the Indian Ocean when monsoonal flow is well established (Gray 1968). Cyclonic wake vortices and twin tropical cyclones have been observed to emanate away from Sumatra and westward into the Indian Ocean between October to December, during the transition period between the summer and winter monsoon (Kuettner 1989).

(5) Convectively coupled wave modes, including equatorial Rossby and Kelvin waves, have been linked to tropical cyclogenesis in the Indian Ocean basin via enhancing low level vorticity or reduce vertical wind shear (e. g., Frank and Roundy 2006; Bessafi and Wheeler 2006). Convectively coupled waves occur more frequently in the vicinity of the active MJO (Schreck et al. 2012).

(6) The MJO itself may also locally modulate tropical cyclone activity when its convective envelope is present in an ocean basin, via producing large, cyclonic Rossby

gyres (Ferreira et al. 1996) or enhancing divergence aloft and making the environment more favorable for tropical cyclogenesis (Liebmann et al. 1994).

CHAPTER 3

Data and Methods

3.1. Data

This research primarily uses the operational analysis (OA) dataset from the European Center for Medium-range Weather Forecasting (ECMWF) for the YOTC period, 1MAY2008 to 30APR2010, and the DYNAMO period, 1OCT2011 to 31DEC2011. The data are available at 18 pressure levels between the surface and 50 hPa, at a spatial resolution of 0.25°, every 6 hours. The OA dataset was generated by the Integrated Forecast System, a component of ECMWF's global model, computed at an enhanced resolution (Ling et al. 2014). In the case of DYNAMO, the model ingested the myriad of observational data from the various DYNAMO observing platforms, including soundings conducted up to eight times a day, shipboard measurements, and aircraft data from 13 research flights during different MJO phases (Johnson and Ciesielski 2013). It was estimated that 95 percent of the sounding data from the northern and southern sounding arrays were assimilated and used to make the DYNAMO operational analysis (Ciesielski and Johnson). While the DYNAMO OA dataset represents well many of the convective events that occurred during DYNAMO, it did display some errors and biases, especially in simulating rainfall and heating and drying activity (Ciesielski and Johnson). In the case of the YOTC dataset, real-time data from sources such as satellites and buoys were assimilated into ECMWF's model (Moncrieff et al. 2012). Primarily, this study will emphasize the October to December (OND) periods of YOTC, in order for results to be comparable to data from DYNAMO.

This research used interpolated outgoing longwave radiation (OLR) to identify convectively coupled equatorial waves. Interpolated OLR data was provided by the NOAA/OAR/ESRL

PSD, Boulder, Colorado, USA, from their Web site at `http://www.esrl.noaa.gov/psd/`. The interpolated OLR data featured daily, 1° resolution.

Best track data from the Joint Typhoon Warning Center (JTWC) were used for tropical cyclone tracks and intensities when necessary. However, the majority of this study focuses on the genesis phase of tropical cyclones and precursor wake vortices, often before the JTWC began to monitor a tropical disturbance, and this study does not analyze systems once they are classified as tropical storms with windspeeds over 35 kt.

3.2. Methods

When referring to the environmental conditions surrounding a pre-tropical cyclogenesis wake vortex, environmental conditions are evaluated in a 10°x10° square box, centered on the wake vortex. The positions of the wake vortices were determined manually, using daily-averaged plan views of wind vectors and geopotential height anomalies. The wake vortex was not removed from the variable fields before analysis, but the weak storms, by definition less than 35 knots, and large reach of the analysis box should lessen the impact of the wake vortex upon the average of a variable within the analysis box. When plotting or calculating anomalies of geopotential height, sea surface temperatures, midlevel moisture (specific humidity between 300-700 hPa), or other variables, anomalies are found by differencing data at some point and time with a seasonal mean (that is, OND2008, OND2009, or OND2011) between 3-7°N or 3-7°S, depending on the hemisphere in which the vortex resides, and 35-120°E, the approximate longitudinal extent of the Indian Ocean basin. Partitioning the data by season and hemisphere is intended to account for any interseasonal and interhemispheric variability that may bias a mean in one direction or another.

To evaluate topographic effects on the flow near Sumatra, zonal wind was examined where easterly wind would impinge upon the island, and relative vorticity was evaluated downstream to capture any topographic effects on the flow. Henceforth, measuring zonal wind incident upon northern Sumatra at 100°E, from 3-7°N, and finding relative vorticity downstream of Sumatra, between 3-7°N and 90-100°E, will be referred to as "Region N" for simplicity. For southern Sumatra, zonal wind will be calculated at 105°E, from 3-7°S, and relative vorticity will be determined between 3-7°S and 95-105°E; these measurement regions will collectively be called "Region S". Regions N and S are depicted in Fig. 3.1.

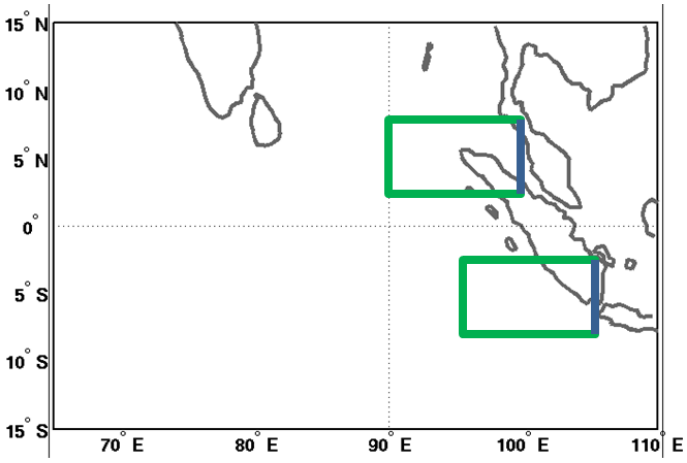

FIGURE 3.1. Analysis Region N is shown near northern Sumatra, where zonal wind is analyzed at the blue line (100°E, 3-7°N) and relative vorticity is analyzed in the green region (90-100°E, 3-7°N). Region S is shown near southern Sumatra, where zonal wind is analyzed at 105°E, 3-7°S, and relative vorticity is analyzed in the region from 95-105°S, 3-7°S.

Extending the latitude band beyond the 3-7°N or 3-7°S range diminishes or erases entirely the enhanced cyclonic vorticity signature that is evident near Sumatra during easterly wind periods, and instead captures just large-scale environmental flow characteristics. Many analyses were performed using daily averages of the 6-hourly data, to reduce influence from the Maritime Continent's pronounced diurnal cycle of convection.

Sumatra is a long, mountainous island that stretches from approximately 6°N to 6°S (Fig. 3.2). Its highest point is 3,805 m, and the mountainous spine averages over 1000 to 1500 m for the length of the island, though these high elevations are confined to a very longitudinally narrow region (Fig. 3.2).

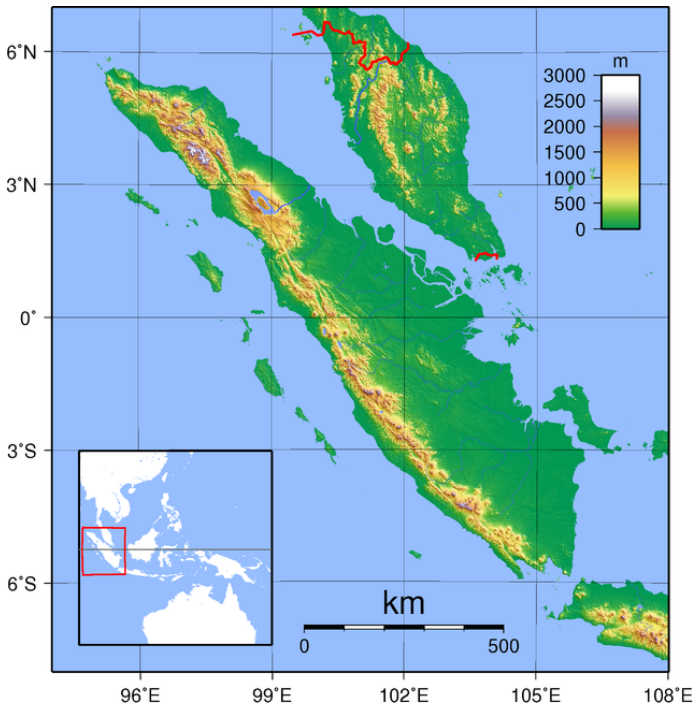

FIGURE 3.2. A topographic map of Sumatra. From wikipedia.org.

Using a 1/16° resolution topographic mesh from the Weather Research and Forecasting (WRF) Model, the average elevation in the region from 3-5°N, 97-99°E is calculated to be 605 m. The average elevation in the region from 3-5°S, 103-105°E was 326 m in the WRF topography. Indeed, the higher mountains of Sumatra are concentrated in the northern tip, while the mountains of the southern tip are lower (Fig. 3.2). Finer resolution topographic data would likely nudge the average calculated elevations at both of Sumatra's tips to be higher. However, an air mass impinging on Sumatra would feel the whole mountain range, not merely the limited areas where elevations exceed 1000 m or 1500 m, and thus the elevation

values of 605 m and 326 m from the WRF topographic data may be usable for determining if flow blocking or splitting is preferred.

When diagnosing convectively coupled equatorial waves, a filter was applied to the NOAA PSD OLR data to select wave types by a prescribed period, equivalent depth, and wavenumber found in OLR anomalies that are distinct from the raw OLR data (K. Straub, 2014, personal communication). The wave characteristics and filtering technique are as in Wheeler and Kiladis (1999) and Wheeler et al. (2000).

CHAPTER 4

Results

This chapter is split into three parts. First, it will be argued that blocking and splitting occur as flow traverses Sumatra and leads to cyclonic vorticity streamers and wake vortices. Second, the propagation of these wake vortices westward from Sumatra will be examined. Results will be presented for the full special observing period during DYNAMO and the following two weeks, comprising the period from 1OCT to 31DEC2011. The 1OCT to 31DEC (henceforth OND) 2008 and 2009 periods of YOTC will be emphasized in order for results to be comparable between YOTC and DYNAMO. Third, three case studies involving cross-equatorial tropical cyclone pairs will be detailed. Two of the tropical cyclone pairs occurred during the YOTC campaign in October 2008 and December 2009, respectively, and one of the tropical cyclone pairs formed during the DYNAMO field campaign from late November to early December 2011.

4.1. Topographic Effects on Flow near Sumatra

Sumatra's length may be roughly estimated as 1200 km, as it is approximately 12 latitudinal degrees long. Using the rounded elevation value at Sumatra's southern tip from the WRF topographic mesh, discussed in section 3.2, of 300m, which is more representative of the whole island, the horizontal aspect ratio β is calculated to be $\approx$4. Then, according to Fig. 2.4, a Froude number ($1/\epsilon$) less than 0.7 would favor flow splitting and lee vortex formation downstream of Sumatra.

Froude numbers were calculated for OND 2008, 2009, and 2011 for all easterly wind days. The flow regime was determined by the direction of zonal wind averaged in Region N or Region S. Zonal wind and static stability were considered as an averaged layer between

1000 and 850 hPa for the northern tip of Sumatra, as 850 hPa is approximately the height of the topography there. For the southern tip of Sumatra, a 1000 to 900 hPa layer was used for all variables. The Brunt–Väisälä frequency or static stability, in the area just upstream of Sumatra in the same location as the zonal wind, was assessed for each easterly wind day and averaged throughout the layers mentioned above.

TABLE 4.1. The mean of Froude numbers calculated for easterly wind days at Sumatra's northern and southern tips. Froude numbers calculated for a 1000 to 850 hPa layer, from 3-7°N at 100°E (Region N), for Sumatras northern tip, and 1000 to 900 hPa layer, from 3-7°S at 105°E (Region S), for Sumatra's southern tip.

Froude No.	Northern Sumatra	Southern Sumatra
OND2008	0.37	0.89
OND2009	0.48	0.9
OND2011	0.46	0.59

In Table 4.1, it is evident that Froude numbers were lower and therefore more favorable for flow blocking and splitting near Sumatra's northern tip when zonal wind was easterly. The southern tip demonstrated slightly higher static stability during all three time periods than did the air masses flowing onto the northern tip of Sumatra. In addition, topography in the south of the island is dramatically lower than the northern topography, which may have permitted more air to flow over the southern mountains, rather than around the southern tip of the island. A preference for air to flow over the southern tip of Sumatra, rather than around it, could have led to more frequent hydraulic jumps, gravity waves, or cyclonic vorticity generation via the conservation of potential vorticity. Froude numbers fluctuated wildly in the other seasons of YOTC, as flow characteristics, direction, and strength varied with the summer and winter monsoons.

A positive vorticity streamer and cyclonic wake vortex are visible west of Sumatra's northern tip for OND2009 in Fig. 4.1a, for composite easterly flow conditions at Sumatra.

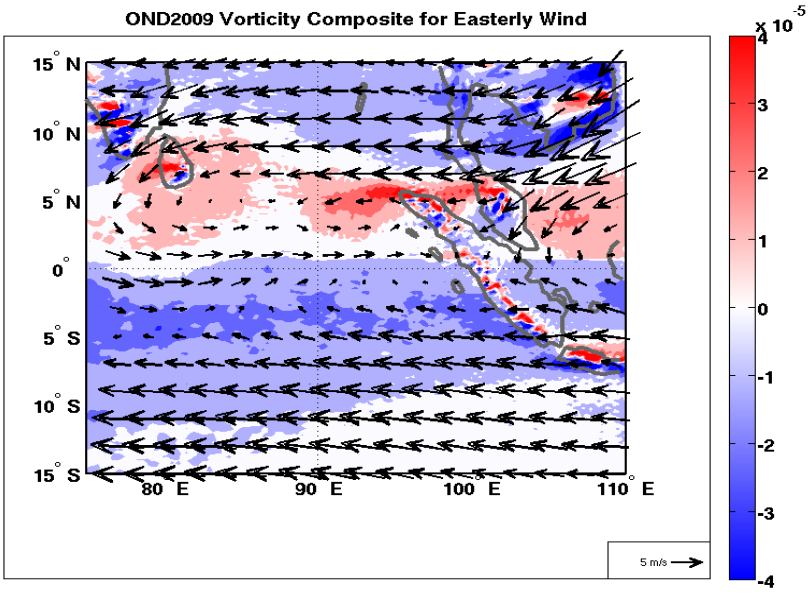

(A)

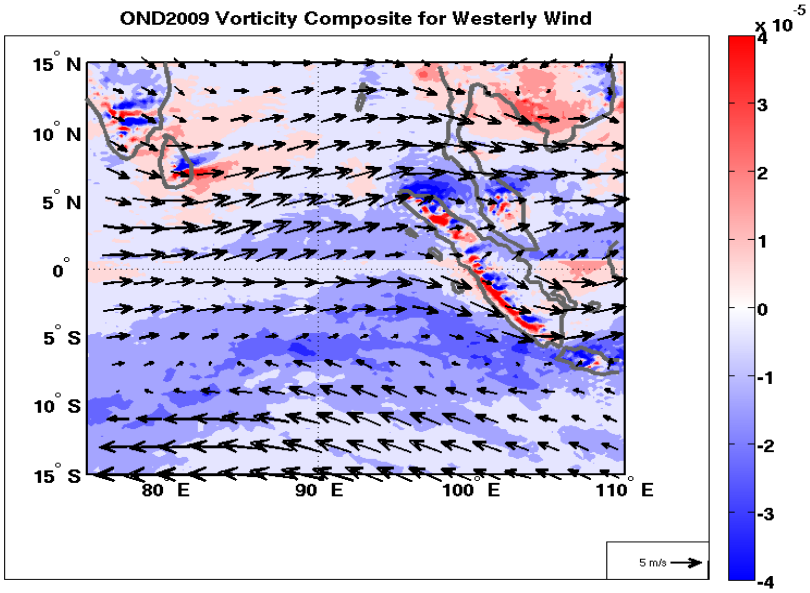

(B)

FIGURE 4.1. Composite plan views of the scaled 850 hPa flow field and relative vorticity during OND2009 for all top, a) easterly and bottom, b) westerly wind days, as determined by the zonal wind incident upon Sumatra in Regions N and S. The easterly wind days and composites are determined separately for each hemisphere, but plotted together. The reference vector in the bottom right of each plot represents 5 m s^{-1}.

The range of wind speeds that would be blocked on any given day depends on the environmental conditions, as described by the Froude number. Easterly winds stronger than 5

m s^{-1} in certain instances produced cyclonic vorticity streamers, but a less distinct wake vortex pattern in the flow field, or no discernible wake vortex at all (not shown). What may be a Rossby gyre in the wake of the active MJO event observed in early November 2009, or could alternately be a wake vortex generated by Sri Lanka's topography, and accompanying equatorial westerly anomalies, are apparent to the south of the Indian Subcontinent in Fig. 4.1a. A negative vorticity streamer is visible to the east of Sumatra in Fig. 4.1b, when flow is westerly upon Sumatra. For both easterly and westerly flow regimes, negative (cyclonic) vorticity extended far to the west of southern Sumatra, in the monsoon trough zone where equatorial westerlies met poleward trade easterlies.

The composite plan views of wind vectors and relative vorticity appear roughly the same for OND2008 and OND2011 (not shown), though the blocking of easterly flow by southern Sumatra appeared more pronounced in OND2011 in both the northward deflection of wind vectors and an area of cyclonic vorticity downstream. It is worth noting that, while correlations between zonal wind and relative vorticity were weak or insignificant at 700 hPa, as will be discussed later, wake vortex and positive vorticity signatures were still evident at 700 hPa (not shown) when all easterly wind times are composited together.

Upon examination of composite wind and relative vorticity fields as in Fig. 4.1, a persistent trough-like pattern emerges south of the equator in the Indian Ocean, wherein equatorial westerlies border trade easterlies farther to the south and create shear and a strip of cyclonic vorticity. Near the Maritime Continent, such a trough in surface flow could be related to the monsoons- a monsoon trough- while in the central Indian Ocean, a trough in surface flow would likely be associated with the ITCZ. These equatorial westerlies divert southward in close proximity to Sumatra, so flow blocking of westerly wind by the center of the island,

where the topography is more pronounced than near the southern tip of the island, is possible. Because Sumatra is diagonally oriented, stretching from northwest to southeast, the magnitude of flow diversion to the south would be greater, and produce more cyclonic vorticity, but production of cyclonic vorticity by westerly flow blocking to the north could also occur. However, if westerly flow is indeed blocked by Sumatra and deflected southwards, the computation box used to compare zonal wind and relative vorticity near Sumatra's southern tip (Region S) would not be ideal for capturing this effect. The monsoon trough or ITCZ wind pattern appeared in all three OND time periods, and seem to be endemic to the southern Indian Ocean during the austral spring, coinciding with or preceding the onset of the Australasian monsoon.

Geopotential height falls are visible within the cyclonic wake vortex present off Sumatra's northern tip when flow is easterly in Fig. 4.2a, which depicts the same flow fields as in Fig. 4.1, with superimposed geopotential height anomalies. In Fig. 4.2a, geopotential height falls are more broadly distributed in the southern Indian Ocean when flow is easterly upon southern Sumatra. This may be due to the monsoon trough-like circulation near Sumatra, or to persistent ITCZ-related convection and rainfall that was concentrated south of the equator during OND2009 (Fig. 4.3), as well as during OND2008 and OND2011. Double ITCZ patterns have been noted in the wake of the active MJO, and there was an active MJO event that crossed Sumatra's latitude in November 2009, but in the northern hemisphere the geopotential height falls appear largely dominated by wake vortex location (Johnson and Ciesielski 2013). Though a cyclonic circulation is present when westerly flow is incident upon southern Sumatra in Fig. 4.2b, the geopotential height falls in the center of that vortex are not as notable.

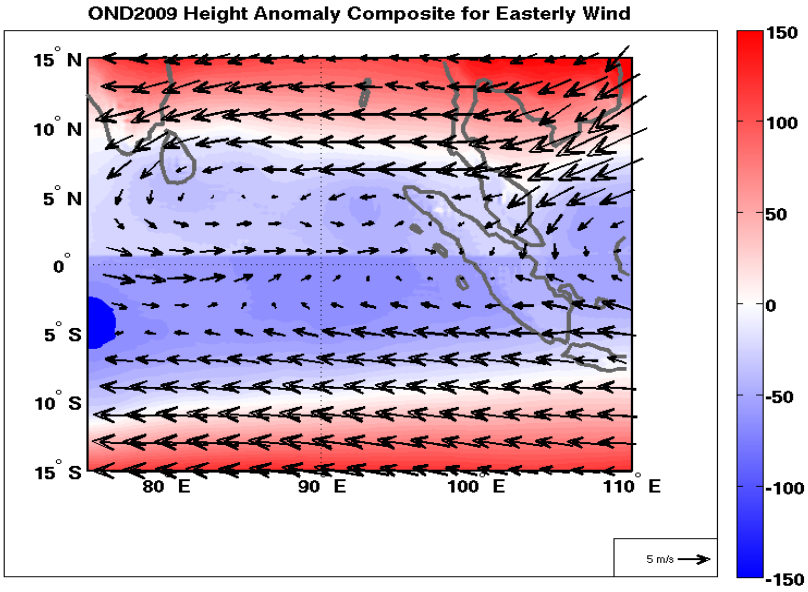

(A)

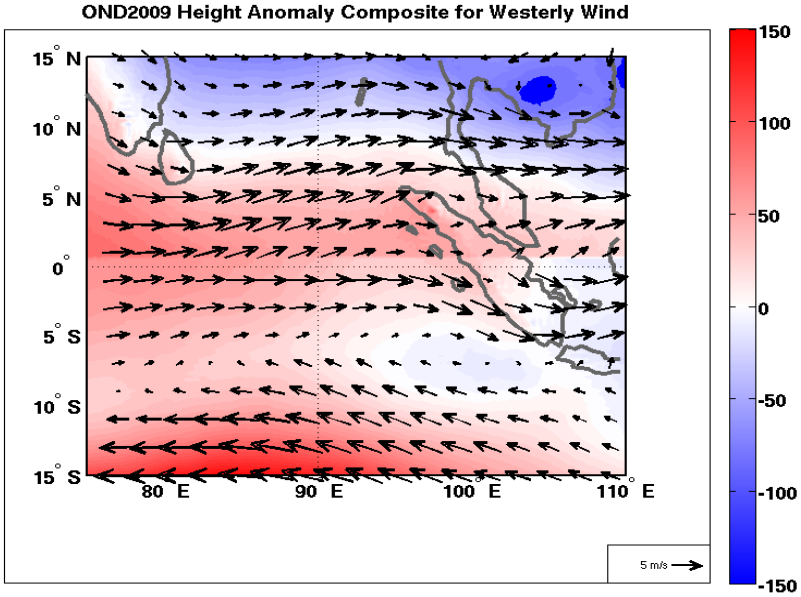

(B)

FIGURE 4.2. Composite plan views of the scaled 850 hPa flow field and geopotential height anomalies during OND2009 for all top, a) easterly and bottom, b) westerly wind days, as determined by the zonal wind incident upon Sumatra in Regions N and S. The geopotential height anomalies were calculated separately for each hemisphere as the difference from a 3-7°N or 3-7°S, Indian Ocean-wide geopotential height mean during OND2009. Slight discontinuities appear along the equator because the easterly wind days and composites are determined separately for each hemisphere, but plotted together. The reference vector in the bottom right of each plot represents 5 m s^{-1}.

Plotting the spatial distribution of rainfall as in Fig. 4.3 reveals frequent and heavy rainfall south of the equator in OND2009, which is attributed to the ITCZ that has migrated southwards towards the summer hemisphere. This pattern was consistent throughout OND2008 and OND2011 as well. The heavy rainfall situated directly on southern Sumatra's west coast has been shown in other studies to be at least partially attributable to interaction between sea breezes, orographic flows, and a strong diurnal cycle of convection (Wu et al. 2009). There is also a rainfall maximum on the mountainous island of Borneo in Fig. 4.3, likely related to similar flow interactions.

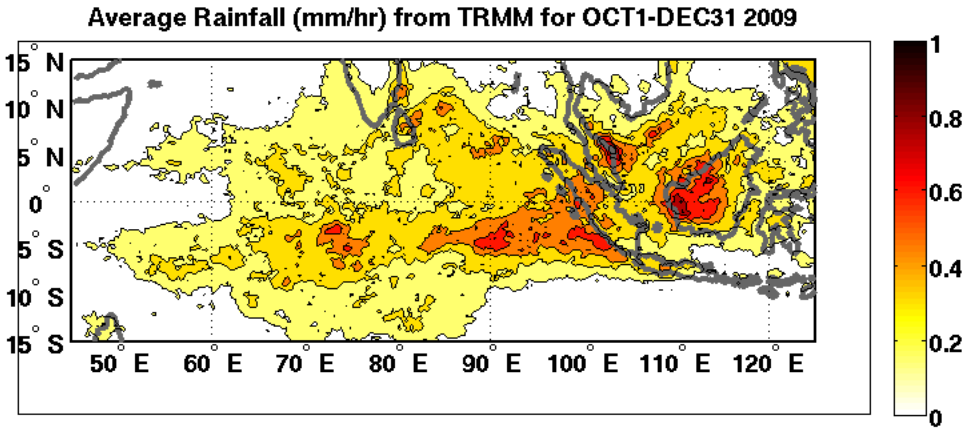

FIGURE 4.3. Averaged rainfall (mm/hr) for OND2009 from the Tropical Rainfall Measurement Mission (TRMM) satellite. Warm colors indicate heavier rain rates.

When using rainfall data with higher temporal resolution (e.g., 3-hourly data), it is possible to stratify these times by the zonal wind direction incident upon Sumatra's tips. Then, periods that experienced an active MJO event (OND2009, OND2011) recorded a large amount of rainfall near Sumatra's northern tip, and south of the Bay of Bengal, when wind was westerly (not shown); this is likely related to the MJO's active envelope, which was accompanied by strong low-level westerly wind, moving into the area. The rainfall

maximum south of the equator was apparent in both the westerly and easterly flow regimes and dominates the overall composite in Fig. 4.3.

Whether the flow splits or surmounts an obstacle, cyclonic vorticity may be generated via several mechanisms, as discussed earlier. To better quantify the relationship between zonal wind and relative vorticity downstream of Sumatra, relative vorticity was linearly regressed onto zonal wind, where both variables were averaged to a daily temporal resolution within Regions N and S.

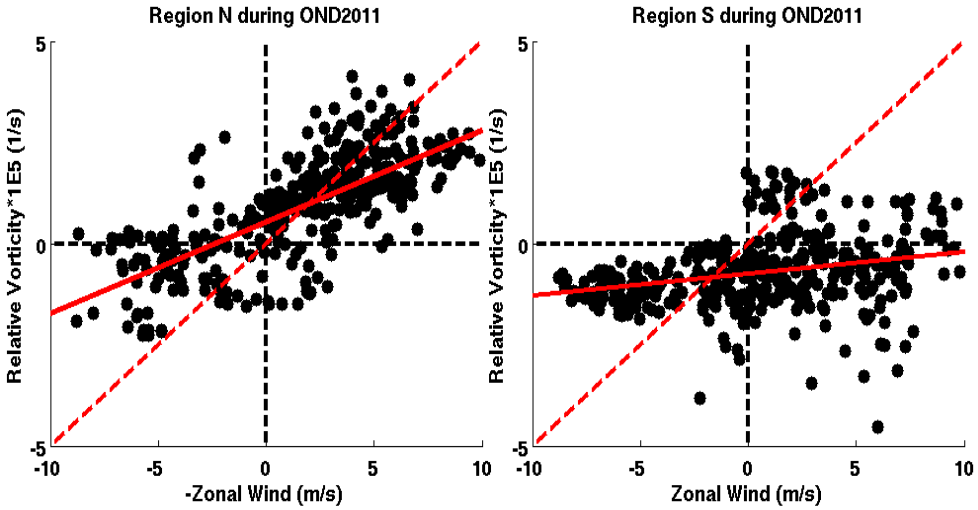

FIGURE 4.4. Relative vorticity regressed onto zonal wind during OND2011, for left, a) Sumatra's northern tip, where variables are averaged within Region N, and right, b) Sumatra's southern tip, where variables are averaged within Region S. Each data point consists of a concurrent relative vorticity and zonal wind value. In a), negative zonal wind is plotted; easterly wind is plotted as positive. The red dashed line indicates where R^2=1; the red solid line is a least-squares fit to the data.

Though only results at 850 hPa are plotted in Fig. 4.4, negative (easterly) zonal wind and positive (cyclonic) relative vorticity were highly significantly correlated (R^2>0.8, P<<0.01) near Sumatra's northern tip for the 1000 to 850 hPa layer during OND2011. The levels 1000, 925, and 850 hPa are all likely impacted by Sumatra's topography. Note the tighter

distribution of relative vorticity and zonal wind when wind is easterly and vorticity is positive in Fig. 4.4a; the relationship becomes more scattered for westerly winds. This finding may be related to the fact that the computation box is centered upstream of Sumatra, not downstream, with regard to westerly flow. The strong relationship between zonal wind and relative vorticity in Region N also held for OND2008 and OND2009, during YOTC (not shown), when zonal wind and relative vorticity were also highly correlated between 1000 hPa and 850 hPa near Sumatra's northern tip (R^2>0.7, P<<0.01). Between 1000 and 850 hPa, for all three time periods, zonal wind at northern Sumatra led relative vorticity downstream by an average of 3-4 days (not shown). A lag between the maximum easterly flow past the northern tip of Sumatra and the vorticity downstream makes physical sense; namely, it is expected that it takes time for the wake vortex to develop and move into the analysis region downstream in Region N. Correlations were middling to insignificant at 700 hPa for the three time periods, which demonstrates that topographic impacts on vorticity diminished as one moved above the height of Sumatra's topography.

Correlations between zonal wind and relative vorticity slightly improved in OND2009 and OND2011 by $R^2 \approx 0.05$ compared to OND2008. One contributing factor may have been the presence of MJO active events in November 2009, October 2011, and November 2011, while there was no distinguishable MJO activity during OND2008. Preceding the passage of the MJO and Kelvin wave convective envelope in November 2009 and October and November 2011, anomalous easterlies incident upon Sumatra's northern tip may have been blocked and formed cyclonic wake vortices; anomalously strong westerlies, including westerly wind bursts, would have accompanied the active envelope, and generated an anticyclonic wake vortex and negative vorticity to the east of Sumatra's northern tip. An active MJO event did not occur in OND2008 to precipitate such flow and vorticity anomalies.

The relationship between zonal wind and relative vorticity was less clear at Sumatra's southern tip (Fig. 4.4b). In OND2011, zonal wind and relative vorticity were moderately correlated (R^2>0.4, P<<0.01) for the 1000 and 925 hPa pressure levels, which are situated within the height of southern Sumatra's mountains. In OND2008 and 2009 (shown in Fig. 4.4b), the relationship between zonal wind and relative vorticity was only weakly significant at 1000 hPa (R^2>0.3, P<0.01), and was insignificant at higher pressure levels. Lead-lag relationships between zonal wind and relative vorticity were difficult to discern and were often insignificant. Mean relative vorticity west of Sumatra's southern tip was negative, or cyclonic, for all three OND time periods, though zonal wind varied in direction.

There is a potential disparity in production or sustainment mechanisms for cyclonic vorticity streamers between Sumatra's northern tip, where wake vortices are apparent, and its southern tip, where flow blocking, stretching and tilting of an atmospheric column by ITCZ convection, or a monsoon trough-like structure, or a combination, may be responsible. Despite this, it will be demonstrated that relative vorticity in both regions was most cyclonic at the approximate height of Sumatra's topography during easterly flow periods.

Vertical profiles of relative vorticity and zonal wind, assessed in Regions N and S, during easterly wind days show prominent maxima of cyclonic relative vorticity around the level of Sumatra's topography for OND2008, OND2009, and OND2011 (Fig. 4.5). In both analysis regions, cyclonic relative vorticity was concentrated in the lower troposphere despite the fact that zonal wind increased with height (Fig. 4.5). During OND2011 in Region N (Fig. 4.5a), the peak positive relative vorticity occurred between 850 and 900 hPa, which encompasses the mountain heights in northern Sumatra, for 50% of all days, and most easterly wind days. In Region S during OND2011 (Fig. 4.5b), relative vorticity was most cyclonic between 925 and 950 hPa for 40% of all days.

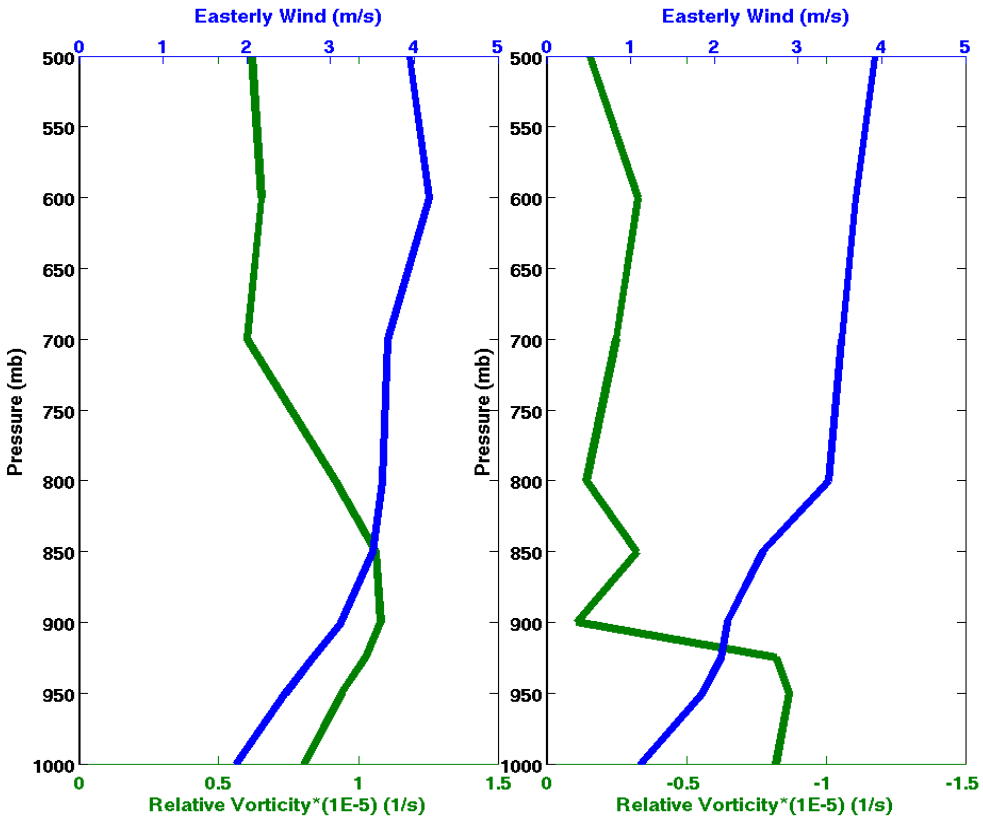

FIGURE 4.5. Composited vertical profiles of zonal wind (blue) and relative vorticity (green) with height during OND2011, where relative vorticity and zonal wind were daily averaged in left, a) Region N and right, b) Region S, when wind was identified as easterly in Regions N or S.

Vertical profiles for Sumatra's northern and southern tips during OND2008 and OND2009 (not shown) resembled those in Fig. 4.5, though the magnitude of cyclonic vorticity during OND2008 was reduced, and the sharpness of the maximum was less pronounced. As in the DYNAMO (OND2011) data, positive relative vorticity near northern Sumatra for OND2009 was concentrated around the topography height; the maximum was found between 850 and 900 hPa on 38% of all days and most easterly wind days. Near southern Sumatra during OND2009, 54% of cyclonic relative vorticity maxima occurred between 925 and 950 hPa. For OND2008, cyclonic relative vorticity maxima were found between 850 and 900 hPa for northern Sumatra less frequently, on only 30% of days, but the southern hemisphere

continued to display a strong signal, with 51% of vorticity maxima located in the 925 to 950 hPa range.

Near northern Sumatra, the low-level maxima in cyclonic relative vorticity appeared attributable to topographic interference with the flow, while distinguishing the cause for cyclonic relative vorticity near southern Sumatra was more difficult. However, it is worth noting that, in composites of all westerly wind days near southern Sumatra for OND2009 and OND2011, the mean relative vorticity profile was negative (cyclonic) but relatively constant with height, and does not display a prominent cyclonic maximum at the topography height (not shown).

In summary, it has been shown that zonal wind and relative vorticity near Sumatra's northern tip were significantly correlated during OND2008, OND2009, and OND2010 up to the mean height of much of Sumatra's topography, approximately 850 hPa. Zonal wind led relative vorticity by 3-4 days, and positive relative vorticity and a wake vortex pattern were visible downstream when easterly wind impinged upon northern Sumatra. In contrast, zonal wind and relative vorticity were weakly or insignificantly correlated near Sumatra's southern tip. Cyclonic relative vorticity, which may be related to ITCZ convection or a monsoon trough, stretched across much of the southern Indian Ocean regardless of the flow characteristics near southern Sumatra. If flow blocking of equatorial westerly wind by central Sumatra were a contributing factor to the long-lasting cyclonic vorticity near southern Sumatra, it would not be readily apparent when analyzing zonal wind and relative vorticity within Region S. Further research would be needed to explore this relationship. Cyclonic relative vorticity maxima occurred most frequently in the pressure levels corresponding approximately to the height of Sumatra's topography for both the northern and southern tips during OND2008, OND2009, and OND2011.

4.2. Wake Vortex Propagation

The wake vortices portrayed in the previous section have been observed to propagate westward into the Indian Ocean basin, where some of them then underwent tropical cyclogenesis. During the two-year YOTC period, 62.5% of positive vorticity streamers at 1000, 925, or 850 hPa, near Sumatra's northern tip (specifically, from 3-7°N at 90°E) that exceeded an empirically determined threshold of 1.6E-5 s^{-1} occurred in the October-December timeframe. The threshold was calculated to reduce noise and erroneous vorticity streamer identification while still retaining the signatures of objectively stronger vorticity streamers.

The preponderance of cyclonic vorticity streamers between October and December of each year is likely because the flow regime is transitioning from summer to winter monsoonal flow; in this shoulder season, flow is easterly throughout much of the troposphere. The principally easterly wind east of Sumatra and multiple vorticity streamers during OND2008 may be seen in Fig. 4.6. During the winter (summer) monsoons, strong easterly (westerly) flow dominates at the surface, and flow is sheared aloft. Several vorticity streamers were also noted from March to April of 2009 and 2010, again during the monsoon transition period (not shown). Climatologically, the northern Indian Ocean experiences a maximum in tropical cyclogenesis in October and November, with a smaller peak in May and June (Schreck et al. 2012). Within the YOTC and DYNAMO periods, it shall be shown, all of the tropical cyclones that spun out of wake vortex precursors emanating from northern Sumatra formed between October and December of each year.

Near Sumatra's southern tip (specifically, from 3-7°S at 95°E), 61% of cyclonic vorticity streamers at either 925 or 1000 hPa with absolute magnitudes greater than 1.6E-5 s^{-1} occurred between October and December 2008 and 2009. The vorticity streamers for OND2008 near southern Sumatra are shown in Fig. 4.6b. More cyclonic vorticity streamers

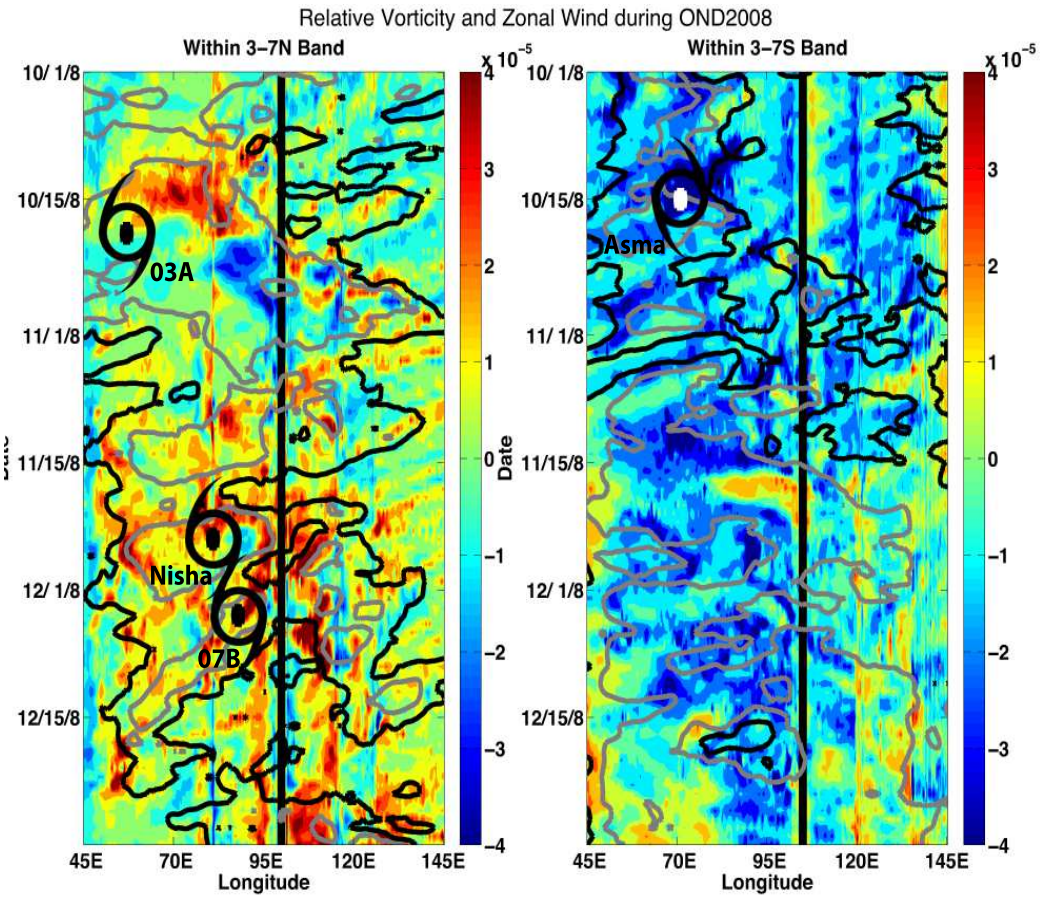

FIGURE 4.6. Longitude vs. time Hovmöller diagrams for OND2008 of 850 hPa daily-averaged relative vorticity (colored) and zonal wind (contoured) for an average at all longitude points between a) 3-7°N and b) 3-7°S. Contours are 2.5 m s^{-1} for zonal wind. Solid gray contours indicate westerly wind, and solid black contours indicate easterly wind. The longitudes and days at which wake vortices reached tropical storm strength are marked by tropical storm symbols. The approximate position of Sumatra is marked by the black line. TCs may move out of the latitude band being averaged and plotted, which may account for apparent discrepancies between the "end" of a vorticity streamer and the location of tropical cyclogenesis.

propagated westward from southern Sumatra from March to May (boreal spring) than were seen near northern Sumatra, possibly due to the differing onset dates and characteristics of the Australian, Indian, and southeast Asian monsoons. Climatologically, tropical cyclogenesis is preferred in a broad timespan between November and May in the southern Indian Ocean (Bessafi and Wheeler 2006). Tropical cyclones related to flow blocking or splitting

near southern Sumatra during the YOTC and DYNAMO campaigns were noted during the months of October through March.

When flow incident upon Sumatra was easterly, multiple wake vortices often formed and detached from Sumatra in succession; the period between streamers during these clusters of activity averaged three days. The impetus for these wake vortices to separate from Sumatra with a three day periodicity is unknown. Studies of vortex shedding indicate a variety of possible mechanisms for this phenomenon (Etling 1989). Such a concentration of positive potential vorticity near the equator may be inherently unstable, as the meridional gradient of potential vorticity would then be reversed from its usual orientation, low at the equator and higher towards the poles (Ferreira and Schubert 1997). In several cases, anomalous equatorial westerlies impacting the center of Sumatra led to counter-rotating wake vortices disengaging from Sumatra and moving westward; one such case, which led to Tropical Cyclone Gael (01S) in early February of 2009, is shown in Fig. 4.7.

In the case of the wake vortex precursor to TC Gael, easterly winds preceding the passage of the MJO convective envelope generated wake vortices. What appeared to be a westerly wind burst raced outwards along the equator and is visible in Fig. 4.7a. Its impact with Sumatra coincided with the detachment of the wake vortex that would become TC Gael (in Fig. 4.7a). It is possible that subsequent interaction between the wake vortex and MJO-related convection, which were in close proximity to one another in Fig. 4.7b, influenced the wake vortex's eventual intensification into a tropical cyclone on 2FEB2009. OND2008 in Fig. 4.1 did not experience an active MJO event, so westerly wind bursts from the MJO active phase could not have generated anomalous westerlies in that instance. Return flow from the counter-rotating wake vortices themselves, if the circulations are mostly closed, could have also provided westerly flow along the equator.

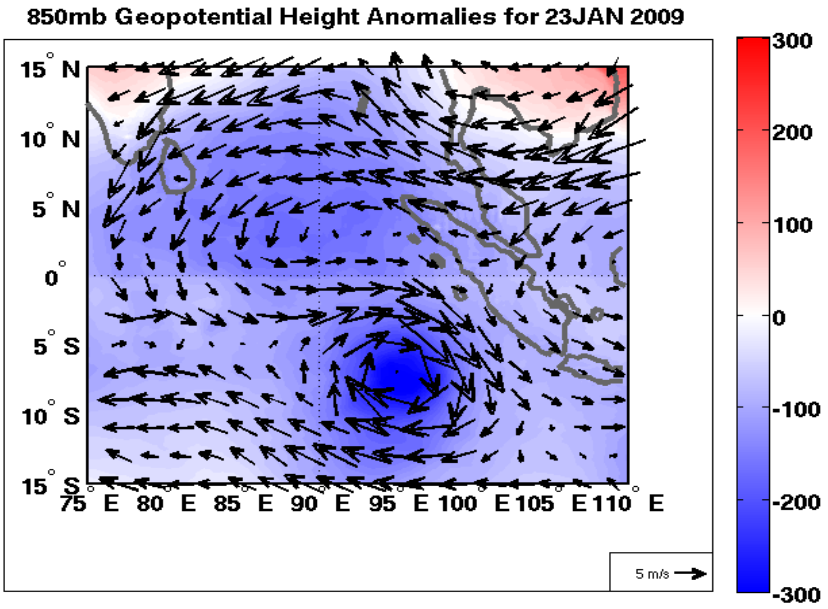

(A)

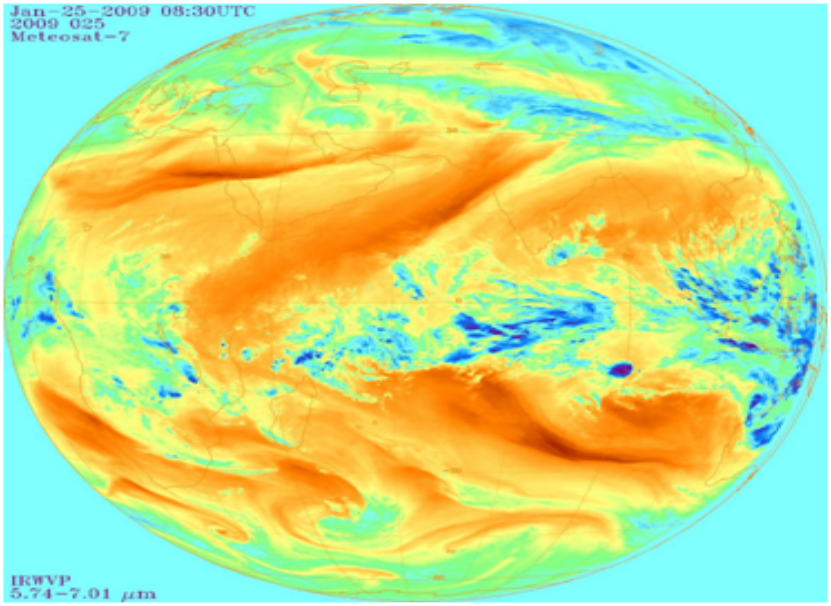

(B)

FIGURE 4.7. (a) Plan view of 850 hPa scaled wind vectors and geopotential height anomalies for 23JAN2009, showing the wake vortex precursor to TC Gael south of the equator. The geopotential height anomalies were calculated separately for each hemisphere as the difference from a 3-7°N or 3-7°S, Indian Ocean-wide (35-120°E) geopotential height mean during DJF2008-2009, then plotted together. b) Meteosat-7 water vapor satellite imagery at 0830Z on 25JAN2009, showing the wake vortex precursor to TC Gael (the concentrated moist area right of and below center) and the MJO convective envelope along the equator. Cooler colors indicate more moisture, and warmer colors indicate drier air.

Convectively coupled waves that bring westerly winds at the surface, such as equatorial Rossby waves, may be another possible source of strong westerlies on the equator. Kelvin waves, which are accompanied by surface easterlies, may be a cause for anomalous easterlies and lead to cyclonic wake vortices on Sumatra's tips, even in the absence of an MJO event. Both Kelvin and equatorial Rossby waves were noted during the YOTC and DYNAMO campaigns, both as isolated events and embedded within the MJO convective envelope (Waliser et al. 2012; Gottschalck et al. 2013).

Eleven tropical cyclones during the YOTC period, and a further two tropical cyclones during the DYNAMO campaign, were subjectively identified as being related to topographic deformation of the flow near Sumatra. The tracks of these TCs are shown in Fig. 4.8. More than three-quarters (ten) of these tropical cyclones occurred during OND2008, OND2009, or OND2011 when flow splitting and cyclonic, counter-rotating wake vortex generation are most frequent near northern Sumatra. The other three tropical cyclones, all in the southern Indian Ocean, formed between January and March of 2009 and 2010, months which exhibited a secondary maximum in cyclonic vorticity streamer frequency near southern Sumatra.

In Fig. 4.8a, TC Asma is the more northerly of the two southern Indian Ocean tropical cyclones that stemmed from Sumatran wake vortices during the 2008 to 2009 season, and brushed the northern tip of Madagascar. TC 03A is depicted in the western Arabian Sea, making landfall in Yemen (Fig. 4.8a). TC Rashmi, which split off from the wake vortex precursor to TC 03A, intensified near the center of the Bay of Bengal (Fig. 4.8a). TC Nisha reached tropical storm strength in the vicinity of Sri Lanka, while TC 07B tracked westward from just downstream of Sumatra's northern tip (Fig. 4.8a). In Fig. 4.6b, TC Asma (01S) is visible streaming off of southern Sumatra in October.

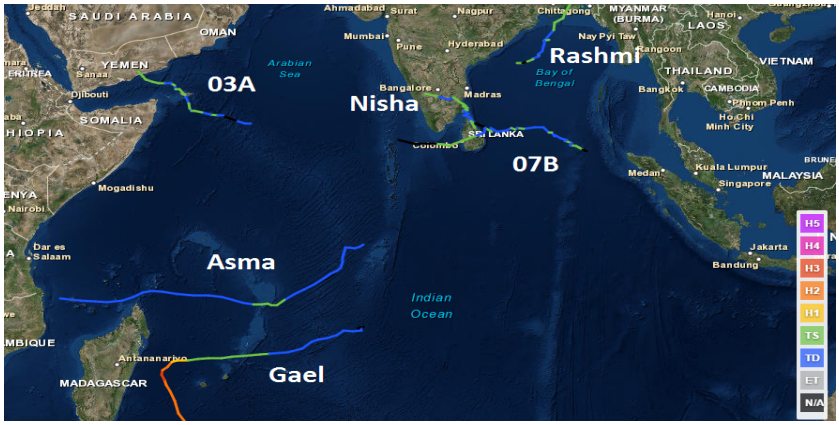

(A)

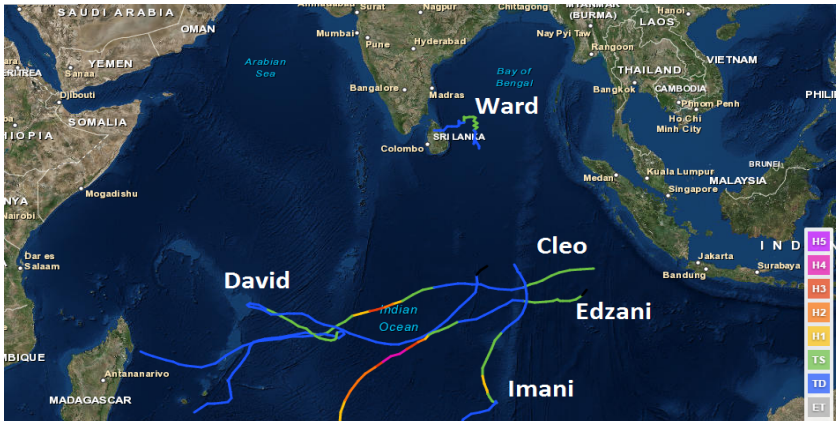

(B)

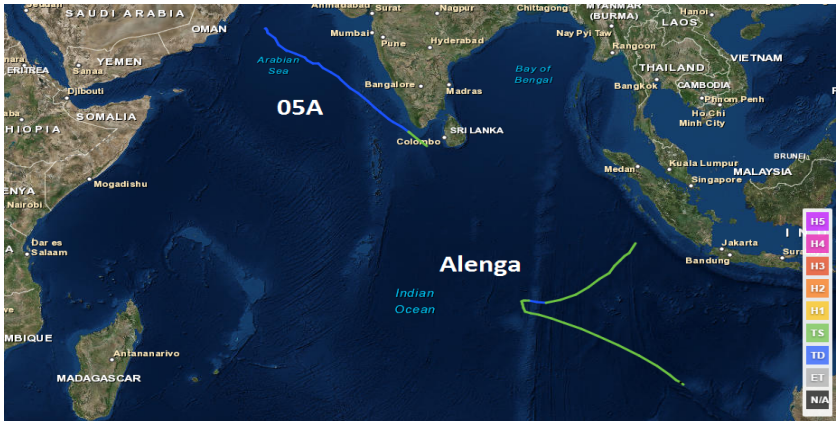

(C)

FIGURE 4.8. Tracks and intensities of tropical cyclones subjectively determined to have formed out of wake vortices generated by Sumatra from a) 1MAY2008 to 30APR2009, b) 1MAY2009 to 30APR2010, and c) 1OCT to 31DEC2011. Track and intensity information are from the International Best Track Archive for Climate Stewardship (IBTrACS). These images generated using the NOAA Historical Hurricane Tracks Viewer at coast.noaa.gov/hurricanes.

In Fig. 4.6a, the wake vortices which became TCs 03A and Rashmi (04B) in October 2008, Nisha (06B) in late November, and 07B in early December, are also apparent as cyclonic vorticity streamers moving westward from Sumatra. TC Gael is not plotted on the Hovmöller diagrams in Fig. 4.6, as it fell outside of the OND2008 time period; it is the southernmost tropical cyclone track in Fig. 4.8a, and also the most intense (120 kt wind speeds) of the tropical cyclones preceded by wake vortices during the late 2008 to early 2009 tropical cyclone season (JTWC 2009).

In Fig. 4.8b, TC Ward (05B) was the lone northern Indian Ocean storm in the late 2009 to early 2010 season; it propagated westward from northern Sumatra and reached tropical storm strength near Sri Lanka. In Fig. 4.8b, TC Cleo (03S) is depicted as the closest track to Sumatra. TC David (05S) achieved tropical storm strength to the west of the two previous storms, then meandered about, even crossing over its previous track twice (Fig. 4.8b). All three tropical cyclones are prominent as vorticity streamers moving westward from Sumatra in early December in Fig. 4.9.

Just to the south of TC Cleo's track is TC Edzani's (07S) track. TC Edzani, in January 2010, was the most intense tropical cyclone to originate from Sumatran wake vortices during the entire YOTC and DYNAMO campaigns; its maximum wind speed was estimated at 140 kt (JTWC 2010). TC Edzani is not plotted in Fig. 4.9, as it existed outside of the OND2009 analysis period. TC Imani was the last wake vortex-related tropical cyclone to form during the YOTC campaign. It propagated westward from Sumatra in mid-March of 2010, then moved almost due south in the south-central Indian Ocean as it intensified into a tropical storm (Fig. 4.8b). TC Imani is also not plotted on the Hovmöller diagrams of relative vorticity and zonal wind in Fig. 4.9, as it did not occur within the months of October to December.

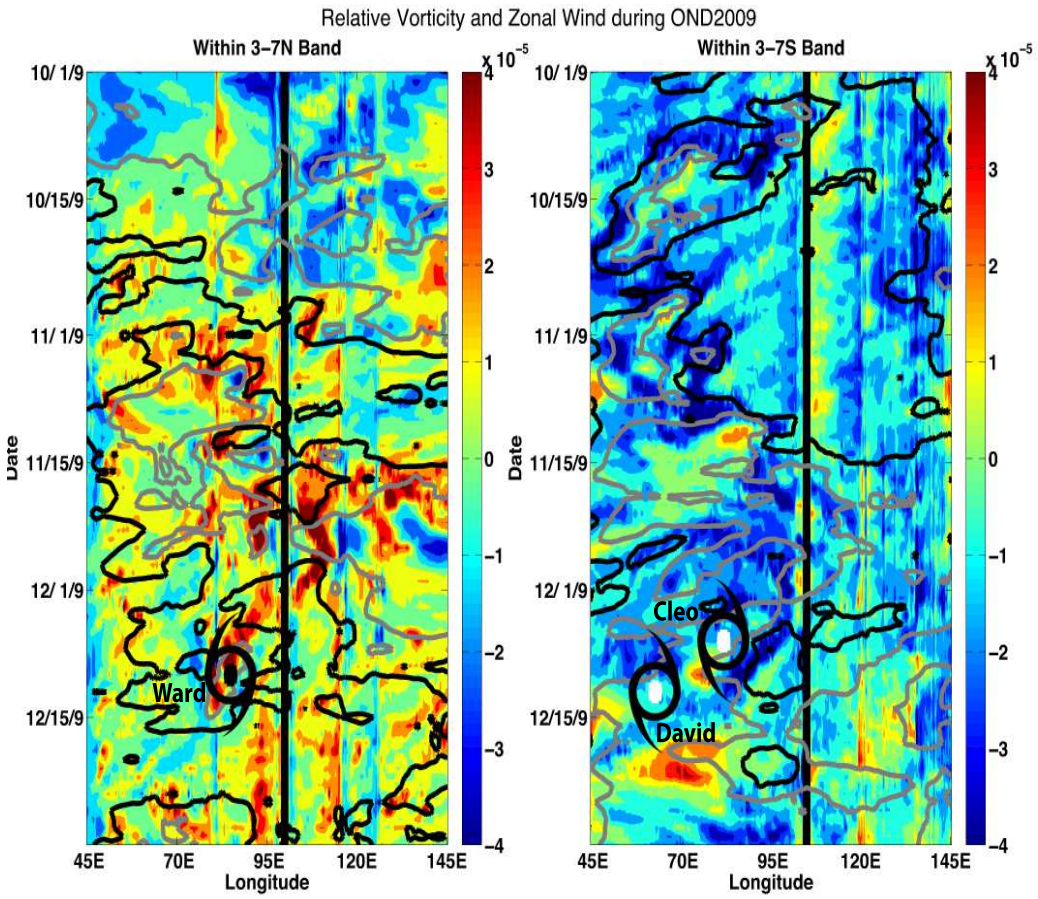

FIGURE 4.9. As in Fig. 4.6, for OND2009.

In Fig. 4.8c, TC 05A is shown tracking northwestward from near Sri Lanka; not shown is the wake vortex transit from Sumatra to Sri Lanka prior to 26NOV2011. TC Alenga is shown spinning up close to Sumatra, moving westward, then recurving later in its life (Fig. 4.8c). In Fig. 4.10a, TC 05A reaches tropical storm strength at the end of a vorticity streamer marked in late November 2011. In Fig. 4.10b, an area of cyclonic vorticity near the line demarcating Sumatra precedes the development of TC Alenga in early December 2011.

Four tropical cyclones, Gael in February 2009, Edzani in January 2010, 05A in November 2011, and Alenga in December 2011, all sprang from wake vortices moving westward from Sumatra and encountered an active MJO envelope at some point in their life cycle. Convectively coupled equatorial Rossby, Kelvin, and mixed Rossby gravity waves were all noted in

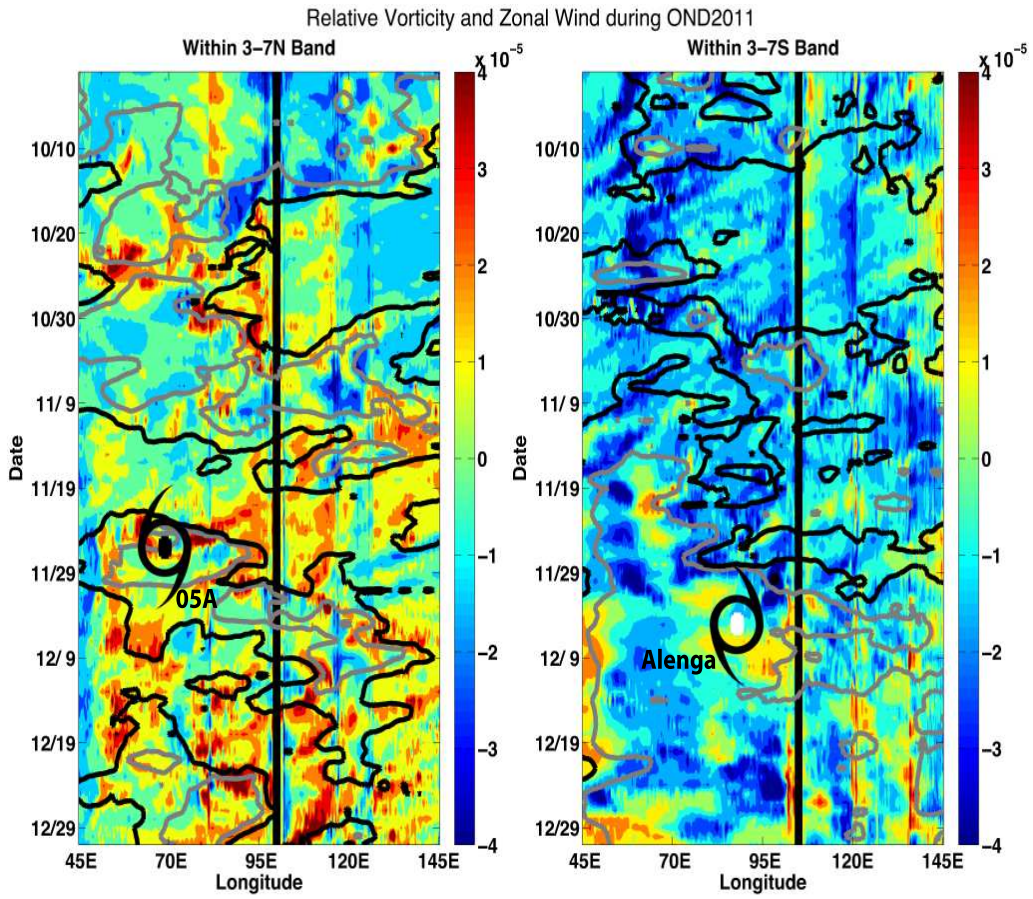

FIGURE 4.10. As in Fig. 4.6, for OND2011.

close proximity to intensifying wake vortices. Three cross-equatorial tropical cyclone pairs or even triplets- Asma and 03A in October 2008 (seen in Figs. 4.6a, 4.6b, and 4.8a), Cleo, Ward, and David in December 2009 (seen in Figs. 4.8b, 4.9a, and 4.9b), and 05A and Alenga in November-December 2011 (seen in Figs. 4.8c, 4.10a, and 4.10b), were observed in all, and will be examined in further detail in section 4.3. On other occasions tropical cyclones developed from wake vortices emanating from one of Sumatra's tips while a counter-rotating, cyclonic wake vortex existed on the other tip, but the second wake vortex dissipated, and thus a cross-equatorial tropical cyclone pair did not form.

4.3. Case Studies

The environmental and dynamic conditions leading to the intensification of three sets of cyclonic, cross-equatorial wake vortices originating from Sumatra will be examined. The analysis of these cases will involve reference to maps of geopotential height anomalies and Hovmöller diagrams of relative vorticity, although owing to space limitations, plan views of the tropical disturbances will be presented for only a few times during their life cycles. Geopotential height anomaly fields are plotted in the plan views instead of relative vorticity fields, because relative vorticity is a somewhat transient feature that may vary as convection appears and causes stretching and tilting, then dies again. The tracks of the tropical cyclone pairs analyzed in this section are shown in Fig. 4.8.

4.3.1. Tropical Cyclones Asma and 03A (October 2008). In 2008, tropical cyclones Asma (01S) and 03A intensified from wake vortices that propagated westward into the Indian Ocean from Sumatra. On 9OCT2008, cyclonic flow curvature of easterly flow around Sumatra's northern and southern tips was visible (not shown).

The western portion of a pre-existing vortex located southeast of Sri Lanka and just south of the equator reinforced anomalous equatorial westerlies, closing the wake vortex circulations on 10OCT (Fig. 4.11a).On 11OCT (not shown), the northern wake vortex separated from Sumatra. Height falls became more prominent as the northern wake vortex and the pre-existing vortex moved westward on 12 OCT, while the wake vortex that had been attached to southern Sumatra dissipated (Fig. 4.11b). The cyclonic vortices appeared to strengthen one another, as the equatorial branches of both vortices provided strong low-level westerly flow (Fig. 4.11b). It is possible that upper-level anticyclonic outflows, evident in Fig. 4.12,

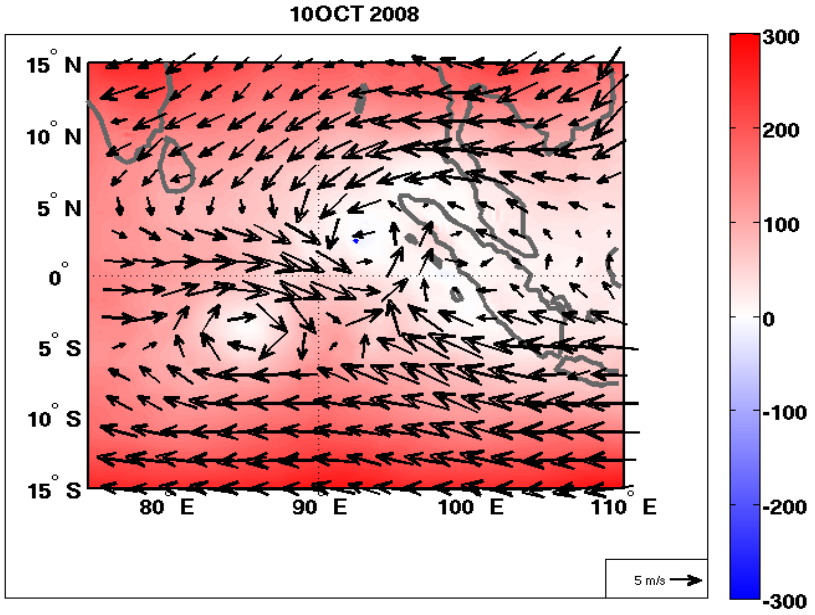

(A)

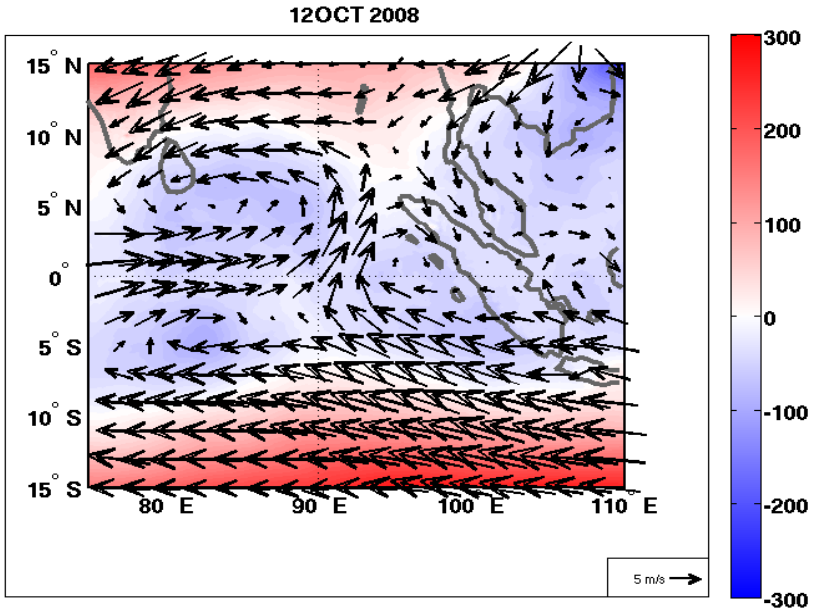

(B)

FIGURE 4.11. Plan view of 850 hPa scaled wind vectors and geopotential height anomalies for top, a) 10OCT2008 and bottom, b) 12OCT2008, showing the wake vortex precursors to TC 03A north of the equator and TC Asma south of the equator. The geopotential height anomalies were calculated separately for each hemisphere as the difference from a 3-7°N or 3-7°S, Indian Ocean-wide (35-120°E) geopotential height mean during OND2008, then plotted together.

in each vortex were mutually advantageous as well; enhanced outflow would lead to greater divergence aloft and promote stronger surface convergence and more efficient convection.

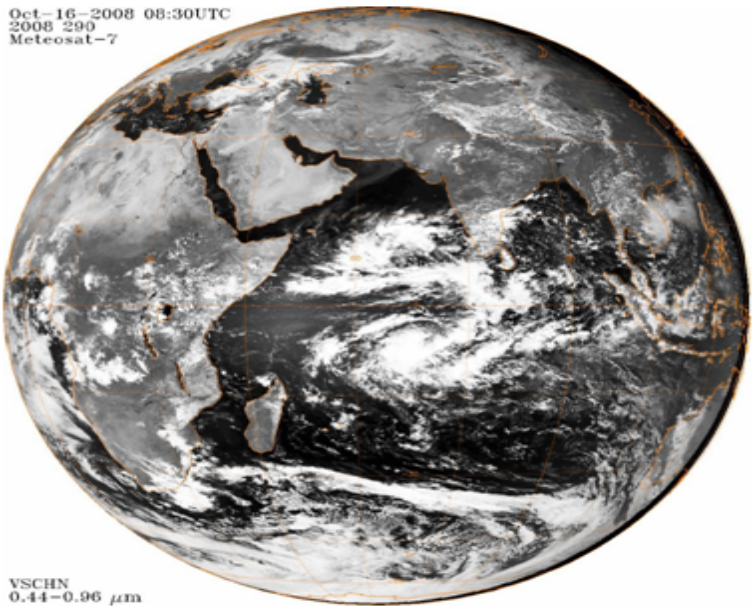

FIGURE 4.12. Meteosat-7 visible satellite imagery at 0830UTC on 16OCT2008, showing Tropical Storm Asma in the southern Indian Ocean, and what would become TC 03A in the Arabian Sea.

As the northern vortex skirted Sri Lanka and moved into the Arabian Sea around 15OCT, a second vortex formed or split from the original vortex near Sri Lanka, possibly due to wave interactions or Sri Lanka's topography (not shown). It is difficult to distinguish any convection related to this new vortex, located south of India, from the cirrus outflow signatures of TCs 03A and Asma in Fig. 4.12. This vortex recurved northeastward into the Bay of Bengal and became Tropical Cyclone Rashmi (04B) on 26OCT2008 (not shown).

Relative vorticity in Region N was maximized at 850 hPa, approximately the level of northern Sumatra's topography, from 9-14OCT 2008, with the exception of 12OCT, when vorticity in the lower levels was weakly negative (Fig. 4.13a). This feature is apparent in Fig. 4.13a prior to 15OCT, just after the vorticity streamer that became TC03A propagated

westward from Sumatra. The wind incident on northern Sumatra shifted from easterly to westerly for 11-12OCT only (visible in Fig. 4.11b), which led to the negative vorticity value in Region N. The average Froude number in OND2008 for Region N under easterly flow was ≈0.4, making conditions favorable for flow splitting, which would lead to cyclonic vorticity in the pressure levels near the height of Sumatra's topography.

In Region S, relative vorticity was most cyclonic at either 925 or 950 hPa, approximately the height of southern Sumatra's mountains, until 15OCT. The OND2008 Froude number in Region S during easterly flow was ≈0.9, and during westerly flow was ≈1, making it difficult to assess whether flow was blocked or traversed the obstacle, which could still produce cyclonic relative vorticity through potential vorticity conservation arguments for easterly flow (Thorpe et al. 1993) or via hydraulic jumps (Schär and Smith 1993a). The Froude number was likely high in Region S due to strong easterly winds, which exceeded 8 m s^{-1} at 850 hPa in mid-October 2008, and the lower topography in southern Sumatra.

The westerly winds that led to the detachment of the wake vortices that developed into TC 03A and TC Asma may have been related to an equatorial Rossby wave that crossed the longitude of Sumatra around the same time, which is shown in Fig. 4.13 as the negative, black contour, which indicates increased cloudiness and convection with equatorial Rossby wave characteristics, around 1OCT.

The low pressure anomalies associated with the convectively coupled phase of an equatorial Rossby wave may have produced anomalous equatorial westerlies that assisted the wake vortices in separating from Sumatra. Equatorial westerlies are visible in Fig. 4.11a on 10OCT, stretching across a large portion of the Indian Ocean. Additionally, two cyclonic circulations on either side of the equator may be related to the equatorial Rossby wave, which could have enhanced cyclonic circulation in the wake vortices. Vertical wind shear

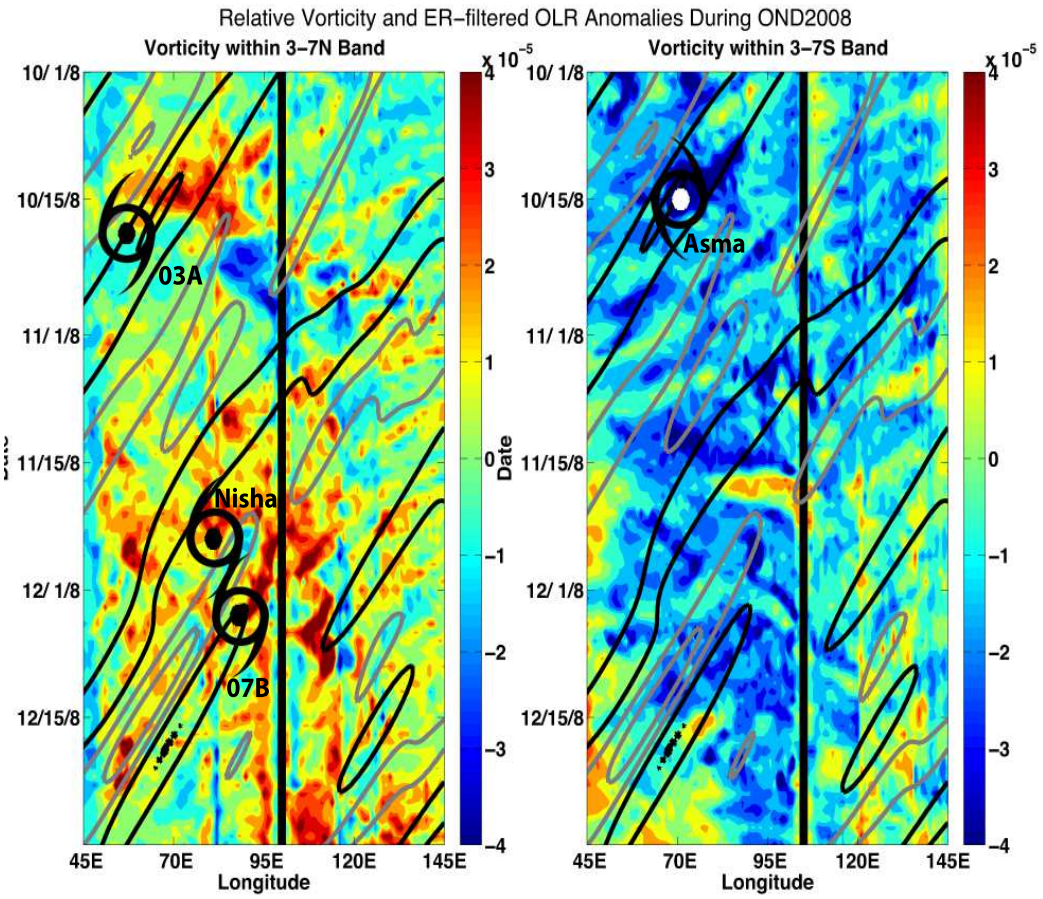

FIGURE 4.13. Longitude vs. time Hovmöller diagrams of 850 hPa daily-averaged relative vorticity (colored) for an average at all longitude points between top, a) 3-7°N and bottom, b) 3-7°S during OND2008. Outgoing longwave radiation (OLR) anomalies (contours) are filtered for equatorial Rossby wave characteristics between 10°S-10°N in both plots. Contours are 5 W m^{-2} and 15 W m^{-2} for OLR anomalies. Solid gray contours indicate positive equatorial Rossby-wave filtered OLR anomalies, and solid black contours indicate negative OLR anomalies (increased cloud cover). The longitudes and days at which wake vortices reached tropical storm strength are marked by tropical storm symbols. The approximate position of Sumatra is marked by the black line. TCs may move out of the latitude band being averaged and plotted, which may account for apparent discrepancies between the end of a vorticity streamer and the location of tropical cyclogenesis.

dropped for several days for both the nascent TC Asma and TC 03A in a period preceding tropical cyclogenesis, though the specific days were different for each vortex (not shown). Vertical wind shear from 850 to 250 hPa around TC Asma's wake vortex precursor decreased

from an average of ≈8 m s^{-1} to ≈5 m s^{-1} after 10OCT (not shown), before the northern wake vortex had even separated from Sumatra. The northern wake vortex experienced relief from moderate (10 m s^{-1}) vertical wind shear after 14OCT (not shown). In Schreck and Molinari (2009), equatorial Rossby waves introduced equatorial westerlies into an area, enhanced low-level cyclonic vorticity, and decreased vertical wind shear to make conditions more favorable for cyclogenesis for three cross-equatorial tropical cyclone pairs in the West Pacific. A similar mechanism may have been operative in the TC 03A and Asma case.

As the wake vortices moved westward, they transitioned from warmer than average sea surface temperatures in the eastern Indian Ocean to a regime of SSTs that were weakly cooler than a seasonal mean (not shown). Both of these cases defied the long-term climatic conditions during YOTC, when the western Indian Ocean was on average ≈0.5°C warmer than the eastern Indian Ocean. That being said, SSTs in the vicinity of the wake vortices were 28°C or greater while the vortices developed (not shown). This sea surface temperature threshold is more than adequate for tropical cyclogenesis, which is a necessary but not sufficient condition for TC genesis (Gray 1968). Both vortices maintained consistently high midlevel (300 to 700 hPa) moisture levels, up to 30% above the OND2008, 35-120°E, 3-7°N or 3-7°S, depending on the hemisphere in which the vortex resided, mean, as they moved from the eastern to western Indian Ocean basin and intensified (not shown).

The diabatic heating in the convection within both wake vortices, located quite close to one another on either side of the equator, may have provided a large enough heating anomaly to initiate a convectively coupled Kelvin wave, which propagated away to the east, as depicted by the negative contours that begin around 15OCT in Fig. 4.14. Even at a lower threshold of wave detection, -5 W m^{-2} (not shown), the Kelvin wave was diagnosed only beginning in the vorticity streamer region.

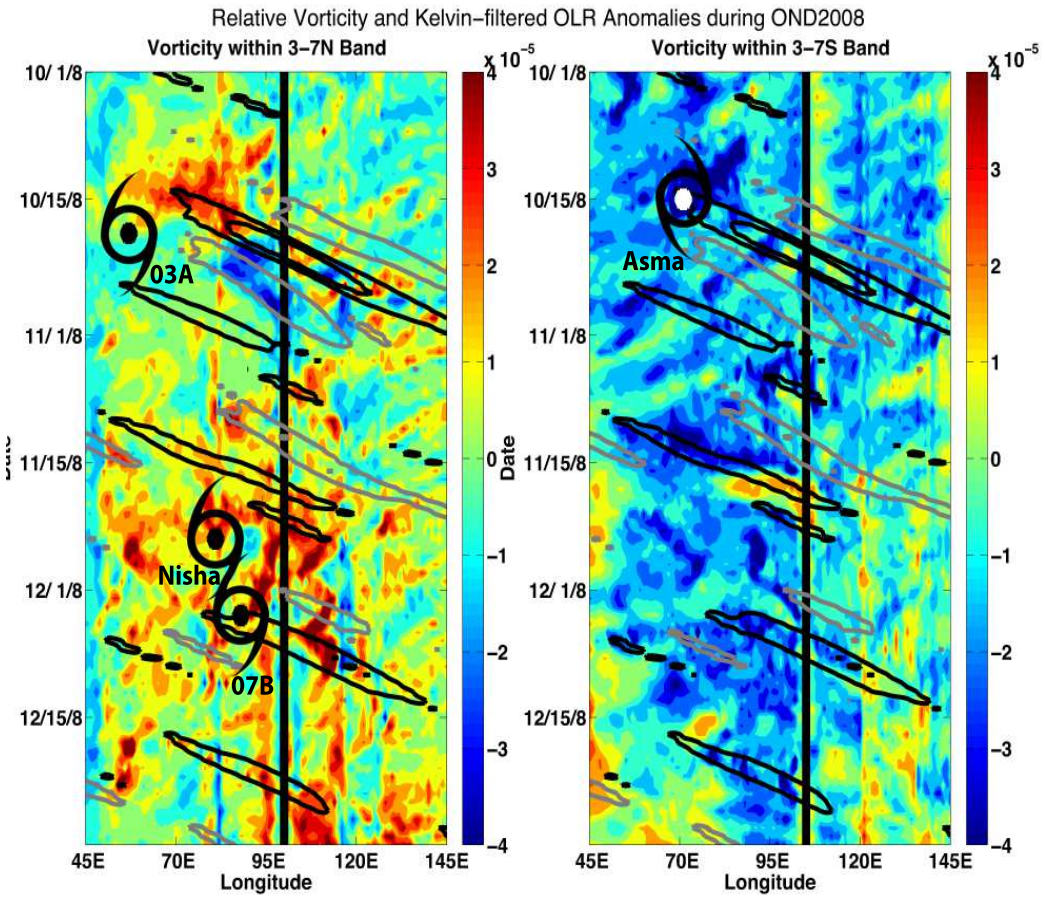

FIGURE 4.14. As in Fig. 4.13, but OLR anomalies are filtered for Kelvin wave characteristics. Contours are 10 W m^{-2} and 20 W m^{-2} for Kelvin wave-filtered OLR anomalies.

In summary, easterly flow curved cyclonically around Sumatra in October 2008, leading to the development of a tropical cyclone pair (or twin tropical cyclones). Anomalous equatorial westerly winds impacted central Sumatra, leading to closed cyclonic wake vortices west of Sumatra's tips on 10OCT. Cyclonic vorticity maxima were located at approximately the height of Sumatra's topography. The equatorial westerlies were partially attributable to a pre-existing cyclonic vortex located south of the equator. Vortex-vortex interactions may have played a role in strengthening the lower level circulation and upper level outflow in both vortices and enabling them to intensify further. An equatorial Rossby wave concurrently

moved through the area and may have induced low-level westerly wind, enhanced low-level vorticity, and reduced vertical wind shear as the wake vortices propagated westward from Sumatra and intensified into tropical storms on 16OCT (TC Asma) and 20OCT (TC 03A). A Kelvin wave was also noted emanating out of the wake vortex path. TC 03A only reached a maximum intensity of 30 kt, just under tropical storm strength, but unleashed torrential rainfall, destroyed over 2000 houses, and killed at least 180 people, with more missing, when it made landfall in Yemen (WHO 2008). TC Asma intensified to 55 kt, then weakened before making landfall and causing flooding in Madagascar (L'Express de Madagascar 2008).

4.3.2. Tropical Cyclones Ward, Cleo, and David (December 2009). Tropical Cyclone Ward (05B) in the northern Indian Ocean, and Tropical Cyclones Cleo (03S) and David (05S) all formed in close succession in December 2009. On 29NOV2009, strong equatorial westerlies exceeding 7 m s^{-1} diverted southward upon approaching central Sumatra's mountains, constituting cyclonic deformation of the flow in the southern hemisphere. On 30NOV, trade easterlies to the south closed the cyclonic circulation, just off Sumatra's southern tip (Fig. 4.15a). Small geopotential height falls were already visible in the center of the circulation (Fig. 4.15a). Meanwhile, easterly flow near Sumatra's northern tip generated a cyclonic wake vortex (Fig. 4.15a).

A cyclonic vortex with slight geopotential height falls is also noted east of Malaysia in Fig. 4.15a, and may be related to a tropical depression that dissipated several days prior in that region of the southern South China Sea. Over the next four days, the two cyclonic wake vortices west of Sumatra continued to deepen (Fig. 4.15b). Their circulations appeared to be complementary at both lower and upper levels, leading to a strong band of lower-level westerlies along the equator and strengthening the cyclonic rotation, evident in Fig. 4.15b.

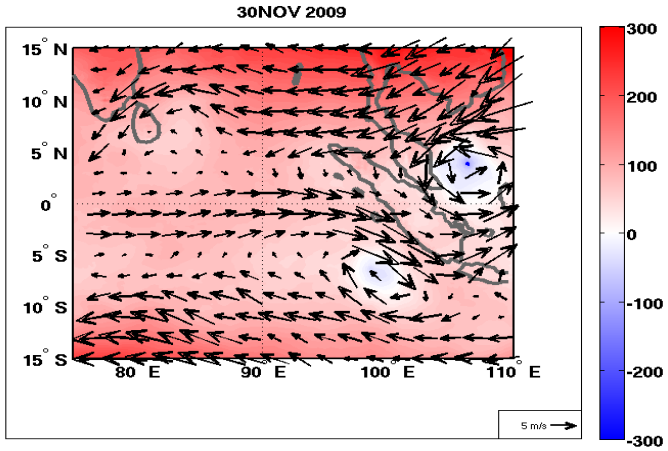

(A)

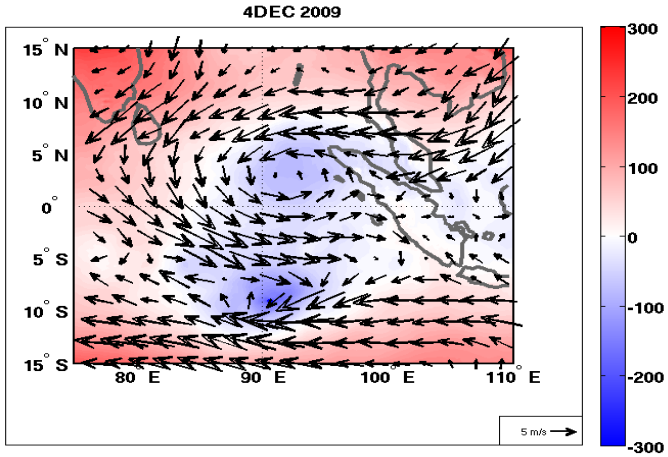

(B)

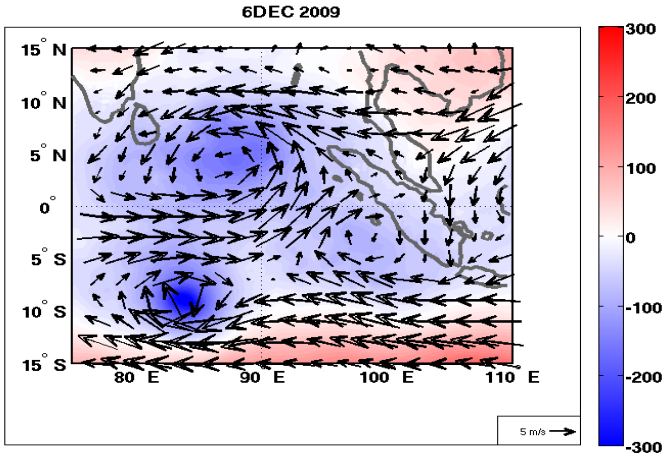

(C)

FIGURE 4.15. As in Fig. 4.11, but for top, a) 30NOV2009, middle, b) 4DEC2009, and bottom, c) 6DEC2009. Geopotential height anomalies were calculated as before, but using an OND2009 geopotential height mean.

On 3DEC (not shown), the southern vortex began to move westward, followed by the northern vortex, which separated from Sumatra's northern tip on 4DEC (Fig. 4.15b). By 6DEC, easterlies split by Sumatra combined with the equatorial westerlies from the two extant vortices to form another wake vortex near southern Sumatra, seen in Fig. 4.15c.

The third wake vortex began to move westward as well on 8DEC (not shown). By this point, TC Cleo was already classified as a tropical storm in the southern Indian Ocean. TC Ward made landfall in Sri Lanka on 14DEC while the wake vortex precursor to TC David propagated further westward and southward before intensifying (not shown). The three tropical cyclones-TC Cleo in the center of the southern Indian Ocean, TC Ward near Sri Lanka, both estimated to possess wind speeds above 35 kt, and the wake vortex precursor to TC David organizing itself and strengthening near Sumatra-are visible in Fig. 4.16.

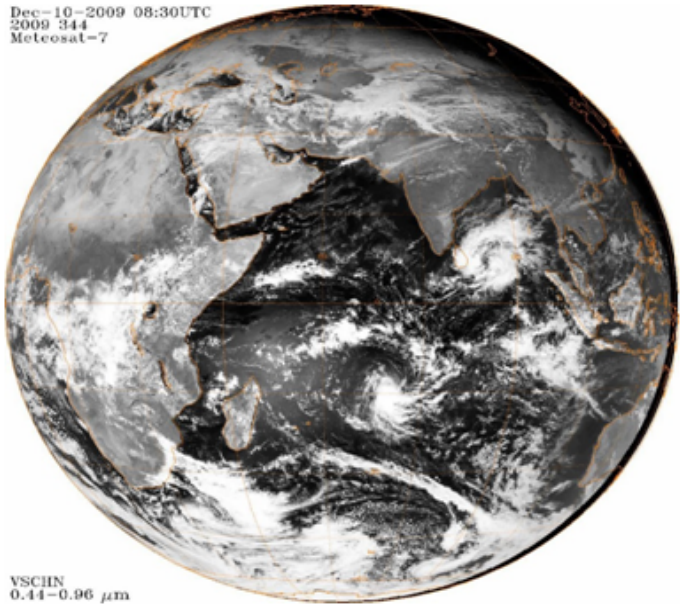

FIGURE 4.16. Meteosat-7 visible satellite imagery at 0830Z on 10DEC2009, showing Tropical Storm Cleo in the southern Indian Ocean, the wake vortex that would become TC David close to Sumatra, and TC Ward, which reached tropical storm strength on 11DEC, near the Bay of Bengal.

From 2 to 12 DEC, cyclonic vorticity in Region S was concentrated between 925 and 950 hPa, an indication that these vortices were likely related to topographic effects on the flow near Sumatra. Froude numbers in Region S during OND2009 for both easterly and westerly flow incident on Sumatra were close to unity, which may have allowed flow to overtop the mountains instead of being blocked. The long duration of cyclonic vorticity near southern Sumatra was likely a result of multiple wake vortices forming and propagating westward from southern Sumatra during that time period. Note the cyclonic wake vortices near southern Sumatra in Figs. 4.15a and 4.15c, a week apart. The cyclonic vorticity maximum in Region N was found between 850 and 900 hPa only between 28NOV and 4DEC, which was before the wake vortex that deepened into TC Ward detached from Sumatra and moved westward and out of the analysis region in early December (Fig. 4.15b). On average, Froude numbers in Region N during OND2009 were $\approx$0.5 during periods of easterly flow, which would favor flow splitting and cyclonic vorticity maxima between 850 and 900 hPa, which were observed.

Like the tropical cyclone pair of 03A and Asma in October 2008, there was an apparent, if weak, equatorial Rossby wave in DEC 2009 that may have provided the equatorial westerlies visible across the region in Fig. 4.15, increased low-level vorticity, reduced vertical wind shear, or made conditions otherwise more favorable for tropical cyclogenesis. In Fig. 4.17, an equatorial Rossby wave was diagnosed in the vicinity of the wake vortices that would become TCs Cleo, Ward, and David; the equatorial Rossby wave is marked by the black contour crossing the thick black line representing Sumatra in late November and early December.

An equatorial Rossby wave also moved westward from the approximate location of the Kelvin wave and MJO convective envelope in early November (seen in Fig. 4.18 with OLR anomalies below -20 W m^{-2}), and a strong equatorial Rossby wave moved into the region near Sumatra in late December 2009. This equatorial Rossby wave was present near Sumatra

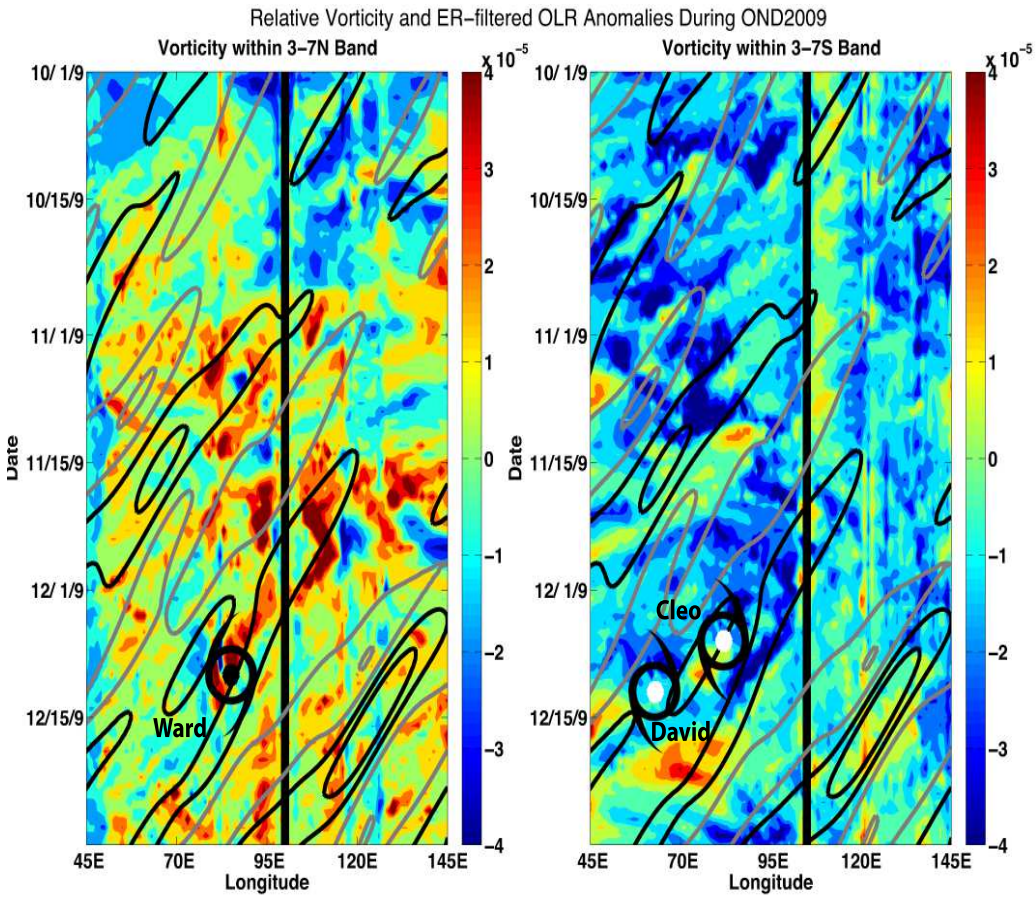

FIGURE 4.17. As in Fig. 4.13, but for OND2009.

in early January 2010 when an active MJO passed through the area and the wake vortex precursor to TC Edzani (07S) formed (not shown).

A weak convectively coupled Kelvin wave, which is the continuation of the Kelvin wave apparent to its west, appeared at the seeming terminus of the vorticity streamers in mid-December which represent the wake vortex precursors to TC Ward in Fig. 4.18a and TC David in Fig. 4.18b. Those are two parts of the same Kelvin wave, but they have more prominent filtered OLR anomalies (below -10 W m^{-2}) than do the other areas of the same wave. The vorticity signature of TC David's precursor disappears in Figs. 4.17 and 4.18b because it moved out of the 3-7°S latitude band, moving farther westward before reaching tropical storm strength where indicated.

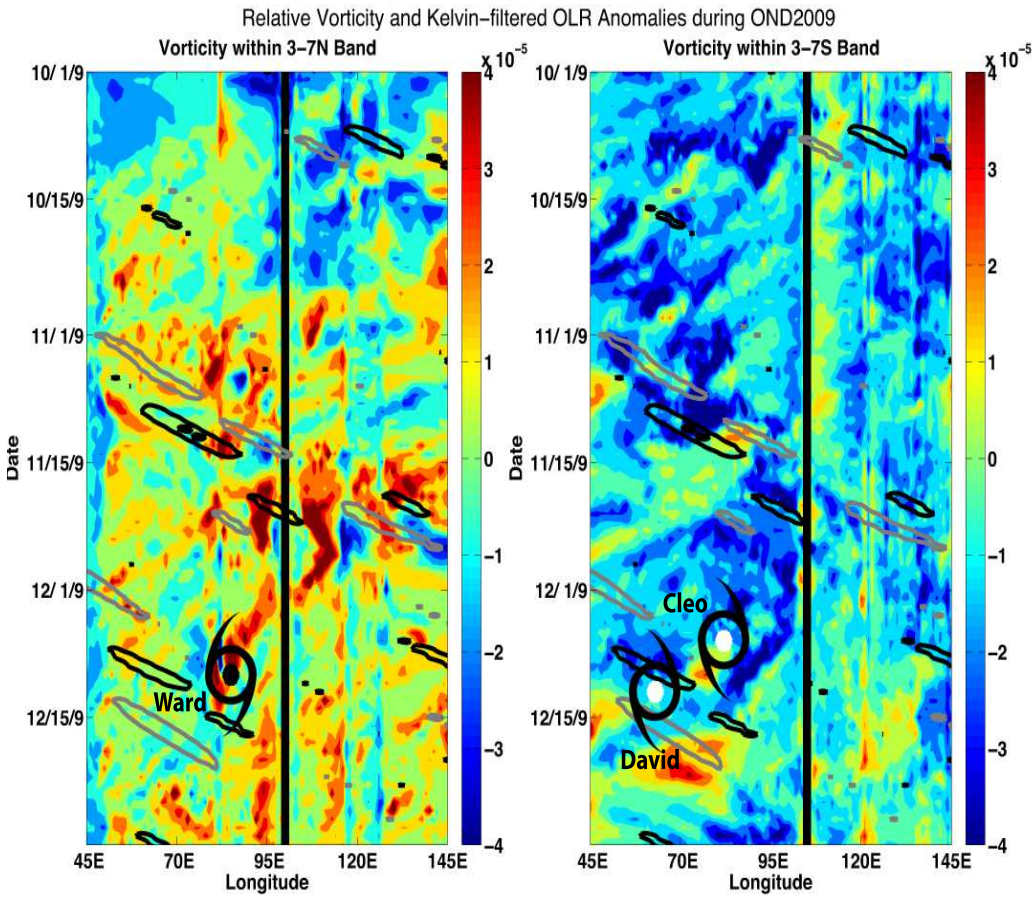

FIGURE 4.18. As in Fig. 4.14, but for OND2009.

It is possible that diabatic heating within the three tropical cyclones in close proximity disturbed the atmosphere enough to invigorate the convectively coupled Kelvin wave. The Kelvin wave in mid-December moved eastward for several days, weakened near Sumatra, then resurged and continued to propagate eastward, though its OLR anomalies at this point were too weak to be detected in Fig. 4.18.

In the northern Indian Ocean, the wake vortex precursor to TC Ward moved over mildly positive SST anomalies while it intensified (not shown). TC Cleo, south of the equator, experienced cool SST anomalies on the order of -0.5°C or greater, as it spun into a tropical storm. TC David, which followed roughly in the path of TC Cleo, also experienced cool SST anomalies. TC David only reached tropical storm wind speeds once it recurved to the east

and south of TC Cleo's track. SSTs around the three wake vortices, all over 28.3°C, were warmer than those SSTs experienced by TC Asma and TC 05A in OND2008, consistent with the interannual warming trend noted by Waliser et al. (2012) during the YOTC period. The three wake vortices all featured enhanced midlevel moisture, 20% or greater than the seasonal OND2009 Indian Ocean basin mean (not shown). As the wake vortices propagated westward, all three moved into a regime of low vertical wind shear, which may have aided their development.

In summary, westerly flow incident upon Sumatra diverted southward, possibly due to flow blocking, in late November 2009. Trade easterlies to the south closed the cyclonic circulation. Splitting of easterly flow by Sumatra led to a concurrent wake vortex near northern Sumatra, and a later wake vortex off southern Sumatra in early December. Cyclonic vorticity maxima were identified at the level of Sumatra's topography while the two southern wake vortices spun up, one after the other, and propagated away, and before the wake vortex precursor to TC Ward propagated away from Sumatra's northern tip. High midlevel moisture levels and low vertical wind shear likely helped the vortices strengthen into tropical storms on 7DEC (TC Cleo), 11DEC (TC Ward), and 13DEC (TC David). Like the OND2008 cross-equatorial tropical cyclone pair case study, there appeared to be interaction between these three wake vortices and equatorial Rossby waves. However, the nascent TCs Cleo, Ward, and David may have produced large enough amounts of diabatic heating via convection that they strengthened a passing Kelvin wave, an event similar to the OND2008 case, which also appeared to excite a convectively coupled Kelvin wave. TC Cleo achieved a maximum windspeed of 115 kt. However, it dissipated before making landfall anywhere in the southwestern Indian Ocean. TC David intensified to 55 kt while meandering in a circuitous track in the southwestern Indian Ocean. Its remnants dumped heavy rain on

Mauritius and Reunion several days after the storm had weakened sufficiently to no longer be warned (La Sentinelle 2009). In the northern Indian Ocean, TC Ward made landfall on Sri Lanka on 14DEC, but no notable damage was reported.

4.3.3. Tropical Cyclones 05A and Alenga (November-December 2011). In 2011, during the intensive observing period of the DYNAMO field campaign, Tropical Cyclones 05A and Alenga (01S) developed from cross-equatorial wake vortices downstream of Sumatra. Anomalously strong easterlies, exceeding 5 m s^{-1} at low levels, impacted Sumatra preceding the passage of a Kelvin wave convective envelope associated with the late November 2011 MJO event. A wake vortex was generated off Sumatra's northern tip during this easterly flow regime on 16NOV2011 (not shown). Geopotential height falls deepened in the center of this cyclonic circulation over time (Fig. 4.19a).

This wake vortex began to propagate westward on 22NOV (not shown). Intense westerly wind bursts along the equator enhanced its low level cyclonic rotation as the vortex neared Sri Lanka and reached tropical storm strength on 26NOV (Fig. 4.19b). TC05A then passed through the Kelvin wave convective envelope (Fig. 4.20a), part of the late November 2011 MJO event, and moved into the Arabian Sea on 26NOV (not shown).

Cyclonic relative vorticity was maximized between 900 and 850 hPa from 13 to 26NOV, while winds were easterly, in Region N. On 26NOV, the wake vortex that became TC 05A had exited Region N. Froude numbers for easterly wind in Region N averaged $\approx$0.45, making wake vortex formation in Region N more likely. By 26NOV, the active MJO and its surface westerlies were approaching (Fig. 4.20a), so topographic cyclonic vorticity production in Region N likely ceased. Between 1 and 8DEC, winds gradually shifted from easterly to westerly incident on southern Sumatra (apparent in the wind vectors in Figs. 4.20b and 4.21).

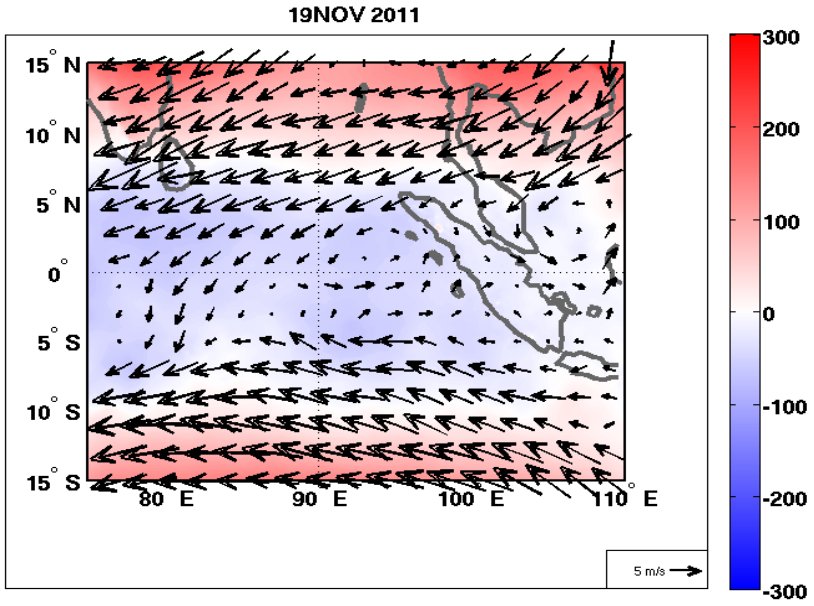

(A)

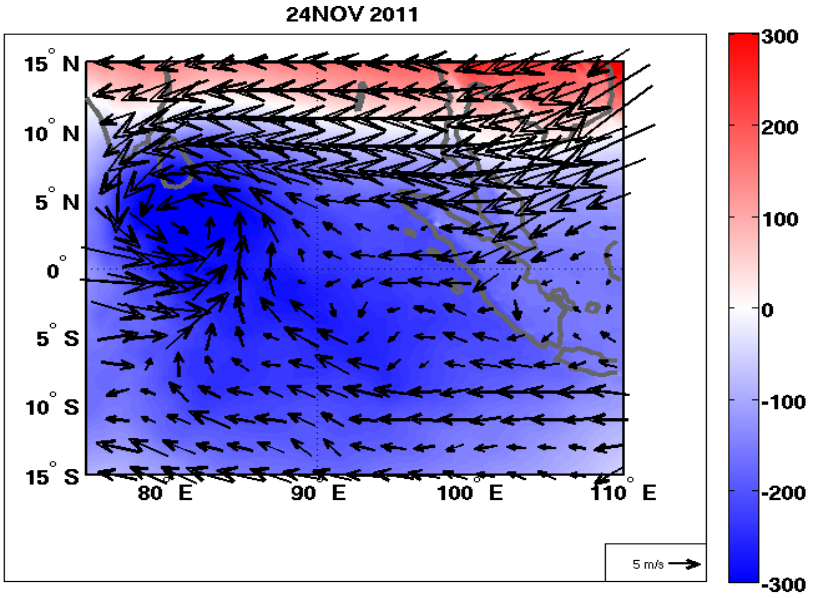

(B)

FIGURE 4.19. As in Fig. 4.11, but for top, a) 19NOV2011, bottom, b) 24NOV2011, showing the wake vortex precursor to TC 05A, north of the equator. Geopotential height anomalies were calculated as before, but using an OND2011 geopotential height mean.

In Region S, the cyclonic vorticity maxima occurred between 1000 and 925 hPa, about the height of southern Sumatra's mountains, only between 1 and 8DEC. So, despite the wind shift, cyclonic vorticity remained maximized in the layer below Sumatra's topography.

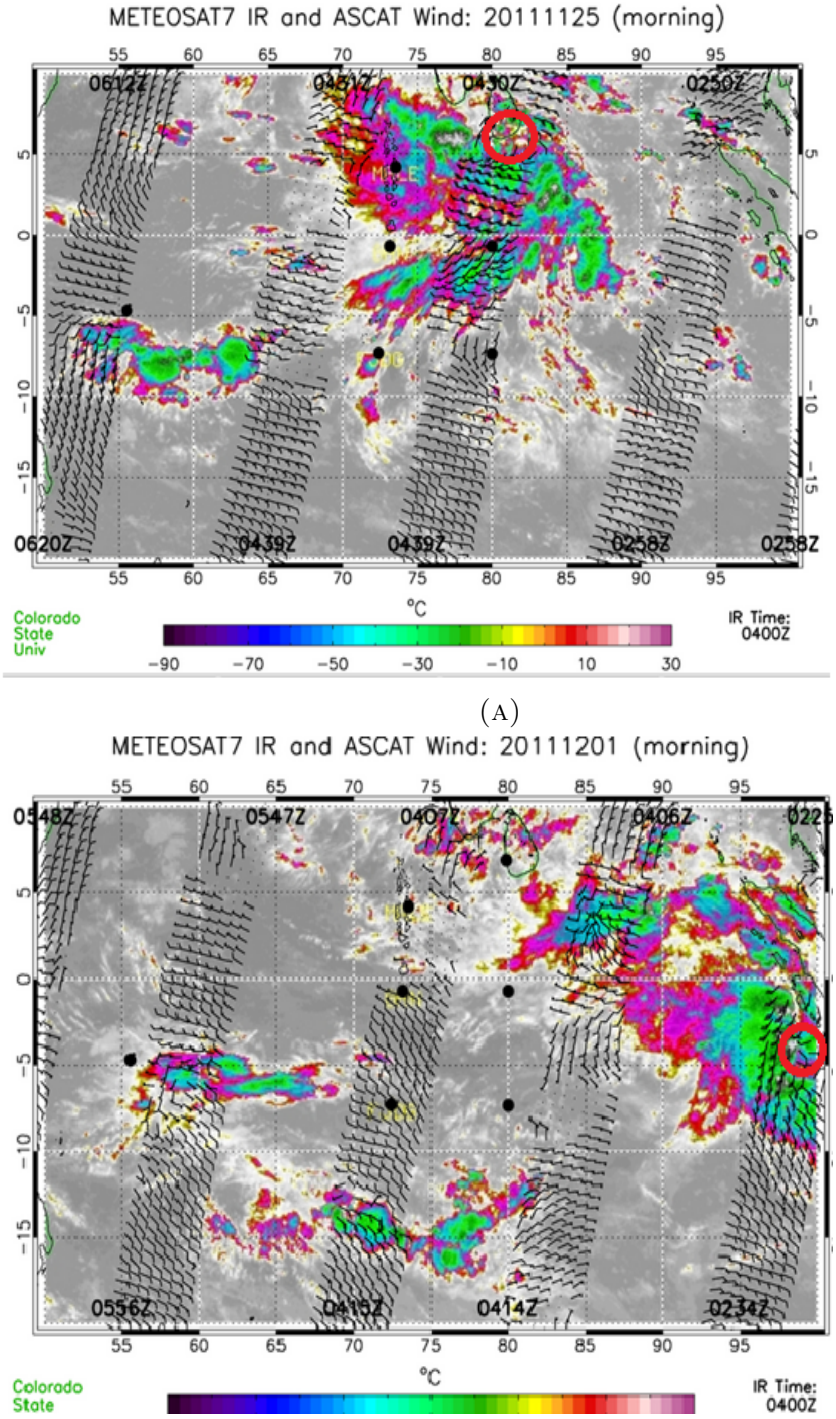

FIGURE 4.20. Meteosat-7 infrared satellite imagery with overlaid ASCAT wind vectors at a) 04Z on 25NOV 2011 and b) 04Z on 1DEC2011. Wake vortices that became a) TC 05A and b) TC Alenga are circled in red, and may be found in wind vectors embedded within the MJO convective envelope near a) Sri Lanka, top-center of the image, and b) southern Sumatra, at the far right of the image. Images produced by Brian McNoldy.

Froude numbers during both the easterly and westerly flow regimes in Region S averaged about ≈0.6, so flow blocking and cyclonic vorticity generation were possible regardless of the wind shift.

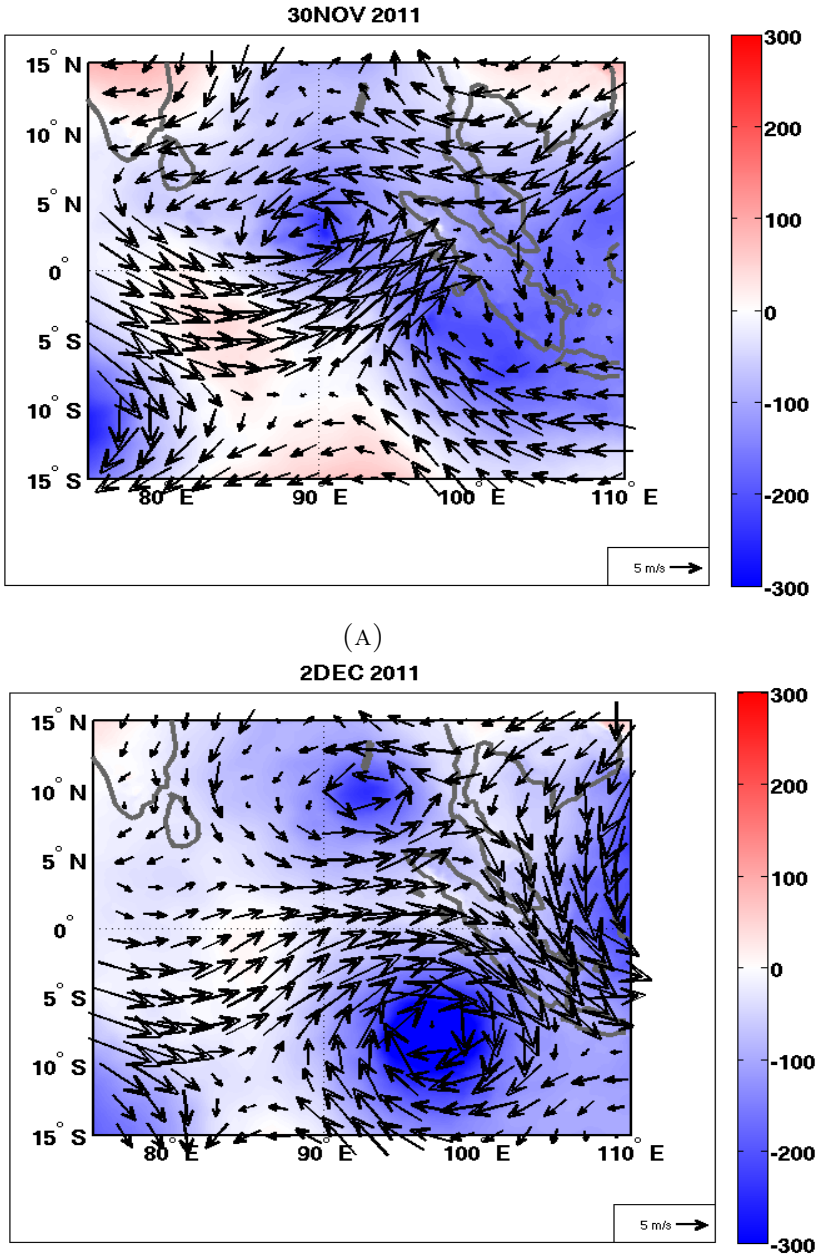

FIGURE 4.21. As in Fig. 4.11, but for top, a) 30NOV2011, and bottom, b) 2DEC2011, showing the wake vortex precursor to TC Alenga, south of the equator. Geopotential height anomalies were calculated as before, but using an OND2011 geopotential height mean.

Easterly flow in late November 2011 resulted in a lee vortex near southern Sumatra, visible in Fig. 4.21a. As for TC 05A, a strong westerly wind burst, likely associated with the MJO convective envelope moving into the region (Fig. 4.20b), enhanced low-level cyclonic vorticity in early December (Fig. 4.21b). Notably, the wake vortex precursor to TC Alenga developed under the MJO convective envelope (Fig. 4.20b), while TC 05A developed ahead of it (Fig. 4.20a). TC Alenga intensified further and reached tropical storm strength once MJO-related convection had propagated away to the east (not shown).

As the wake vortex precursor to TC 05A journeyed westward, it encountered warm SSTs, 0.5 °C above average. The warm SST anomalies in the pre-onset phase of the MJO may have been enhanced by calm conditions, which minimized mixing and enabled the formation of diurnal surface warm layers, several degrees above the mean (Moum et al. 2014). The atmosphere gradually moistened as the Kelvin wave and MJO convective envelope approached the vortex that became TC 05A (Fig. 4.20a); midlevel moisture (300 to 700 hPa) was as much as 30% above the mean in the vicinity of the intensifying wake vortex. The southern wake vortex formed under the convective envelope (Fig. 4.20b), where gusty winds and precipitation mixed the upper ocean and cooled the sea surface. SSTs remained below average, but still more than adequate to fuel tropical cyclogenesis, after the wake vortex propagated westward and emerged from under the MJO convection. Midlevel moisture was also close to 30% above average for the southern wake vortex within the moist MJO convective envelope, which likely assisted its development into TC Alenga.

The superposition of an equatorial Rossby wave, Kelvin wave, and the MJO was noted before the northern wake vortex intensified into TC 05A (Gottschalck et al. 2013). That equatorial Rossby wave, the black contour crossing over a vorticity streamer around 25NOV, was rather weak as seen in Figs. 4.22a and 4.22b. It moved westward for ≈10 days after

passing over the wake vortex precursor to TC 05A (Fig. 4.22a). A separate equatorial Rossby wave propagated westward from the Maritime Continent and passed over the wake vortex precursor to TC Alenga, west of Sumatra, in early December 2011 (Fig. 4.22b).

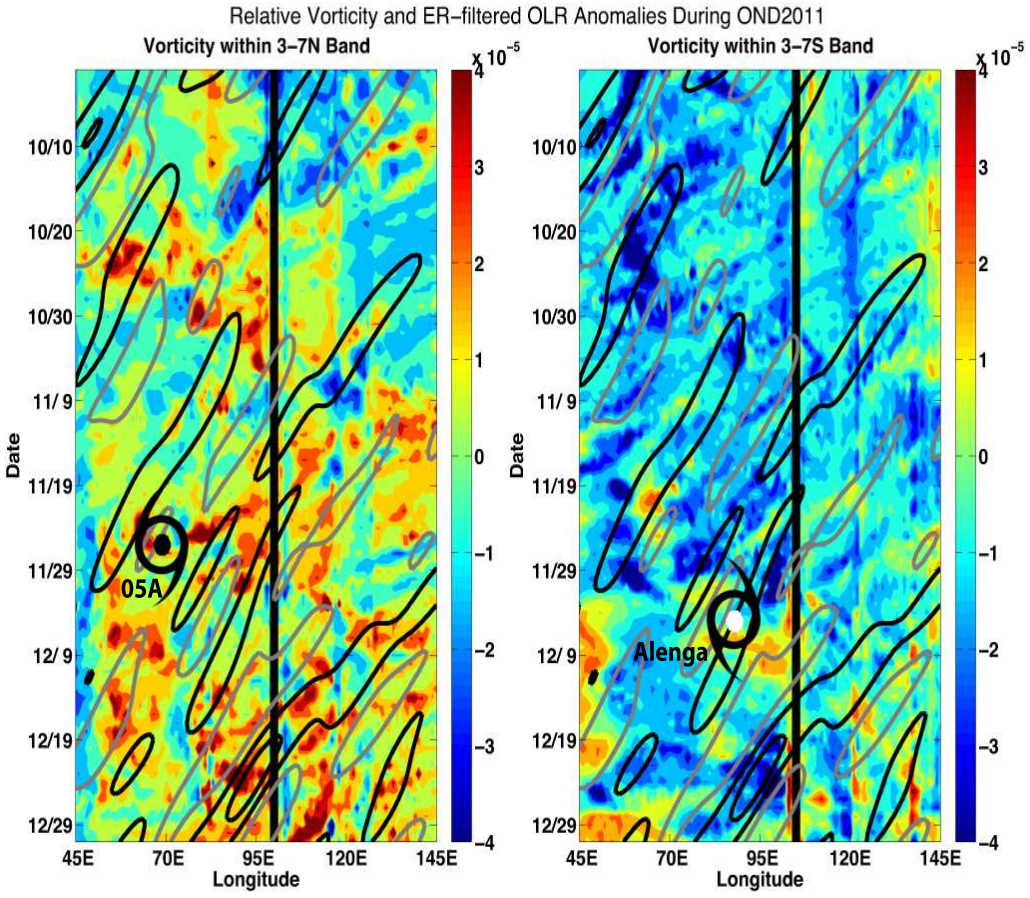

FIGURE 4.22. As in Fig. 4.13, but for OND2011.

These equatorial Rossby waves may have contributed to low-level cyclonic vorticity or lowered vertical wind shear to make the environment more favorable for tropical cyclogenesis, as in previous case studies of equatorial Rossby waves and tropical cyclogenesis (e. g. Schreck and Molinari 2009). However, vertical wind shear in both vortices increased dramatically around when they encountered equatorial Rossby waves and the Kelvin wave convective

envelope (in Figs. 4.23a and 4.23b) likely associated with shear between incoming surface flow and diverging flow aloft in the MJO convective envelope in late November 2011.

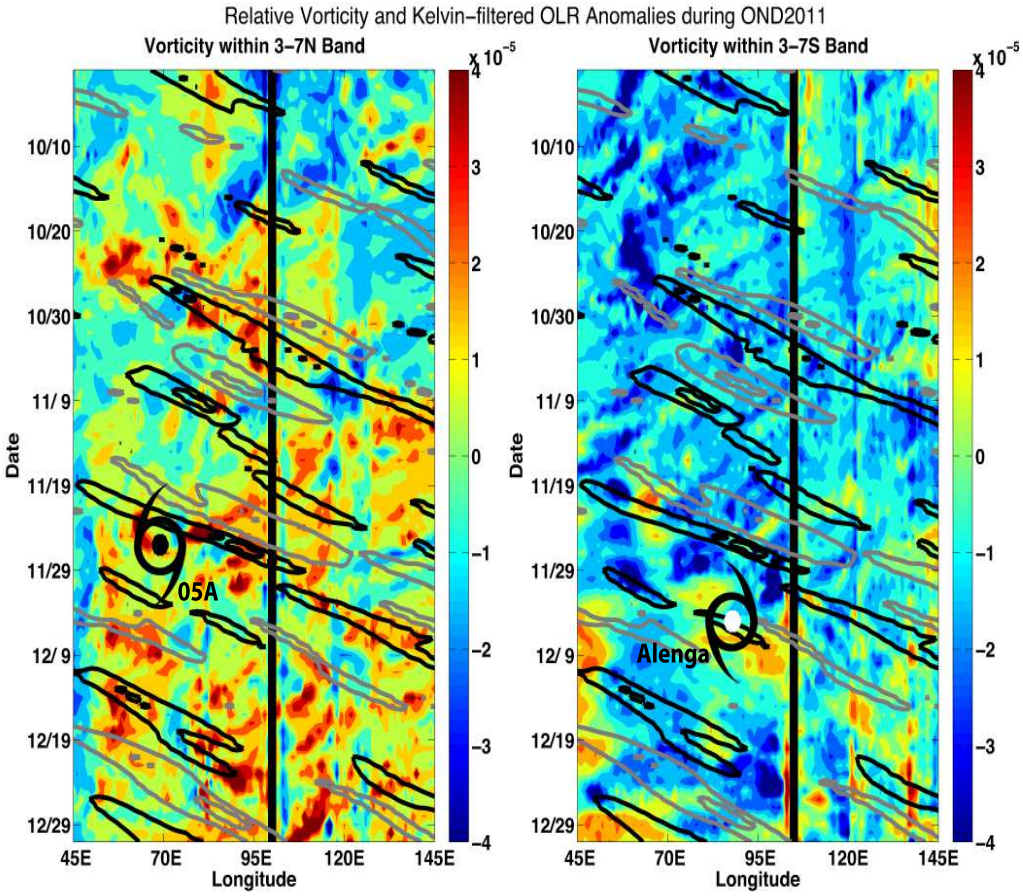

FIGURE 4.23. As in Fig. 4.14, but for OND2011.

A strong Kelvin wave signature is visible in Figs. 4.23a and 4.23b, embedded within the active MJO itself in mid to late November. This Kelvin wave passed directly over the wake vortex precursors to TC Alenga and TC 05A before they achieved tropical storm force winds. The large cyclonic gyres left in the wake of the MJO and Kelvin wave convective envelope may have also reinforced cyclonic circulation in the wake vortices.

TC 05A and TC Alenga were the only cross-equatorial cyclone pair during the YOTC or DYNAMO campaigns that encountered the MJO as they intensified and stemmed from

wake vortices generated near Sumatra. Two other tropical cyclones with wake vortex origins, TC Gael (13S) in February 2009 and TC Edzani (07S) in January 2010, also intersected the MJO active envelope and concurrent other convectively coupled equatorial wave types, but were not discussed at length here.

In summary, a wake vortex formed off northern Sumatra during a period of easterly winds preceding the active MJO in mid-November 2011. Westerly wind bursts racing ahead of the Kelvin wave convective envelope increased low-level vorticity in the region. After encountering an equatorial Rossby wave, Kelvin wave, and the active MJO itself, TC 05A made landfall in Sri Lanka on 26NOV, the same day that it reached tropical storm strength winds; despite the low wind speeds, TC 05A caused flooding, damaged thousands of homes, and contributed to nearly 20 deaths, mostly fishermen (Agence France-Presse 2011). The wake vortex that became TC Alenga formed slightly later, on 30NOV, under easterly flow around or over southern Sumatra's mountains. Westerlies associated with the passage of the active phase MJO strengthened that cyclonic circulation and helped to separate the wake vortex from Sumatra. Because TC 05A was located in the Arabian Sea at that point, there was little chance of mutually beneficial vortex-vortex interaction to strengthen lower-level cyclonic circulation and upper-level outflow, as in the other two case studies. It is possible that MJO-related convection and outflow aloft, as well as interaction between the MJO, a Kelvin wave, and an equatorial Rossby wave, helped the wake vortex precursor to TC Alenga to intensify as it moved westward and emerged from the MJO convective envelope. TC Alenga reached maximum wind speeds of 95 kt but diminished while at sea.

CHAPTER 5

Conclusions

5.1. Overview and Discussion of Results

Splitting of easterly flow by the cross-equatorial island of Sumatra and the subsequent formation of counter-rotating wake vortices was first noted by Kuettner (1989) (Fig. 2.9). Kuettner noted that since Sumatra straddles the equator, both vortices are cyclonic during easterly flow regimes. In this study, flow blocking and splitting were demonstrated for low-level easterly flow encountering Sumatra from October to December of 2008, 2009, and 2011. OND2008 and 2009 were part of the YOTC virtual field campaign, which emphasized increased assimilation and usage of extant data, such as satellite imagery, while OND2011 encompassed the special observing period of the DYNAMO field campaign, which featured frequent radiosonde launches, multiple radar placements, and ocean observations from two research vessels. Principally due to higher topography, Froude numbers were lower during all three periods for Sumatra's northern tip than its southern tip, indicating that flow blocking and splitting were more preferred in the north (Table 4.1). However, Froude numbers near Sumatra's southern tip were still marginally less than one during OND2008 and 2009, and close to 0.6 in 2011, so flow blocking and splitting were still possible.

Under easterly flow regimes, streamers of cyclonic vorticity were visible emanating from both of Sumatra's tips, manifested as cyclonic wake vortices or flow curvature downstream over the Indian Ocean (e.g., Figs. 4.1, 4.6). Cyclonic flow curvature and vorticity were noted near southern Sumatra for westerly flow as well (Fig. 4.1b). This phenomenon may be related to a monsoon trough-like pattern west of southern Sumatra noted during all three OND periods, a strong diurnal cycle of convection involving interaction between sea breezes,

orographic flow, and the ITCZ, or it may be that equatorial westerlies were blocked, then diverted southwards, which constituted cyclonic movement, by the mountains of central Sumatra.

Daily-averaged zonal wind at northern Sumatra and relative vorticity downstream were highly significantly correlated ($R^2>0.7$, $P<<0.01$) from the surface to the approximate level of Sumatra's topography, 850 hPa, for OND2008, 2009, and 2011 (Fig. 4.4a). The relationship between zonal wind and relative vorticity was more muddled near southern Sumatra, where multiple processes may have influenced flow and relative vorticity; correlations between zonal wind and relative vorticity near southern Sumatra were moderately significant at 1000 and 925 hPa, roughly from the surface to the elevation of southern Sumatra's mountains, during OND2011 (Fig. 4.4b), and only weakly significant at 1000 hPa during OND2008 and 2009. Near northern Sumatra, zonal wind led relative vorticity by approximately 3-4 days, but the lead-lag relationship at lower pressure levels near southern Sumatra was insignificant. On over 30% of days, and the majority of easterly wind days during the three studied periods, cyclonic vorticity maxima were found in the Indian Ocean just west of Sumatra, at approximately the level of the island's topography, from 850 to 900 hPa near northern Sumatra, and 925 to 950 hPa near southern Sumatra, another indication that topographic effects on the flow were at least partially responsible for forming cyclonic vorticity downstream (Fig. 4.5).

The majority (roughly 60%) of sufficiently cyclonic (exceeding an empirically defined threshold) wake vortices at low levels that propagated westward from Sumatra were observed between October and December of the entire YOTC campaign, which spanned two full years. Between October and December, the dominant interseasonal circulation in the Indian Ocean basin, the monsoons, transition from flowing into southeast Asia and India, to

flowing outward from the continents. The prevailing winds near Sumatra shift from strong surface westerlies to surface easterlies during the winter monsoon. However, during the winter monsoon, the low-level wind regime across Sumatra may shift from easterly to westerly in association with the passage of the Madden Julian Oscillation (MJO). Another monsoonal transition period exists from March to May, when cyclonic vorticity streamers were also frequently detected downstream of southern Sumatra. When winds incident upon Sumatra were easterly, cyclonic vorticity streamers were observed moving westward from Sumatra, with a mean period of 3 days between each streamer. The cause or causes for wake vortices to detach from Sumatra with a 3-day period in between each vortex is unclear, although vortex shedding is a frequent occurrence in flow past islands attributable to a variety of mechanisms (Etling 1989). Many of these cyclonic circulations downstream of Sumatra developed corresponding geopotential height minima at 850 hPa, and in some of these cases tropical cyclogenesis was observed. Thirteen tropical cyclones were determined to be related to cyclonic wake vortices or flow curvature near Sumatra during the combined YOTC and DYNAMO periods, and ten of those tropical cyclones occurred between October and December of a given year, when climatological vertical wind shear was reduced compared to during the winter or summer monsoons.

Three twin tropical cyclone case studies have been identified in the data sets, wherein equatorial westerlies impacted Sumatra before some of the studied wake vortices separated from Sumatra and began to move westward. These twin tropical cyclone pairs- TCs 03A and Asma in October 2008, TCs Cleo, Ward, and David in December 2009, and TCs 05A and Alenga in November and December 2011- arose from counter-rotating, cyclonic wake vortices on Sumatra's tips. In several instances, wake vortices propagated far to the west and remained coherent into the Arabian Sea or southwestern Indian Ocean before undergoing

tropical cyclogenesis and reaching intensities anywhere between 35 and 115 kt. Like the other two tropical cyclone pairs, the wake vortex precursors to TC 05A and TC Alenga enjoyed elevated midlevel (300 to 700 hPa) moisture as they intensified, likely due in this case to the approaching MJO-related convection, which moistened the midlevels.

All three case studies were observed to coincide with convectively coupled equatorial Rossby and Kelvin wave activity. For TC 05A and TC Alenga, Kelvin waves were embedded within the MJO (Fig. 4.23). For TCs 03A and Asma, and TCs Cleo, Ward, and David, OLR anomalies associated with Kelvin waves strengthened as the waves passed over convection in the burgeoning vortices (Figs. 4.14 and 4.18). For the tropical cyclone pairs in OND2008 and 2009, equatorial Rossby waves moved into the region (Figs. 4.13 and 4.17), bringing with them low-level equatorial westerly winds, preceding the detachment and intensification of wake vortices (Figs. 4.11 and 4.15). During OND2011, equatorial westerly winds associated with the active phase of the MJO impinged upon Sumatra before the wake vortex precursor to TC Alenga separated from Sumatra (Fig. 4.21). Kelvin and equatorial Rossby waves were noted within the MJO convective envelope when the wake vortices transited through it in late November and early December 2011, prior to the intensification of those wake vortices (Figs. 4.20, 4.22, and 4.23). Two other tropical cyclones, in early 2009 and 2010, both formed out of wake vortices generated by southern Sumatra and encountered the MJO convective envelope as well, but were not described in detail here.

Equatorial Rossby waves, such as those identified in the vicinity of all three wake vortex pairs, encouraging tropical cyclogenesis and intensification by lowering vertical wind shear and providing cyclonic relative vorticity at low levels would echo the results of other studies (e. g., Bessafi and Wheeler 2006; Frank and Roundy 2006; Schreck and Molinari 2009). However, a reduction in vertical wind shear in the presence of an equatorial Rossby wave was

not seen for the twin tropical cyclone case in late 2011, which may be related to the arrival of the Madden-Julian Oscillation's convective envelope at that time. In previous studies, Kelvin waves and the MJO convective envelope have been linked to cyclonic gyres or potential vorticity generation, which assisted tropical cyclogenesis in analyzed cases (e. g., Ferreira et al. 1996; Roundy 2008; Schreck and Molinari 2011). The same mechanisms may have been operative in abetting intensification of these twin wake vortices, which encountered Kelvin waves as they spun up. In the OND2008 and OND2009 case studies, Kelvin waves were generated or strengthened in the vicinity of the twin tropical cyclones, an impact of twin tropical cyclones which has not been suggested in previous work.

In summary, this study examined cyclonic wake vortex generation downstream of Sumatra over the Indian Ocean, the subsequent propagation of these wake vortices westward, and tropical cyclogenesis in three cases where cross-equatorial cyclone pairs developed, from October to December of 2008, 2009, and 2011. The main findings of this research are as follows:

(1) Between October and December in the analyzed data, counter-rotating wake vortices and cyclonic relative vorticity generation were frequently observed downstream of Sumatra. Froude numbers less than unity, significant correlations between zonal wind and relative vorticity, and cyclonic vorticity maxima at the level of Sumatra's topography suggest topographic influence on vorticity generation. On some occasions, the flow anomalies that precipitated the formation of wake vortices were related to an active MJO envelope in the Indian Ocean. Vortex development and separation from Sumatra was aided in several cases by equatorial westerlies impinging upon central Sumatra.

(2) Because Sumatra straddles the equator, both wake vortices emanating from the islands tips are cyclonic under easterly flow regimes, and may serve as incipient disturbances preceding tropical cyclogenesis, as originally proposed by Kuettner (1989).

(3) Thirteen total cases of tropical cyclogenesis from cyclonic wake vortices downstream of Sumatra were identified during the YOTC and DYNAMO campaigns. Ten (or 77%) of these tropical cyclones formed between October and December of each year. Seven of these tropical cyclones formed in the southern Indian Ocean, while the other six cyclones formed in the northern Indian Ocean.

(4) Wake vortex intensification and development into tropical cyclones was aided by midlevel moistening and equatorial wave activity, which increased during the MJO's active phase in the Indian Ocean.

(5) Sumatra stretches across the equator. Unique among tropical islands, its topography interacts with flow to produce cyclonic wake vortices on either side of the equator which may then propagate into a large stretch of warm, open ocean, and develop into twin tropical cyclones.

5.2. Future Work

Further research is needed into the sources and role of equatorial westerly wind in cyclonic flow curvature and vorticity production near southern Sumatra. Correlations between zonal wind and relative vorticity were poor in the defined southern analysis region, Region S, and westerly wind regimes evaluated there featured cyclonic relative vorticity on average, but this cyclonic vorticity was constant with height, instead of displaying a maximum at the topography height as did easterly flow. Adjusting the analysis location to evaluate truly

equatorial westerly winds and relative vorticity near central Sumatra may yield a more accurate picture of the impacts of Sumatra upon westerly flow.

Numerical simulations that remove the diurnal cycle of heating, convection, or Sumatra's mountainous terrain, could also be performed to isolate the effects of the ITCZ, complex interactions between sea and mountain flows, and potential flow blocking or splitting by southern Sumatra.

Running a spatial filter on the wind or relative vorticity fields could also remove large scale features in space and time, such as the persistent monsoon trough south of the equator, thus enabling a focused analysis of smaller-scale features, such as wake vortices.

With many more years of observations, a representative composite or dataset could be constructed for wake vortices in the northern and southern hemisphere. Such a dataset could then be stratified by those vortices that do and do not reach tropical storm strength, and further divided by those vortices that do and do not encounter convectively coupled equatorial waves or the active MJO. That may illuminate the mechanism by which most vortices detach from Sumatra 3 days apart, the environmental conditions surrounding both developers and non-developers, patterns in tropical cyclogenesis related to wake vortices and modes of variability, or the potential importance of convectively coupled equatorial waves, which were often diagnosed in the vicinity of developing wake vortices.

Further research is needed into interaction between these burgeoning wake vortices and convectively coupled equatorial waves. More years of data, as mentioned above, would aid in this investigation, and support or rebut the theory that convectively coupled equatorial waves positively impact the development of Sumatran wake vortices, and conversely, that Sumatran wake vortices may invigorate Kelvin waves. Removing the effects of wake vortices upon the flow and environmental conditions, as has been performed in other tropical cyclogenesis

studies, would better facilitate the diagnosis of environmental modification, such as low level vorticity enhancement, by convectively coupled equatorial waves. Flow anomalies related to the MJO were shown to lead to wake vortex generation, which raises the question: could flow blocking, or the diabatic energy release or circulations of tropical cyclones also project onto the MJO? An upcoming field project, the Year of the Maritime Continent, intends to examine the behavior of the MJO in the vicinity of the mountainous Maritime Continent. An improved understanding of the interaction between topography and flow processes near Sumatra may enhance tropical cyclone prediction for vulnerable populations around the Indian Ocean basin, and could improve predictive capability for the MJO and its many worldwide impacts as well.

Bibliography

Agence France-Presse, 2011: Sri Lanka storm kills 19, damages 5700 homes. [Available online at http://www.webcitation.org/63Vnhm01u].

Ashok, K., Z. Guan, N. Saji, and T. Yamagata, 2004: Individual and combined influences of ENSO and the Indian Ocean dipole on the Indian summer monsoon. *J. Climate*, **17 (16)**, 3141–3155.

Avila, L. A., and R. J. Pasch, 1992: Atlantic tropical systems of 1991. *Mon. Wea. Rev.*, **120 (11)**, 2688–2696.

Baines, P. G., 1997: *Topographic effects in stratified flows*. Cambridge University Press, 482 pp.

Bender, M. A., R. E. Tuleya, and Y. Kurihara, 1987: A numerical study of the effect of island terrain on tropical cyclones. *Mon. Wea. Rev.*, **115 (1)**, 130–155.

Bessafi, M., and M. C. Wheeler, 2006: Modulation of South Indian Ocean tropical cyclones by the Madden-Julian Oscillation and convectively coupled equatorial waves. *Mon. Wea. Rev.*, **134 (2)**, 638–656.

Brand, S., and J. W. Blelloch, 1973: Changes in the characteristics of typhoons crossing the Philippines. *J. Appl. Meteor.*, **12 (1)**, 104–109.

Briegel, L. M., and W. M. Frank, 1997: Large-scale influences on tropical cyclogenesis in the western North Pacific. *Mon. Wea. Rev.*, **125 (7)**, 1397–1413.

Camargo, S. J., K. A. Emanuel, and A. H. Sobel, 2007: Use of a genesis potential index to diagnose ENSO effects on tropical cyclone genesis. *J. Climate*, **20 (19)**, 4819–4834.

Ciesielski, P. E., and R. H. Johnson, ????: .

Clark, T., and W. Peltier, 1977: On the evolution and stability of finite-amplitude mountain waves. *J. Atmos. Sci.*, **34 (11)**, 1715–1730.

de Szoeke, S. P., J. B. Edson, J. R. Marion, C. W. Fairall, and L. Bariteau, 2015: The MJO and air-sea interaction in TOGA COARE and DYNAMO. *J. Climate*, **28**, 597–622.

Dickinson, M., and J. Molinari, 2002: Mixed Rossby–gravity waves and western Pacific tropical cyclogenesis. part I: Synoptic evolution. *J. Atmos. Sci.*, **59 (14)**, 2183–2196.

Epifanio, C. C., 2003: Lee vortices. *Encyclopedia of Atmospheric Sciences, JR Holton, J. Pyle, and JA Curry, Eds*, 1150–1160.

Etling, D., 1989: On atmospheric vortex streets in the wake of large islands. *Meteor. Atmos. Phys.*, **41 (3)**, 157–164.

Farfán, L. M., and J. A. Zehnder, 1997: Orographic influence on the synoptic-scale circulations associated with the genesis of Hurricane Guillermo (1991). *Mon. Wea. Rev.*, **125 (10)**, 2683–2698.

Feng, Z., S. A. McFarlane, C. Schumacher, S. Ellis, J. Comstock, and N. Bharadwaj, 2014: Constructing a merged cloud–precipitation radar dataset for tropical convective clouds during the DYNAMO/AMIE experiment at Addu Atoll. *J. Atmos. Oceanic Technol.*, **31 (5)**, 1021–1042.

Ferreira, R. N., and W. H. Schubert, 1997: Barotropic aspects of ITCZ breakdown. *J. Atmos. Sci.*, **54 (2)**, 261–285.

Ferreira, R. N., W. H. Schubert, and J. J. Hack, 1996: Dynamical aspects of twin tropical cyclones associated with the Madden-Julian oscillation. *J. Atmos. Sci.*, **53 (7)**, 929–945.

Flatau, M., 2015: Wave/wave and atmosphere/ocean interaction in MJO initiation. *Proc. 95th Annual Meeting of the American Meteorological Society*, Phoenix, AZ, Amer. Meteor. Soc.

Frank, W. M., 1977: The structure and energetics of the tropical cyclone I. Storm Structure. *Mon. Wea. Rev.*, **105 (9)**, 1119–1135.

Frank, W. M., and P. E. Roundy, 2006: The role of tropical waves in tropical cyclogenesis. *Mon. Wea. Rev.*, **134 (9)**, 2397–2417.

Frank, W. M., and G. S. Young, 2007: The interannual variability of tropical cyclones. *Mon. Wea. Rev.*, **135 (10)**, 3587–3598.

Gill, A., 1980: Some simple solutions for heat-induced tropical circulation. *Quart. J. Roy. Meteor. Soc.*, **106 (449)**, 447–462.

Goswami, B., 2011: South Asian monsoon. *Intraseasonal variability in the atmosphere-ocean climate system, W.K.-M. Lau and D.E. Waliser, Eds*, 21–72.

Gottschalck, J., P. E. Roundy, C. J. Schreck III, A. Vintzileos, and C. Zhang, 2013: Large-scale atmospheric and oceanic conditions during the 2011–12 DYNAMO field campaign. *Mon. Wea. Rev.*, **141 (12)**, 4173–4196.

Gray, W. M., 1968: Global view of the origin of tropical disturbances and storms. *Mon. Wea. Rev.*, **96 (10)**, 669–700.

Hanley, D., J. Molinari, and D. Keyser, 2001: A composite study of the interactions between tropical cyclones and upper-tropospheric troughs. *Mon. Wea. Rev.*, **129 (10)**, 2570–2584.

Hendon, H. H., and M. L. Salby, 1996: Planetary-scale circulations forced by intraseasonal variations of observed convection. *J. Atmos. Sci.*, **53 (12)**, 1751–1758.

Holland, G., 1995: Scale interaction in the western Pacific monsoon. *Meteor. Atmos. Phys.*, **56 (1-2)**, 57–79.

Holton, J., 2004: An introduction to dynamic meteorology. *International geographics series (*, **88**.

Houghton, D. D., and A. Kasahara, 1968: Nonlinear shallow fluid flow over an isolated ridge. *Communications on Pure and Applied Mathematics*, **21 (1)**, 1–23.

Hsu, H.-H., 2011: East Asian monsoon. *Intraseasonal variability in the atmosphere-ocean climate system, W.K.-M. Lau and D.E. Waliser, Eds*, 73–110.

Inness, P. M., and J. M. Slingo, 2006: The interaction of the Madden–Julian oscillation with the Maritime Continent in a GCM. *Quart. J. Roy. Meteor. Soc.*, **132 (618)**, 1645–1667.

Johnson, R. H., and P. E. Ciesielski, 2013: Structure and properties of Madden–Julian oscillations deduced from DYNAMO sounding arrays. *J. Atmos. Sci.*, **70 (10)**, 3157–3179.

JTWC, 2009: Annual Tropical Cyclone Report 2009. 109 pp., [Available online at http://www.usno.navy.mil/NOOC/nmfc-ph/RSS/jtwc/atcr/2009atcr.pdf].

JTWC, 2010: Annual Tropical Cyclone Report 2010. 93 pp., [Available online at http://www.usno.navy.mil/NOOC/nmfc-ph/RSS/jtwc/atcr/2010atcr.pdf].

JTWC, 2011a: Annual Tropical Cyclone Report 2011. 108 pp., [Available online at http://www.usno.navy.mil/NOOC/nmfc-ph/RSS/jtwc/atcr/2011atcr.pdf].

JTWC, 2011b: Significant tropical weather advisory for the Indian Ocean 0300Z 24DEC2011. [Available online at http://www.webcitation.org/648qKk5Xg].

JTWC, 2012: Annual Tropical Cyclone Report 2012. 118 pp., [Available online at http://www.usno.navy.mil/NOOC/nmfc-ph/RSS/jtwc/atcr/2012atcr.pdf].

Jury, M. R., 1993: A preliminary study of climatological associations and characteristics of tropical cyclones in the SW Indian Ocean. *Meteor. Atmos. Phys.*, **51 (1-2)**, 101–115.

Kerns, B. W., and S. S. Chen, 2014: Equatorial dry air intrusion and related synoptic variability in MJO initiation during DYNAMO. *Mon. Wea. Rev.*, **142 (3)**, 1326–1343.

Khouider, B., Y. Han, A. J. Majda, and S. N. Stechmann, 2012: Multiscale waves in an MJO background and convective momentum transport feedback. *J. Atmos. Sci.*, **69 (3)**, 915–933.

Kiladis, G. N., J. Dias, K. H. Straub, M. C. Wheeler, S. N. Tulich, K. Kikuchi, K. M. Weickmann, and M. J. Ventrice, 2014: A comparison of OLR and circulation-based indices for tracking the MJO. *Mon. Wea. Rev.*, **142 (5)**, 1697–1715.

Klemp, J., and D. Lilly, 1975: The dynamics of wave-induced downslope winds. *J. Atmos. Sci.*, **32 (2)**, 320–339.

Kuettner, J., 1989: Easterly flow over the cross equatorial island of Sumatra and its role in the formation of cyclone pairs over the Indian Ocean. *Wetter und Leben*, **41 (1)**, 47–55.

La Sentinelle, 2009: Pluies diluviennes: les pompiers et la Special Mobile Force en é'tat d'alert. [Available online at http://www.lexpress.mu/article/pluies-diluviennes-les-pompiers-et-la-special-mobile-force-en-%C3%A9tat-d%E2%80%99alerte/].

Lander, M. A., 1996: Specific tropical cyclone track types and unusual tropical cyclone motions associated with a reverse-oriented monsoon trough in the western North Pacific. *Wea. Forecasting*, **11 (2)**, 170–186.

Lau, W., and D. Waliser, 2011: El-Nino Southern Oscillation connection. *Intraseasonal variability in the atmosphere-ocean climate system, W.K.-M. Lau and D.E. Waliser, Eds*, 291–334.

L'Express de Madagascar, 2008: Le cyclone Asma fait une victim á andapa. [Available online at http://www.lexpressmada.com/pub/2008?p=display&id=21986/].

Liebmann, B., H. H. Hendon, and J. D. Glick, 1994: The relationship between tropical cyclones of the western Pacific and Indian Oceans and the Madden-Julian oscillation. *J. Meteor. Soc. Japan*, **72 (3)**, 401–412.

Lindstrom, E., R. Lukas, R. Fine, E. Firing, S. Godfrey, G. Meyers, and M. Tsuchiya, 1987: The western equatorial Pacific Ocean circulation study.

Lindzen, R. S., and T. Matsuno, 1968: On the nature of large scale wave disturbances in the equatorial lower stratosphere. *J. Meteor. Soc. Japan*, **46**, 215–221.

Ling, J., P. Bauer, P. Bechtold, A. Beljaars, R. Forbes, F. Vitart, M. Ulate, and C. Zhang, 2014: Global versus local MJO forecast skill of the ECMWF model during DYNAMO. *Mon. Wea. Rev.*, **142 (6)**, 2228–2247.

Luther, D., D. Harrison, and R. Knox, 1983: Zonal winds in the central equatorial Pacific and El Niño. *Science*, **222 (4621)**, 327–330.

MacRitchie, K., and P. E. Roundy, 2012: Potential vorticity accumulation following atmospheric Kelvin waves in the active convective region of the MJO. *J. Atmos. Sci.*, **69 (3)**, 908–914.

Madden, R. A., and P. R. Julian, 1971: Detection of a 40-50 day oscillation in the zonal wind in the tropical Pacific. *J. Atmos. Sci.*, **28 (5)**, 702–708.

Madden, R. A., and P. R. Julian, 1972: Description of global-scale circulation cells in the tropics with a 40-50 day period. *J. Atmos. Sci.*, **29 (6)**, 1109–1123.

Madden, R. A., and P. R. Julian, 1994: Observations of the 40-50-day tropical oscillation-a review. *Mon. Wea. Rev.*, **122 (5)**, 814–837.

Mahrer, Y., and R. A. Pielke, 1977: The effects of topography on sea and land breezes in a two-dimensional numerical model. *Mon. Wea. Rev.*, **105 (9)**, 1151–1162.

Matsuno, T., 1966: Quasi-geostrophic motions in the equatorial area. *J. Meteor. Soc. Japan*, **44 (1)**, 25–43.

Matthews, A. J., 2000: Propagation mechanisms for the Madden-Julian Oscillation. *Quart. J. Roy. Meteor. Soc.*, **126 (569)**, 2637–2651.

McPhaden, M., 2008: Evolution of the 2006–2007 El Niño: the role of intraseasonal to interannual time scale dynamics. *Adv. Geosci.*, **14 (14)**, 219–230.

McPhaden, M. J., 1999: Genesis and evolution of the 1997-98 El Niño. *Science*, **283 (5404)**, 950–954.

McPhaden, M. J., 2004: Evolution of the 2002/03 El Niño. *Bull. Amer. Meteor. Soc.*, **85 (5)**, 677–695.

McPhaden, M. J., F. Bahr, Y. Du Penhoat, E. Firing, S. Hayes, P. Niiler, P. Richardson, and J. Toole, 1992: The response of the western equatorial Pacific Ocean to westerly wind bursts during November 1989 to January 1990. *J. Geophys. Res.*, **97 (C9)**, 14 289–14 303.

Milliff, R. F., and R. A. Madden, 1996: The existence and vertical structure of fast, eastward-moving disturbances in the equatorial troposphere. *J. Atmos. Sci.*, **53 (4)**, 586–597.

Moncrieff, M. W., D. E. Waliser, M. J. Miller, M. A. Shapiro, G. R. Asrar, and J. Caughey, 2012: Multiscale convective organization and the YOTC virtual global field campaign. *Bull. Amer. Meteor. Soc.*, **93 (8)**, 1171–1187.

Mori, S., and Coauthors, 2004: Diurnal land-sea rainfall peak migration over Sumatera Island, Indonesian maritime continent, observed by TRMM satellite and intensive rawinsonde soundings. *Mon. Wea. Rev.*, **132 (8)**, 2021–2039.

Moum, J. N., and Coauthors, 2014: Air-sea interactions from westerly wind bursts during the November 2011 MJO in the Indian Ocean. *Bull. Amer. Meteor. Soc.*, **95 (8)**, 1185–1199.

Nakazawa, T., 1988: Tropical super clusters within intraseasonal variations over the western Pacific. *J. Meteor. Soc. Japan*, **66 (6)**, 823–839.

Ooyama, K., 1969: Numerical simulation of the life cycle of tropical cyclones. *J. Atmos. Sci.*, **26 (1)**, 3–40.

Peatman, S. C., A. J. Matthews, and D. P. Stevens, 2014: Propagation of the Madden–Julian Oscillation through the Maritime Continent and scale interaction with the diurnal cycle of precipitation. *Quart. J. Roy. Meteor. Soc.*, **140 (680)**, 814–825.

Pierrehumbert, R., 1984: Local and global baroclinic instability of zonally varying flow. *J. Atmos. Sci.*, **41 (14)**, 2141–2162.

Qian, J.-H., 2008: Why precipitation is mostly concentrated over islands in the Maritime Continent. *J. Atmos. Sci.*, **65 (4)**, 1428–1441.

Rao, S. A., J.-J. Luo, S. K. Behera, and T. Yamagata, 2009: Generation and termination of Indian Ocean dipole events in 2003, 2006 and 2007. *Clim. Dyn.*, **33 (6)**, 751–767.

Red Cross, 2011: Myanmar: Cyclone Nargis 2008 facts and figures. [Available online at http://www.ifrc.org/en/news-and-media/news-stories/asia-pacific/myanmar/myanmar-cyclone-nargis-2008-facts-and-figures/].

Riehl, H., 1948: On the formation of typhoons. *J. Meteor.*, **5 (6)**, 247–265.

Roundy, P. E., 2008: Analysis of convectively coupled Kelvin waves in the Indian Ocean MJO. *J. Atmos. Sci.*, **65 (4)**, 1342–1359.

Ruppert, J. H., and R. H. Johnson, 2015: Diurnally modulated cumulus moistening in the pre-onset stage of the Madden-Julian Oscillation during DYNAMO. *J. Atmos. Sci.*, **72 (4)**, 1622–1647.

Sadler, J. C., 1976: A role of the tropical upper tropospheric trough in early season typhoon development. *Mon. Wea. Rev.*, **104 (10)**, 1266–1278.

Saji, N., B. N. Goswami, P. Vinayachandran, and T. Yamagata, 1999: A dipole mode in the tropical Indian Ocean. *Nature*, **401 (6751)**, 360–363.

Schär, C., and D. R. Durran, 1997: Vortex formation and vortex shedding in continuously stratified flows past isolated topography. *J. Atmos. Sci.*, **54 (4)**, 534–554.

Schär, C., and R. B. Smith, 1993a: Shallow-water flow past isolated topography. Part I: Vorticity production and wake formation. *J. Atmos. Sci.*, **50 (10)**, 1373–1400.

Schär, C., and R. B. Smith, 1993b: Shallow-water flow past isolated topography. Part II: Transition to vortex shedding. *J. Atmos. Sci.*, **50 (10)**, 1401–1412.

Schreck, C. J., and J. Molinari, 2009: A case study of an outbreak of twin tropical cyclones. *Mon. Wea. Rev.*, **137 (3)**, 863–875.

Schreck, C. J., and J. Molinari, 2011: Tropical cyclogenesis associated with Kelvin waves and the Madden-Julian Oscillation. *Mon. Wea. Rev.*, **139 (9)**, 2723–2734.

Schreck, C. J., J. Molinari, and A. Aiyyer, 2012: A global view of equatorial waves and tropical cyclogenesis. *Mon. Wea. Rev.*, **140 (3)**, 774–788.

Schubert, W. H., and M. T. Masarik, 2006: Potential vorticity aspects of the MJO. *Dyn. Atmos. Oceans*, **42 (1)**, 127–151.

Seiki, A., and Y. N. Takayabu, 2007: Westerly wind bursts and their relationship with intraseasonal variations and ENSO. Part I: Statistics. *Mon. Wea. Rev.*, **135 (10)**, 3325–3345.

Singh, O., T. A. Khan, and M. S. Rahman, 2000: Changes in the frequency of tropical cyclones over the North Indian Ocean. *Meteor. Atmos. Phys.*, **75 (1-2)**, 11–20.

Smith, R. B., 1979: The influence of mountains on the atmosphere. *Advances in Geophysics*, **21**, 87–230.

Smith, R. B., 1982: Synoptic observations and theory of orographically disturbed wind and pressure. *J. Atmos. Sci.*, **39 (1)**, 60–70.

Smith, R. B., 1989: Hydrostatic flow over mountains. *Advances in Geophysics*, **31**, 1–41.

Smolarkiewicz, P. K., and R. Rotunno, 1989: Low Froude number flow past three-dimensional obstacles. Part I: Baroclinically generated lee vortices. *J. Atmos. Sci.*, **46 (8)**, 1154–1164.

Straub, K. H., and G. N. Kiladis, 2002: Observations of a convectively coupled Kelvin wave in the eastern Pacific ITCZ. *J. Atmos. Sci.*, **59 (1)**, 30–53.

Thorpe, A. J., H. Volkert, and D. Heimann, 1993: Potential vorticity of flow along the Alps. *J. Atmos. Sci.*, **50 (11)**, 1573–1590.

Vitart, F., A. Leroy, and M. C. Wheeler, 2010: A comparison of dynamical and statistical predictions of weekly tropical cyclone activity in the Southern Hemisphere. *Mon. Wea. Rev.*, **138 (9)**, 3671–3682.

Waliser, D. E., and Coauthors, 2012: The "Year" of Tropical Convection (may 2008-april 2010): Climate variability and weather highlights. *Bull. Amer. Meteor. Soc.*, **93 (8)**, 1189–1218.

Wallace, J. M., and V. Kousky, 1968: Observational evidence of Kelvin waves in the tropical stratosphere. *J. Atmos. Sci.*, **25 (5)**, 900–907.

Wang, S.-T., 1980: Prediction of the movement and strength of typhoons in Taiwan and its vicinity (in Chinese). National Science Research Council Report 108, Taipei, Taiwan, 100 pp.

Wei-Jen Chang, S., 1982: The orographic effects induced by an island mountain range on propagating tropical cyclones. *Mon. Wea. Rev.*, **110 (9)**, 1255–1270.

Wheeler, M., and G. N. Kiladis, 1999: Convectively coupled equatorial waves: Analysis of clouds and temperature in the wavenumber-frequency domain. *J. Atmos. Sci.*, **56 (3)**, 374–399.

Wheeler, M., G. N. Kiladis, and P. J. Webster, 2000: Large-scale dynamical fields associated with convectively coupled equatorial waves. *J. Atmos. Sci.*, **57 (5)**, 613–640.

Wheeler, M. C., and H. H. Hendon, 2004: An all-season real-time multivariate MJO index: Development of an index for monitoring and prediction. *Mon. Wea. Rev.*, **132 (8)**, 1917–1932.

Wheeler, M. C., H. H. Hendon, S. Cleland, H. Meinke, and A. Donald, 2009: Impacts of the Madden-Julian oscillation on Australian rainfall and circulation. *J. Climate*, **22 (6)**, 1482–1498.

WHO, 2008: Heavy flooding in yemen situation report no. 3- 27 oct 2008. [Available online at http://reliefweb.int/report/yemen/heavy-flooding-yemen-situation-report-no-3-27-oct-2008/].

Wu, C.-H., and H.-H. Hsu, 2009: Topographic influence on the MJO in the Maritime Continent. *J. Climate*, **22 (20)**, 5433–5448.

Wu, P., M. Hara, J.-i. Hamada, M. D. Yamanaka, and F. Kimura, 2009: Why a large amount of rain falls over the sea in the vicinity of western Sumatra Island during nighttime. *J. Climate Appl. Meteor.*, **48 (7)**, 1345–1361.

Yanai, M., and T. Maruyama, 1966: Stratospheric wave disturbances propagating over the equatorial Pacific. *J. Meteor. Soc. Japan*, **44**, 291–294.

Yang, G.-Y., and J. Slingo, 2001: The diurnal cycle in the tropics. *Mon. Wea. Rev.*, **129 (4)**, 784–801.

Yoneyama, K., C. Zhang, and C. N. Long, 2013: Tracking pulses of the Madden-Julian Oscillation. *Bull. Amer. Meteor. Soc.*, **94 (12)**, 1871–1891.

Zangvil, A., and M. Yanai, 1980: Upper tropospheric waves in the tropics. Part I: Dynamical analysis in the wavenumber-frequency domain. *J. Atmos. Sci.*, **37 (2)**, 283–298.

Zehnder, J. A., D. M. Powell, and D. L. Ropp, 1999: The interaction of easterly waves, orography, and the intertropical convergence zone in the genesis of eastern Pacific tropical cyclones. *Mon. Wea. Rev.*, **127 (7)**, 1566–1585.

Zhang, C., 2005: Madden-Julian Oscillation. *Rev. Geophys.*, **43 (2)**.

Zhang, C., 2013: Madden-Julian Oscillation: Bridging weather and climate. *Bull. Amer. Meteor. Soc.*, **94 (12)**, 1849–1870.

Zhang, C., and J. Ling, 2012: Potential vorticity of the Madden-Julian Oscillation. *J. Atmos. Sci.*, **69 (1)**, 65–78.

Zhang, L., B. Wang, and Q. Zeng, 2009: Impact of the Madden-Julian Oscillation on summer rainfall in southeast China. *J. Climate*, **22 (2)**, 201–216.